FACULTY OF ENGINEERING
AND ARCHITECTURE

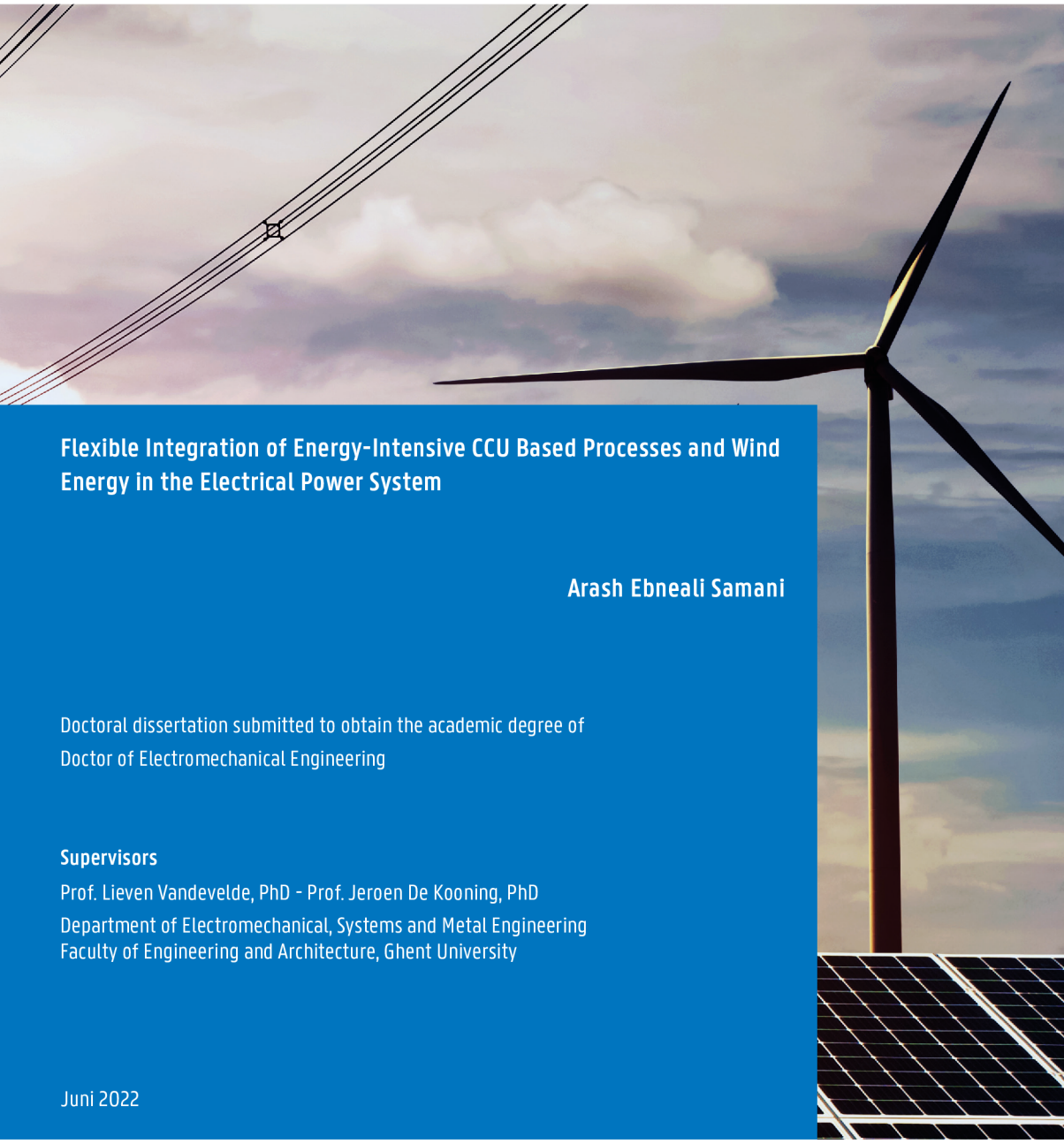

Flexible Integration of Energy-Intensive CCU Based Processes and Wind Energy in the Electrical Power System

Arash Ebneali Samani

Doctoral dissertation submitted to obtain the academic degree of
Doctor of Electromechanical Engineering

Supervisors
Prof. Lieven Vandevelde, PhD - Prof. Jeroen De Kooning, PhD
Department of Electromechanical, Systems and Metal Engineering
Faculty of Engineering and Architecture, Ghent University

Juni 2022

GHENT
UNIVERSITY

FACULTY OF ENGINEERING AND ARCHITECTURE

Flexible Integration of Energy-Intensive CCU Based Processes and Wind Energy in the Electrical Power System

Arash Ebneali Samani

Doctoral dissertation submitted to obtain the academic degree of
Doctor of Electromechanical Engineering

Supervisors
Prof. Lieven Vandevelde, PhD - Prof. Jeroen De Kooning, PhD

Department of Electromechanical, Systems and Metal Engineering
Faculty of Engineering and Architecture, Ghent University

June 2022

GHENT UNIVERSITY

ISBN 978-94-6355-606-4
NUR 959, 961
Wettelijk depot: D/2022/10.500/47

Members of the Examination Board

Chair

Prof. Em. Luc Taerwe, PhD, Ghent University

Other members entitled to vote

Prof. Emmanuel De Jaeger, PhD, Université catholique de Louvain
Prof. Clara-Mihaela Ionescu, PhD, Ghent University
Prof. Mark Saeys, PhD, Ghent University
Prof. Paolo Silva, PhD, Politecnico di Milano, Italy

Supervisors

Prof. Lieven Vandevelde, PhD, Ghent University
Prof. Jeroen De Kooning, PhD, Ghent University

Contents

Summary

Global warming and climate change are the most prominent issues of concern today. Over recent decades, various strategies and universal agreements have been set to combat climate change. In this framework, governments have adopted various climate, energy, and taxation policies to reduce net greenhouse gas emissions and meet the global climate target. However, there are several technical and economic challenges in the transition towards a low-carbon future and a circular economy. Renewable energy sources, power systems and carbon dioxide-based processes play a significant role in this paradigm shift. However, these technologies face barriers to effectively contribute to reduce emissions.

One of the key solutions to reducing greenhouse gas emissions is to expand renewable energy installations and to move towards predominantly or entirely renewable power generation. However, the electrical grid is not designed to accommodate a high level of renewable power generation. The intermittent and inertia-less nature of renewable energy sources reduces the grid's reliability and increases the pressure on the conventional power plants to balance the grid. Therefore, the power system needs to become more flexible and adaptive. The increasing penetration of renewable energy in power systems is expected to increase curtailment due to a lack of system flexibility. Alternatively, renewables can be operated flexibly according to the grid's condition. However, this leads to a sub-optimal operation of renewables and negatively impacts these systems, e.g., it can increase structural loads on wind turbines. Novel chemical processes with innovative technologies are under development to reduce carbon dioxide emissions. These processes, which are referred to as Carbon dioxide Capture and Utilisation (CCU), use carbon dioxide as a raw material for the chemical synthesis, e.g., formic acid, methane or methanol. CCU based processes have the potential to reshape the chemical industry in the low carbon paradigm. However, CCU based processes for the direct conversion of CO_2 into value-added chemicals are energy-intensive and have a poor economic viability. Therefore, new strategies are required to address these challenges, to accelerate the deep decarbonisation process and to reach the net-zero emissions target.

In this PhD research, we searched for solutions to enhance the flexibility

of power systems for further integration of renewables and CCU based processes into the electrical grid, facilitating the transition towards a low carbon paradigm. In this framework, various sources of flexibility are researched to extend the system flexibility on both the electricity supply and demand sides. This dissertation introduces four flexible operating strategies addressing challenges concerning the integration of wind energy and energy-intensive chemical processes into the power grid.

Firstly, the optimal demand response operation of power-to-hydrogen technology is investigated. The techno-economic analysis is performed for the flexible operation of a large-scale PEM electrolyser under two scenarios. First, the economic performance of the PEM electrolyser is assessed for a price-based scenario where the power consumption of the electrolyser is regulated based on the electricity price. Then, the potential economic benefits of the flexible operation are investigated for fast-paced ancillary services where the electrolyser's power input is regulated based on the grid frequency. Moreover, an electrochemical model and a control system are developed to evaluate the technical feasibility of the proposed strategy. The techno-economic analysis shows that operating the electrolyser at the optimum baseload and providing Frequency Containment Reserve (FCR) for the grid can generate extra revenue and improve economic performance. The dynamic simulation shows that the PEM system represents a high degree of flexibility and can react to the grid frequency variation with a response time of less than five seconds.

The second research topic investigates the flexible operation of energy-intensive CCU based processes with two objectives: to provide ancillary services for the grid and to operate on renewable electrical energy. A flexible operating strategy and a control architecture are developed, addressing the challenges of demand response operation of chemical processes, i.e., the constraints and nonlinear dynamics of chemical systems. The developed strategy increases the process's flexibility by adaptively regulating the setpoints of process components based on input power variations. Therefore, the chemical process reacts to the grid frequency by controlling the power consumption of the PEM electrolyser while maintaining the reactor's optimal operating conditions through the adaptive operation of the H_2 and CO_2 multi-stage compression systems. The results show that the proposed strategy enables the CCU based process to provide FCR while minimising the impact on the reactor efficiency. Moreover, the techno-economic analysis shows that operating the process at optimal baseload and providing the remaining capacity as a power reserve can create additional revenue and improve the economic profit.

Thirdly, the advantages of pitch-to-stall control are investigated for the effective integration of wind energy into the power grid. The purpose of this research study was to identify the potential benefits of stall regulation to improve the capability of wind turbines in the active power control for

FCR provision while minimising the impact on the structural loads and pitch mechanism. Two control systems are designed for pitch-to-stall and pitch-to-feather control concepts to address the aerodynamic nonlinearity of the system. Then, the dynamic response of three wind turbine models is compared, focusing on control performance and the effect on the pitch mechanism and structural loads. The wind turbines performance is examined in uniform wind and turbulent wind in the whole operating region, i.e., Maximum Power Point Tracking (MPPT), the transition zone, and the full load region. The results show that the pitch-to-stall strategy with a stall-regulated blade design offers comparative advantages in terms of active power control and load reduction on the tower and pitch mechanisms. However, stall regulation might increase the risk of surface damage in the rolling bearings of the blades and increase the loading on the rotor blades to some degree.

Finally, a novel flexible operating strategy is developed based on the collaborative operation of a CCU based process with wind energy. In this strategy, the chemical process is coupled with wind turbines, and they participate in the energy and reserve markets as a hybrid system. To effectively integrate this system into the power grid, an optimisation framework is required to deal with wind and grid uncertainties and support optimal operating decisions. Therefore, an optimal two-stage stochastic programming model is developed to enable FCR provision through the cooperative operation of the CCU based process and wind turbines. The Group Method of Data Handling (GMDH) algorithm is used to predict stochastic variables and make the optimisation computationally efficient. The developed dynamic model of the process and the wind turbine in the previous research studies allows the detailed coupling of dynamic models and validate the proposed optimisation framework under operational restrictions. The results demonstrate that the proposed approach enables the hybrid system to make the optimal decision when offering its bidding quantity in the day-ahead electricity and reserve market.

In conclusion, various flexible operating strategies are proposed to facilitate the integration of power-to-hydrogen technology, wind turbines, and CO_2-based processes into the power grid. The results show the significance of the developed strategies for optimal participation in the energy and ancillary markets, which can have a valuable contribution to the development of the future grid under the high-level penetration of renewable energy sources.

Samenvatting

De opwarming van de aarde en de klimaatverandering zijn de meest prominente problemen van vandaag. De afgelopen decennia zijn verschillende strategieën en politieke akkoorden opgesteld om klimaatverandering tegen te gaan. In dit kader hebben regeringen verschillende klimaat-, energie- en belastingsbeleidsmaatregelen getroffen om de netto-uitstoot van broeikasgassen te verminderen en de wereldwijde klimaatdoelstellingen te halen. Er zijn echter verschillende technische en economische uitdagingen in de transitie naar een koolstofarme toekomst en een circulaire economie. Hernieuwbare energiebronnen, energiesystemen en op koolstofdioxide gebaseerde processen spelen een belangrijke rol in deze paradigmaverschuiving. Deze technologieën hebben echter te maken met belemmeringen om effectief bij te dragen aan het verminderen van emissies.

Een van de belangrijkste oplossingen om de uitstoot van broeikasgassen te verminderen, is het uitbreiden van installaties voor hernieuwbare energieopwekking en het overstappen op overwegend of volledig hernieuwbare energieopwekking. Het elektriciteitsnet is echter niet ontworpen om een grote hoeveelheid aan duurzame energieopwekking op te vangen. De intermitterende en inertieloze aard van hernieuwbare energiebronnen vermindert de betrouwbaarheid van het net en verhoogt de druk op de conventionele elektriciteitscentrales om het net in evenwicht te houden. Daarom moet het energiesysteem flexibeler en adaptiever worden. Het toenemende aandeel van hernieuwbare energie in elektriciteitssystemen zal naar verwachting leiden tot meer inperkingen vanwege een gebrek aan systeemflexibiliteit. Als alternatief kunnen hernieuwbare energiebronnen flexibel worden beheerd, afhankelijk van de toestand van het net. Dit leidt echter tot een suboptimale werking van hernieuwbare energiebronnen en heeft een negatieve invloed op deze systemen. Het kan bijvoorbeeld de structurele belasting van windturbines verhogen. Nieuwe chemische processen met innovatieve technologieën zijn in ontwikkeling om de uitstoot van kooldioxide te verminderen. Deze processen, die worden aangeduid als 'Carbon dioxide Capture and Utilization' (CCU), gebruiken koolstofdioxide als grondstof voor de chemische synthese van o.a. mierenzuur, methaan of methanol. Op CCU gebaseerde processen hebben het potentieel om de chemis-

che industrie een nieuwe vorm te geven in het koolstofarme paradigma. Op CCU gebaseerde processen voor de directe omzetting van CO_2 in chemicaliën met toegevoegde waarde zijn echter energie-intensief en leveren tegenvallende economische prestaties. Daarom zijn nieuwe strategieën nodig om deze uitdagingen aan te pakken, het proces van verregaande decarbonisatie te versnellen en het streefcijfer voor netto-koolstofvrije emissies te bereiken.

In dit doctoraatsonderzoek hebben we gezocht naar oplossingen om de flexibiliteit van energiesystemen te vergroten voor verdere integratie van hernieuwbare energiebronnen en CCU gebaseerde processen in het elektriciteitsnet, waardoor de overgang naar een koolstofarm paradigma wordt vergemakkelijkt. In dit kader worden verschillende bronnen van flexibiliteit onderzocht om de systeemflexibiliteit aan zowel de aanbod- als de vraagzijde van elektriciteit te vergroten. Dit proefschrift introduceert vier flexibele operationele strategieën die uitdagingen aangaan met betrekking tot de integratie van windenergie en energie-intensieve chemische processen in het elektriciteitsnet.

Ten eerste wordt de optimale vraagresponswerking van waterstoftechnologie onderzocht. Een technisch-economische analyse wordt uitgevoerd voor de flexibele werking van een grootschalige PEM-elektrolyser in twee scenario's. Eerst worden de economische prestaties van de PEM-elektrolyser beoordeeld voor een prijsgebaseerd scenario waarbij het stroomverbruik van de elektrolyser wordt gereguleerd op basis van de elektriciteitsprijs. Vervolgens worden de potentiële economische voordelen van de flexibele werking onderzocht voor snelle net-ondersteunende diensten waarbij het opgenomen vermogen van de elektrolyser wordt geregeld op basis van de netfrequentie. Bovendien worden een elektrochemisch model en een controlesysteem ontwikkeld om de technische haalbaarheid van de voorgestelde strategie te evalueren. Uit de technisch-economische analyse blijkt dat het gebruik van de elektrolyser bij de optimale basislast en het leveren van 'Frequency Containment Reserve' (FCR) voor het net extra inkomsten kan genereren en de economische prestaties kan verbeteren. De dynamische simulatie laat zien dat het PEM-systeem een hoge mate van flexibiliteit vertegenwoordigt en kan reageren op de variaties in de netfrequentie met een responstijd van minder dan vijf seconden.

Het tweede onderzoeksthema bestudeert de flexibele werking van energie-intensieve CCU gebaseerde processen met twee doelstellingen: het leveren van ondersteunende diensten voor het net en het werken op hernieuwbare elektrische energie. Er wordt een flexibele bedrijfsstrategie en een controle-architectuur ontwikkeld die de uitdagingen van vraagrespons van chemische processen aanpakken, d.w.z. de beperkingen en de niet-lineaire dynamica van chemische systemen. De ontwikkelde strategie vergroot de flexibiliteit van het proces door adaptief de setpoints van procescomponenten te regelen op basis van variaties in het ingangsvermogen. Daarom reageert het chemische proces op de netfrequentie door het stroomverbruik van de PEM-elektrolyser te regelen

terwijl de optimale bedrijfsomstandigheden van de reactor worden gehandhaafd door de adaptieve werking van de H_2 en CO_2 meertraps compressoren. De resultaten laten zien dat de voorgestelde strategie het CCU gebaseerde proces in staat stelt om FCR te leveren terwijl de impact op de reactorefficiëntie wordt geminimaliseerd. Bovendien toont de technisch-economische analyse aan dat het proces met optimale basislast en het verstrekken van de resterende capaciteit als reserve extra inkomsten kan opleveren en de economische winst kan verbeteren.

Ten derde worden de voordelen van pitch-to-stall-regeling onderzocht voor de effectieve integratie van windenergie in het elektriciteitsnet. Het doel van deze studie was om de potentiële voordelen van overtrekregeling te identificeren om het vermogen van windturbines in de actieve vermogensregeling voor FCR-voorziening te verbeteren, terwijl de impact op de structurele belastingen en het hellingsmechanisme wordt geminimaliseerd. Er zijn twee regelsystemen ontworpen voor de bedieningsconcepten van pitch-to-stall en pitch-to-feather om de aerodynamische niet-lineariteit van het systeem aan te pakken. Vervolgens wordt de dynamische respons van drie windturbinemodellen vergeleken, waarbij de nadruk ligt op de regelprestaties en het effect op het pitchmechanisme en structurele belastingen. De prestaties van de windturbines worden onderzocht in uniforme wind en turbulente wind in het hele werkgebied, d.w.z. Maximum Power Point Tracking (MPPT), de overgangszone en het werkingsgebied bij vol vermogen. De resultaten laten zien dat de pitch-to-stall-strategie met een overtrek-gereguleerd bladontwerp voordelen biedt in termen van actieve vermogensregeling en belastingvermindering op de toren- en pitch-mechanismen. Overtrekregeling kan echter het risico op oppervlaktebeschadiging in de wentellagers van de schoepen vergroten en de belasting van de rotorschoepen tot op zekere hoogte verhogen.

Ten slotte wordt een nieuwe flexibele strategie ontwikkeld op basis van de samenwerking van een CCU-gebaseerd proces met windenergie. In deze strategie wordt het chemisch proces gekoppeld aan windturbines en nemen ze als hybride systeem deel aan de energie- en reservemarkten. Om dit systeem effectief in het elektriciteitsnet te integreren, is een optimalisatiekader nodig om met wind- en netonzekerheden om te gaan en optimale operationele beslissingen te ondersteunen. Daarom is een optimaal tweetraps stochastisch programmeermodel ontwikkeld om FCR-voorziening mogelijk te maken door de samenwerking tussen het op CCU gebaseerde proces en windturbines. Het 'Group Method of Data Handling' (GMDH) algoritme wordt gebruikt om stochastische variabelen te voorspellen en de optimalisatie rekenkundig efficiënt te maken. Het ontwikkelde dynamische model van het proces en de windturbine uit de vorige studies maken het mogelijk om dynamische modellen gedetailleerd te koppelen en het voorgestelde optimalisatiekader onder operationele beperkingen te valideren. De resultaten tonen aan dat de voorgestelde aanpak het hybride

systeem in staat stelt de optimale beslissing te nemen bij het aanbieden van zijn energie en reserves op de day-ahead elektriciteits- en reservemarkten.

Concluderend worden verschillende flexibele strategieën voorgesteld om de integratie van waterstoftechnologie, windturbines en op CO_2 gebaseerde processen in het elektriciteitsnet te vergemakkelijken. De resultaten tonen het belang aan van de ontwikkelde strategieën voor een optimale deelname aan de energie- en aanverwante markten, die een waardevolle bijdrage kunnen leveren aan de ontwikkeling van het toekomstige net met een groot aandeel aan hernieuwbare energiebronnen.

List of Figures

List of Tables

Chapter 1

Introduction

1.1 Challenges of renewable energy penetration on power systems

Electricity is critical to all modern economies, enabling essential services from healthcare to all kinds of transactions, from information exchange to transportation. A reliable power system is thus of paramount importance for a secure electricity supply and for sustaining long term economic growth. In the past two decades, the electrical power system has been extensively changing due to the energy mix transformation with the fast-growing share of renewable energy sources. According to the International Energy Agency (IEA), renewable electricity generation increased at its fastest rate in two decades in 2020, and it is set to increase by more than 8% in 2021, the fastest annual growth since the 1970s. Fig. 1.1 illustrates the renewable electricity generation expansion by country, region and technology. As shown, wind and solar energy continued to dominate in the renewable capacity increase in 2020 and 2021. The growth of renewable capacity is expected to accelerate in the next few years, accounting for almost 95% of the increase in global power capacity through 2026. Renewed energy policies and COP26 climate goals are set to higher targets for renewable electricity growth. Therefore, the global renewable electricity capacity is predicted to grow by over 60% between 2020 and 2026, reaching more than 4800 GW [1].

The renewable capacity growth in the European Union (EU) over 2021-26 is set to outpace the current envision for 2030. According to the European Green Deal in 2014, in line with the Paris Agreement, the EU aimed to increase the renewable energy share by at least 32% and reduce greenhouse emissions by at least 40% (compared to 1990 levels) by 2030. However, the European Commission adopted a package of proposals for higher greenhouse emission reduction and outlined the required transformational change. The new commis-

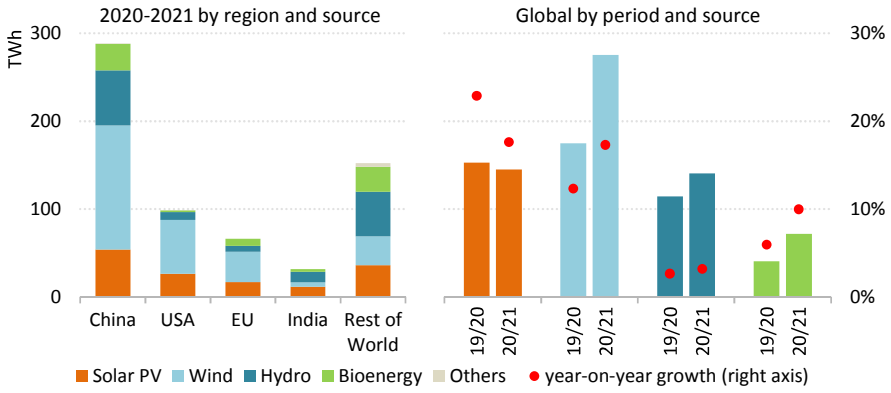

Figure 1.1: Renewable electricity generation increase by technology, country and region [2].

sion proposal, referred to as the "Fit for 55" program, increases the greenhouse gas emissions reduction by at least 55% and raises the current EU target of renewables in the overall energy mix to at least 40% by 2030. This is two times higher than the current renewable energy share of 19.7% [3]. Although the deployment of renewable energy sources reduces greenhouse gas emissions, technical barriers need to be addressed to accelerate these sources into the power system. The increasing growth of renewable energy sources introduces new challenges to the operation of power systems due to the intermittent and inertia-less nature of these sources. The higher penetration of renewables complicates maintaining the stability and reliability of the power system. Therefore, new technologies and operating strategies are needed to enable the system to cope with renewable generation uncertainty and availability.

The variable renewable output increases the load on conventional power plants to compensate for supply-demand mismatches. The intermittency of renewable output implies that the remaining resources on a power system must respond to variations in renewable output to maintain the balance between supply and demand. The remaining load, referred to as net load or residual load, is the required level of non-variable power after deducting the variable renewable generation, i.e., wind and solar. Variable power generation can lead to ramps of extreme steepness or duration in net load caused by large swings in renewable power output over short periods, for instance, when electricity demand increases while wind generation drops. Also, sun rising/setting can lead to daily ramps. In regions with high penetration of solar power, the grid operators have to deal with ramps in net load occurring over a few hours due to solar output declining and rising during sunset/sunrise periods and weather changes. Variable energy sources can increase the ramping range, leading to

dispatchable generator turn-downs [4]. The associated reduction in minimum net load can force the dispatchable generators to reduce output to low levels or even cycle off during low demand and high wind speed periods while remaining available to rise again. Moreover, intermittent wind power can also increase the net load's short-term variability, increasing the need for frequency regulation [5].

With increasing penetration of renewable energy sources, the power system inertia is changing due to the inertia-less nature of these sources. In power systems, inertia refers to the kinetic energy stored in large rotating machinery, which gives them the tendency to remain rotating. This stored energy can be valuable to stabilise the grid when a large power plant or transmission fails. The stored energy can temporarily compensate for the power lost from the failed generator and provide the grid time to respond to the failure. The inertia in the power system is provided by spinning generators in conventional power plants, i.e., fossil, nuclear and hydroelectric power plants. Most conventional power plants use synchronous generators to generate electricity, rotating with the same frequency (50 Hz in Europe). However, wind turbines, PV and batteries use inverters to inject power at 50 Hz. These technologies, referred to as inverter-based resources, are not directly coupled with rotating inertia. Therefore, when a major generation from synchronous generators is replaced by renewable generation, the total amount of inertia during these periods will decrease. Therefore, in the case of a contingency event, the frequency falls faster due to the lower available inertia. Therefore, potential declines in inertia that can result from increased integration of inverter-based resources need to be addressed in the planning and operations of the system to maintain reliable operation.

There are several possible and proven approaches to respond to the declining role of inertia due to the increased penetration of renewables. The power system's inertia can be maintained using synchronous condensers, i.e., synchronous motors/generators that draw and inject energy into the grid to maintain rotating inertia. Also, synchronous renewable energy sources, e.g., hydropower, geothermal, and biomass, can provide inertia to the grid. Moreover, the fast decline in frequency resulting from lower inertia can be compensated by the rapid response from fast frequency response. In this context, there are several electrical loads and inverter-based technologies, e.g., wind, solar and storage, that are able to respond to system imbalances and increase the energy supply much faster than synchronous generators. Therefore, the electronic-based frequency response from inverter-based resources and fast response from loads can offset the declines in inertia. Although the accelerating integration of renewable energy sources into the power system will reduce the grid inertia, there are multiple solutions for enhancing system reliability. Therefore, reduction in inertia is not a barrier to the significant growth of wind

and solar energy [6].

1.2 Solutions to provide power system flexibility

All power systems are designed with an inherent level of flexibility to balance electricity consumption and production. Flexibility is a characteristic of a power system, primarily defined as the ability to vary system generation to respond to changes in load or sudden unexpected situations, such as faults or accidents in transmission lines or generators. However, with higher levels of grid-connected variable renewable energy, the flexibility concept needs to be reconsidered beyond conventional flexibility to include renewables with variable and hardly predictable power generation. Therefore, the flexibility of the power system can be defined as the ability to respond to changes in both demand and supply, coping with uncertainty on supply-demand sides.

1.2.1 Energy Storage Systems

Energy Storage Systems (ESS) can provide flexibility to the energy system and support power systems by balancing supply and demand mismatches. This is achieved by storing energy and releasing it whenever required. EES can be used in a wide range of applications in power systems, including reserve services, transmission and distribution and bulk power management. These technologies are mainly classified as chemical, electrochemical, mechanical and electrical storage systems. Several storage technologies have been developed, providing a wide range of storage capacity and discharge times, e.g., batteries, supercapacitors, flywheels, Superconducting Magnetic Energy Storage (SMES), Compressed-Air Energy Storage (CAES), pumped hydro and hydrogen storage systems. Fig. 1.2 illustrates the power ranges and discharge times at the rated power of different energy storage technologies. As shown, a wide range of power capacity and discharge times can be provided by EES, depending on the characteristics of the storage systems.

Pumped hydroelectric energy storage (PHES) is already an established technology for several decades and holds more than 99% of the installed ESS capacity [8]. PHESs provide important capacity for grid stability and reliability while utilising hydro potential to store electrical energy [9, 10]. PHESs store electrical energy in the form of the gravitational potential of water by pumping water from a reservoir at a low height to a higher water reservoir. Then, energy can be generated by releasing water from the upper reservoir to the lower, activating hydraulic turbines to generate electricity. As illustrated in Fig. 1.2, PHESs can store a large amount of power (up to some GW) with a long discharge time. In addition to the large power volumes in PHES installations, their high

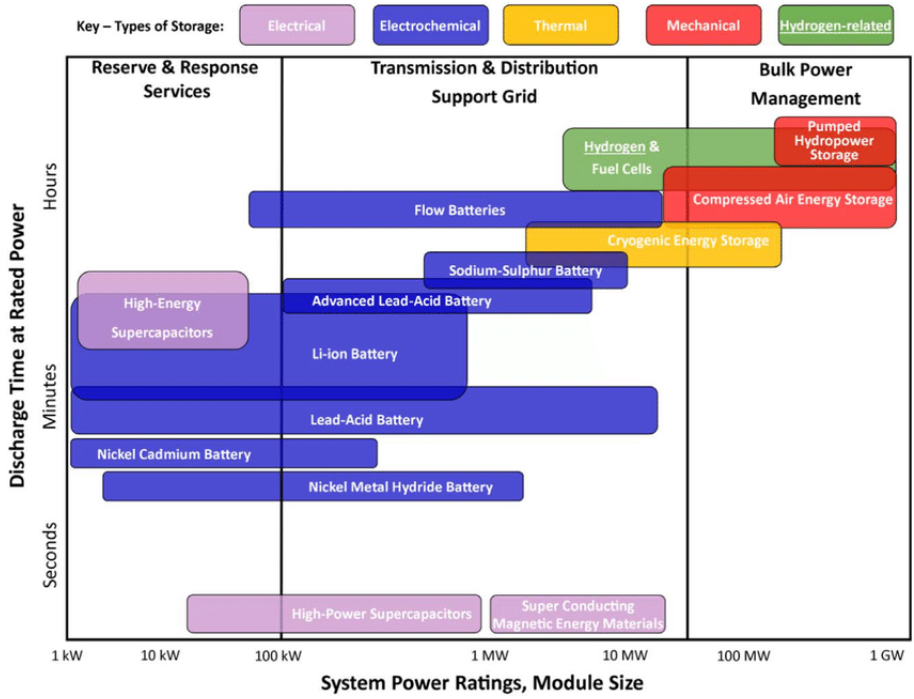

Figure 1.2: Comparison of energy storage technologies in terms of storage capacity and discharge power duration [7].

degree of reactivity, i.e., response times below 1 min [11], enables them to provide frequency regulation and spinning reserve services. Despite these advantages of PHES, these are large units with high capital costs. Also, they are limited to the topographic conditions, i.e., the available elevation difference between both reservoirs.

Although PHES dominates current EES, electrochemical storage systems can offer valuable options such as self-discharging and higher efficiency. Among the available technologies, capacitors and batteries can store electrical energy in electrochemical form. Capacitors can both handle high currents, but only for extremely short periods due to their very low energy density. Therefore, double-layer capacitors, referred to as supercapacitors (SC), are being used with larger energy storage capabilities. Batteries have a higher energy density than SCs, storing almost 30 times higher energy with the same mass [12]. However, capacitors can deliver higher power and run for a longer span when compared to batteries [13]. Amid different battery technologies, significant progress was made for lithium-based (Li-based) batteries due to their relatively higher energy density and specific energy. In [14], it is shown that Li-air and Li-sulfur were cost-effective compared to Li-ion batteries. Despite the advantages of

lithium-based batteries, they cannot store significant power fluctuation in grid applications due to their low specific energy, i.e., 250 Wh/kg. A large number of batteries are required to provide sufficient reserve for the grid. In [15], it is shown that combining metal-ion batteries and capacitors in a hybrid system can comply with future energy storage requirements. In addition, flow battery technologies can provide energy storage with higher power capacity and discharge time. Flow batteries use two electrolyte reservoirs for electrolyte flow which are separated by a membrane. The storage volume of the electrolyte determines the energy capacity, and the power is a function of the electrodes surface area. Redox flow battery technologies have improved to be employed in storage applications with renewable energy sources, providing higher performance, e.g., power capacity, density and charge and discharge rates, while using non-toxic material [16, 17].

Hydrogen storage is among the most promising technologies to support the integration of renewable energy sources into the power system. In off-grid applications, hydrogen storage devices have been considered as one viable solution for power generation and energy storage [18]. Also, hydrogen energy systems integrated into a network offer significant advantages by providing flexibility to the power system, which helps to maintain the balance between electricity generation and consumption. The intermittent renewable electricity can be reversibly stored as hydrogen and re-injected in the grid by using a fuel cell, in the scale from kWh to GWh of energy. In large scale applications, where the volume occupied by the storage system can be of concern, hydrides and intermetallic alloys are promising and competitive solutions [19, 20]. In [21], it is shown that hydride, i.e., AB_5, $NaAlH_4$, and MgH_2, can considerably reduce the volume required to store a large amount of energy. Hydrogen-based systems allow the decoupling of the power and energy characteristics of the system, which makes them more expandable and leads to a longer storage period and lower capital energy costs compared to batteries [18]. Further, hydrogen is not necessarily need to be processed in a fuel cell. It can be coupled within a natural gas combined cycle plant or hydrogen fuel stations as a clean energy vector, allowing decarbonisation of electricity and automotive sectors [22]. Given these advantages, hydrogen can play a fundamental role in future power systems to provide flexibility for higher integration of renewable energy sources and accelerate the reduction of carbon emissions.

1.2.2 Curtailment

The rapid growth of variable renewable generation has resulted in system integration challenges and has increased curtailment levels in the last few years. Therefore, the grid operational strategies need to be adapted to ensure secure and cost-effective integration of the increasing share of renewables and prevent

a higher level of curtailment in the coming years. The term curtailment refers to reducing renewable electricity output below what could have been produced at that moment due to the system requirements, e.g., inertia and priority dispatch, or transmission constraints, e.g., grid congestion and faults. As illustrated in Fig. 1.3, the share of dispatched-down increased in the countries with wind and solar PV generation. This was because of the change in load patterns caused by the Covid – 19 demand shock and higher variable renewable generation. As shown, the share of curtailed wind and solar PV increased in the United States, Australia, Spain and Italy while remaining stable in Germany and Great Britain [23]. The curtailment level in China has been reduced from 20% of VRG in 2012 to less than 5% in 2020. This improvement is despite the fact that China's renewable capacity has grown during this period and currently accounts for 50% of the global growth. The curtailment was mainly caused by insufficient transmission capacity, lack of flexible generating units and demand-side flexibility. Therefore, China started to improve the curtailment situation by commissioning additional inter-provincial transmission capacity, improving market operations and grid operational strategies, e.g., generation scheduling, forecasting, and constructing wind power dispatch systems [23, 24].

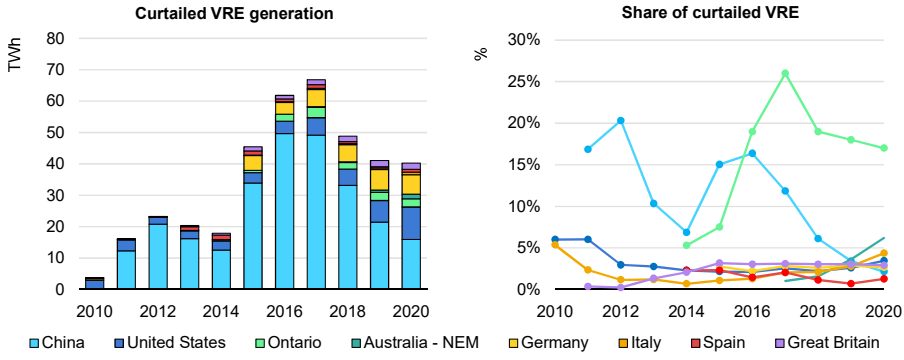

Figure 1.3: Wind and solar PV generation curtailment by country [23].

Although regular curtailment of variable renewable sources has not been critical in many power systems so far, the rapid increasing share of VRE means that dispatch-down of non-synchronous generation may be required in the future. In [25], it is discussed that although curtailment of renewable generation might appear as a loss, it can be a rational option to avoid high grid investment and operational costs when expanding the renewable variable generation capacity. Curtailment can be an optimal option from a power systems operation and cost-efficient perspective up to a point where the marginal cost of not curtailing equals the total value of the lost energy. However, curtailment

has also negative influences on the systems operation costs. As a result of the renewable curtailment during excess power supply, conventional power plants must compensate for the reduced share of the consumer load covered by renewable energy. Also, the curtailed energy cannot be restored to the system later when the electrical load increases. Therefore, curtailment gives rise the higher fossil fuel consumption and corresponding emissions of conventional power plants.

In [26], it is shown that sub-optimal operation of non-dispatchable energy sources, and using that headroom, can create marginal reserves and enables renewable plants to participate in the ancillary market. The flexible operation of variable renewable energy sources can provide the opportunity to support the electric power system while creating economic revenue for VRE owners. Wind power plants can respond to grid frequency increases by reducing the output power through torque or pitch control [27]. However, downward frequency regulation can only be provided by operating them below maximum output levels [28], creating enough headroom to increase the power at the operating wind speed. Solar plants can also provide frequency regulation by regulating output power through electronic controls [29]. However, curtailment or sub-optimal operation could have a significant economic impact on wind or solar power plants.

1.2.3 Demand-side management

One of the solutions to accommodate increasing variable energy sources in the power system is to develop a new dynamic equilibrium by increasing the flexibility on the electricity demand side. Demand-side management (DSM) or demand-side response (DSR) is the modification of the consumers' electricity demand to match/accommodate changes in power generation. Changing load patterns of residential, commercial and industrial users to provide flexibility to the power system is a bilateral scope. From the electricity consumers perspective, energy consumption schedules can minimise the operating costs with financial incentives or an advantageous tariff offer strategy. While, from the Transmission System Operator (TSO) perspective, the goal is to utilise demand-side management to maintain the grid stability and minimise the operating cost of the power system. Demand-response regulation and implementation have progressed further in 2020 and 2021 by developing favourable policies in several countries to facilitate widespread demand-response deployment in power markets. However, the global capacity of flexible assets in the residential, commercial and industrial sectors must be ten times higher than today by 2030 to support Net Zero Emissions by 2050 trajectories. The electricity system flexibility, i.e., hour-to-hour ramping ability, need to be enhanced more than double by 2030 to accommodate the expanded variable renewable sources. According

to [23], battery storage and demand-side response should become significant sources of flexibility in 2030, providing a quarter of flexibility needs globally. From the technological perspective, a certain level of technical adaptation of residential and industrial users is required, e.g., smart control and automation systems, to ensure the effective contribution of electricity loads in demand response programs. Fig. 1.4 illustrates the increasing volumes of demand-side response in the central scenario.

1.3 Demand response operation of chemical processes

The intermittent and inertia-less nature of renewable sources threatens the grid robustness with significant disturbances, e.g., capacity losses and frequency deviations. Therefore, the need for demand-side management/demand response of industrial loads has become of great importance. The contribution of industrial users in demand-side management has largely involved a price-based response, in which plant operations are scheduled in response to variable electricity prices. In [31], it is concluded that energy-intensive industrial processes with high specific electricity costs, i.e., electricity costs per gross value added, have a high potential to participate in demand response programs. The electricity cost thereby comprises a considerable share of the total operation cost of the processes. Also, the industrial plant must be able to modify its power demand quickly without affecting the production quality. A price-based demand response can be applied in different industrial applications such as steel furnaces [32], chlorine production [33], air separation units [34, 35], cement plants [36], pulp mills [37] and glass furnaces [38]. In this context, several operating strategies have been developed for the optimal coordination of electricity consumption and production. In [39,40], the power consumption of steel plants is scheduled in a price-based demand response framework. In [41, 42], the process scheduling is assessed for air-separation units for optimal contribution in demand-side response programs. Although price-based demand response allows the TSOs to estimate electrical loads, it does not guarantee the loads behaviour and the resulting impact on the grid operation. Also, priced-based demand response might lead to rebound peaks. These are large increases in electricity consumption after a demand response event in off-peak conditions [43, 44]. Therefore, some uncertainties remain regarding industrial load behaviour and its impact on the operation of the grid. Moreover, price-based demand response is slow, and it does not provide direct control to react to fast frequency variations to stabilise the power grid.

The deficiencies of price-based demand response have led to the increasing need for fast demand response programs that provide the TSOs with direct control of electrical loads. In this context, grid balancing services can rebal-

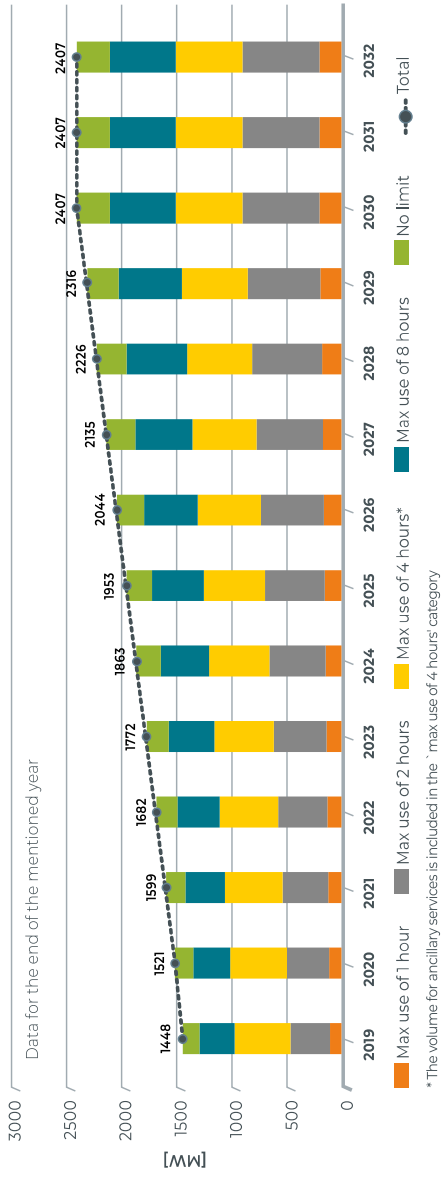

Figure 1.4: Evolution of demand-side response volumes per year in the central scenario [30].

ance supply and demand and maintain grid frequency at the reference value (50 Hz). The services for frequency regulation can be implemented using fast ramping reserves that can react to the grid frequency variations. The chemical processes with adequate flexibility potential can contribute to fast-paced demand response programs by flexible operation of their components with a fast dynamic response, e.g., electrolysers, compressors, pumps, fans and electric heaters. Several energy-intensive chemical industries can provide frequency regulation services as Balancing Service Providers (BSPs) or Flexibility Service Providers (FSPs). In [31, 45, 46], it is shown that processes such as chloralkali electrolysis, Liquefied Natural Gas (LNG) plants, cement processing plants, and aluminium smelters have the technical potential to provide balancing services. In [47–50], it is shown that the processes with the capability of discrete power changes, e.g., bitumen, cement, paper production processes and industrial meting pots, can provide continuous power regulation through combining on/off switching of discrete load units, e.g., bitumen processes, cement crushers or paper mills. Moreover, it is shown that frequency regulation can be provided by applying proper optimal scheduling and control algorithms with a limited impact on the process units. In [51, 52], ancillary service provision is assessed for aluminium smelters.

Moreover, there are several chemical processes whose slow dynamics can absorb fast power input variation with negligible impact on product quality. These processes consist of subsystems with higher time constants in the order of minutes to hours. Therefore, they can absorb the fast variation in input signals such as frequency dispatch signals. In [53], the feasibility of providing frequency regulation by conventional chemical processes with slow dynamics, e.g., distillation and cooling towers, is investigated. The authors have stated that chemical processes such as water-methanol distillation systems can participate in the ancillary market due to their capacity in damping the dominant high-frequency harmonic content of frequency dispatch signals. These systems can absorb the fast variations of the power offtake with negligible impact on product quality, similar to electric arc furnaces that treat the dispatch signal as a disturbance instead of a reference signal.

1.4 Frequency control and ancillary services

In electrical power systems, the active power generation and consumption must be maintained in constant equilibrium. The grid frequency reflects the ability of a system to balance electricity supply and demand, and it is determined by the rotational speed of the synchronous generators. Disruptions in this balance lead to a deviation of the system frequency from its nominal value. Therefore, grid frequency is a measure to prevent grid instability and undesired technical

and economical problems. The current grid operating rules apply tight grid frequency tolerances to ensure a full and rapid response to disturbances. Fig. 1.5 illustrates the reserve capacities used by TSOs to cover the system imbalances and restore the frequency to its setpoint value. Three reserves are activated consecutively to restore the frequency after an imbalance:

- **Frequency Containment Reserve (FCR):** A frequency disturbance impacts the entire synchronous zone when power imbalance events occur. Therefore, all interconnection partners collectively provide FCR to restore the equilibrium between power generation and consumption, ensuring that the grid frequency is maintained within allowed limits. The synchronous power plants detect changes in frequency and automatically adjust operations of online generators to maintain frequency within the desired range. Historically, primary frequency response was provided by a series of synchronous generators. However, many other technologies with high reactivity, such as electrolysers, can also provide FCR and support the power grid. FCR is activated within the time frame of 30 seconds and reacts proportionally to the frequency deviation. According to the TSO regulation, 50% of the contracted volume must be activated within 15 seconds and 100% within 30 seconds.

- **Automatic Frequency Restoration Process (aFRR)**: The primary control can rebalance power and stabilise the frequency, but it does not restore the grid frequency to its nominal frequency. Moreover, the contribution of control blocks in the primary control in the interconnected system leads to the deviation of power interchanges between individual control blocks from the scheduled values. Therefore, the activation of aFRR is required to cancel the steady-state frequency error and restore the system frequency to its nominal value of 50 Hz. Also, the function of aFRR is to drive the power flows with adjacent control areas back to their scheduled values, thus ensuring that the full reserve of activated FCR will be available again. Based on the TSO regulation, the aFRR provider must deliver the contracted volume within 30 seconds and be able to supply this reserve for at least 7.5 consecutive minutes.

- **Frequency restoration via manual activation (mFRR)**: mFRR is manually activated at the TSOs request in the event of a substantial significant or systematic imbalance and significant congestion that cannot be corrected by FCR or aFRR. mFRR is activated to schedule the output levels of online generators and the interarea power flows. mFRR must be fully available within 12.5 minutes.

Ancillary services refer to a series of services that help the TSOs maintain a secure and stable operation of the power system. The Belgian TSO (Elia)

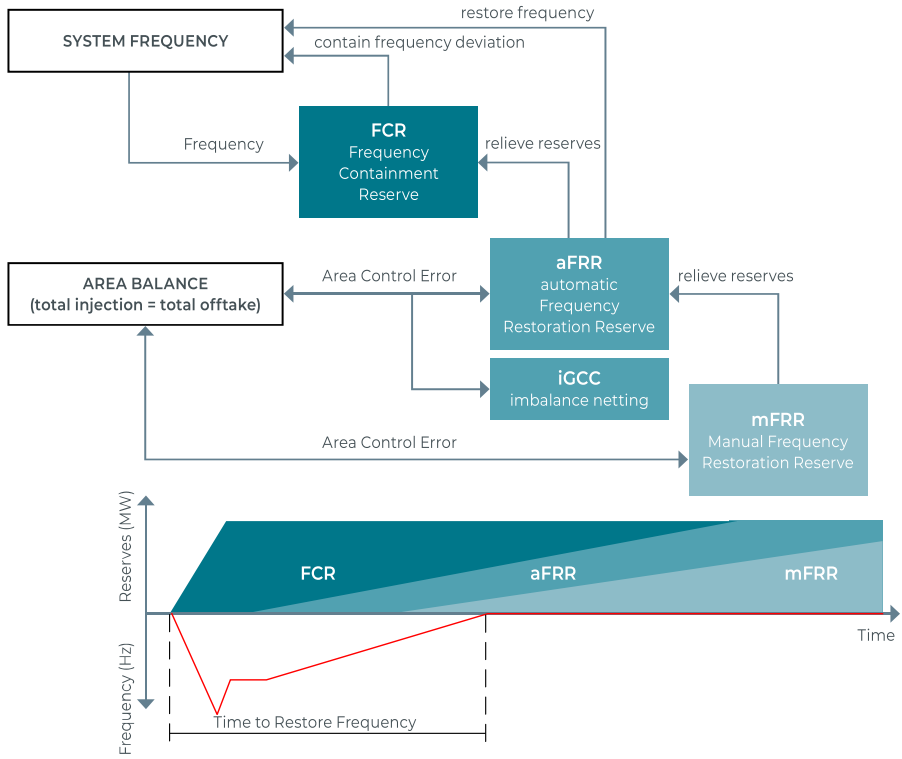

Figure 1.5: Activation process of Elia's reserve capacity [30].

arranged a balancing market to utilise the flexibility offered by Balancing Service Providers (BSPs) to maintain the balance on the Belgian grid in real-time. BSPs can participate in FCR, aFRR or mFRR, depending on the flexibility of their systems. Elia has developed different ancillary products to exploit the wide range of potential flexibility sources. The diagram in Fig. 1.6 illustrates the time horizon of the ancillary market mechanisms to support the grid. In this mechanism, the BSPs must nominate an energy portfolio one day in advance (day-ahead) that guarantees the power equilibrium in the coming day. Market parties and system operators use forecast tools to anticipate the system variations with the highest possible accuracy on a day-ahead and intraday basis. Therefore, they can schedule their portfolio, manage their operations, and cope with the uncertainties in the demand and supply. By moving further, closer to real-time, intraday and real-time flexibility will be used to solve possible imbalances in the system. Therefore, the market must have adequate flexibility to offset forecast errors in electricity generation and consumption, particularly with regard to renewable energy sources.

Figure 1.6: Time horizon of ancillary market mechanisms [30].

1.5 Objectives and challenges

The transition towards low carbon energy systems with the increasing share of intermittent renewable energy has led to a paradigm shift in the power sector. In these circumstances, the active participation of large electricity consumers in the ancillary market becomes more important in order to provide flexibility to the power system and to stabilise the future grid. The flexibility provided by the frequency adaptive electricity consumers will also allow the power system to accommodate the more stochastically fluctuating power generation of renewable energy sources. In this context, several energy-intensive industries have the potential to engage in demand response programmes. However, the demand response operation of industrial loads has not been taken forward swiftly due to a number of uncertainties, i.e., of economical, technical or regulatory nature. Therefore, the following challenges should be addressed to ensure the secure and cost-efficient contribution of chemical processes in the ancillary market:

Technical feasibility
Classically, chemical processes are planned to run continuously at their nominal capacities with predetermined setpoints, or their operating point is only varied slowly based on product demand. The electrical flexible operation of chemical plants as BSPs or FSPs is usually not foreseen in the planning phase of a plant. Moreover, the operation of a process is subject to strict constraints, i.e., with regards to safety and product quality. Therefore, the demand response operation of chemical processes without extending the flexibility of the process can violate these restrictions and lead to severe economic losses or threaten operational safety. The ramp rate of the process, i.e., rate of change in power demand, is restricted to its nonlinear dynamics and operational constraints, e.g., safety, product quality and wear. Therefore, applying fast ramp rates and fulfilling the grid requirements is not straightforward. Therefore, a suitable control architecture is required for the flexible operation of chemical processes to satisfy grid services requirements while maintaining process efficiency.

Economic viability
The economic performance of chemical plants is questioned under flexible operation dealing with grid and market uncertainties. For active participation of the chemical processes in the ancillary market, careful analysis is required to ensure the economic viability of the ancillary service provision. The lack of a proper operating/investment decision-making framework in current market structures is one of the most significant barriers to the demand response operation of industrial loads. Therefore, a decision-making algorithm is needed to maximise the economic performance of chemical processes in the

presence of uncertainties in the energy and ancillary market.

Based on the above, the research objectives of this PhD thesis are:

1. to analyse the technical feasibility and economic viability of the flexible operation of a chemical CCU process supplied with wind energy
2. to develop the necessary tools to operate such a system flexibly, i.e., models, control algorithms and decision support systems

1.6 Thesis outline

The following chapters of the thesis contain the research results of this PhD. Combined, these results answer the two objectives defined above. Fig. 1.7 graphically shows the coherence of the different chapters and helps to understand how the topics are related.

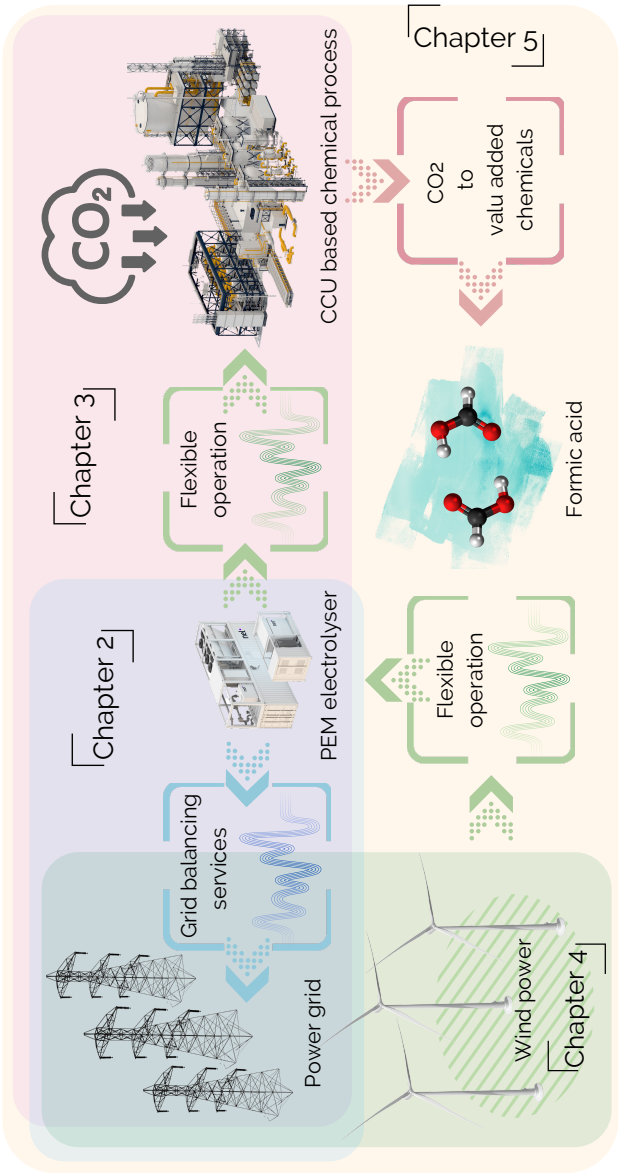

Figure 1.7: Overview of the chapters in this dissertation.

Chapter 2

Chapter 2 focuses on the flexible operation of a large PEM electrolyser connected to the grid. Electrolysers are energy-intensive systems with favourable dynamic properties, making them particularly suitable to provide frequency support services. The results presented in chapter 2 are published in [54].

Chapter 3

Electrolysis provides an essential source of hydrogen in many CCU based chemical processes. Hence, chapter 3 expands the topic of chapter 2 into a study on the flexible operation of an entire chemical process for the synthesis of formic acid. Next to the flexible operation of an electrolyser, this study adds flexible operation of multiple compression stages and the reactor itself. The results presented in chapter 3 are published in [55].

Chapter 4

In chapters 2 and 3 the electrolyser and chemical process are connected to the grid. A renewable energy source is not yet involved in the analysis. However, the flexible operation of wind turbines was also a topic of investigation throughout the PhD work. Several control methodologies to control the torque, pitch and power were developed in the research group to allow for this flexible operation. Also, the impact of these control methodologies on the structural loads and pitching system were analysed. Chapter 4 presents the portion of this research for which the author is the main investigator, which is published in [56]. Next to this, the author contributed considerably to the related study published in [57], which is not reported in this PhD manuscript.

Chapter 5

Chapters 2, 3 and 4 respectively study the flexible operation of electrolysers, chemical processes and wind turbines. These topics are brought together in chapter 5 in which a novel flexible operation strategy is presented for a chemical CCU process supplied with wind energy. Chapter 5 fuses the research presented in the previous chapters and realizes the general research objectives of the PhD.

Chapter 6

Chapter 6 presents a summary of the research outcomes of this thesis and concludes this dissertation. The potential future research topics and further possible flexibility challenges are consulted regarding chemical processes in combination with wind energy.

1.7 Scientific publications by the author

The following list gives a complete overview of all articles published in the frame of this PhD research.

1. **Samani, A. E.**, D'Amicis, A., De Kooning, J. D. M., Bozalakov, D., Silva, P. and Vandevelde, L. (2020), Grid balancing with a large-scale electrolyser providing primary reserve. *IET Renewable Power Generation*, 14: 3070-3078, DOI: 10.1049/iet-rpg.2020.0453.

2. **Samani, A. E.**, De Kooning, J. D. M., Kayedpour, N., Singh, N., and Vandevelde, L. (2020). The Impact of Pitch-To-Stall and Pitch-To-Feather Control on the Structural Loads and the Pitch Mechanism of a Wind Turbine. *Energies*, DOI: 10.3390/en13174503.

3. **Samani, A. E.**, De Kooning, J. D. M., Urbina Blanco, C. A., and Vandevelde, L. (2022). Flexible operation strategy for formic acid synthesis providing frequency containment reserve in smart grids, *International Journal of Electrical Power & Energy Systems*, DOI: 10.1016/j.ijepes.2022.107969.

4. **Samani, A. E.**, Kayedpour, N., Kayedpour, F., De Kooning, J. D. M., Crevecoeur, G., and Vandevelde, L. An optimal cooperative strategy for flexible operation of a CCU process with wind energy (Under review for IEEE Transactions on Sustainable Energy).

5. Kayedpour, N., **Samani, A. E.**, De Kooning, J. D. M., Vandevelde, L., and Crevecoeur, G. (2021). Model Predictive Control with a Cascaded Hammerstein Neural Network of a Wind Turbine Providing Frequency Containment Reserve. *IEEE Transactions on Energy Conversion*, *Early access*, DOI: 10.1109/TEC.2021.3093010.

6. De Kooning, J. D. M., **Samani, A. E.**, De Zutter, S., De Maeyer, J., and Vandevelde, L. (2021). Techno-economic optimisation of small wind turbines using co-design on a parametrised model. *Sustainable Energy Technologies and Assessments*, 45, DOI: 10.1016/j.seta.2021.101165.

7. Asiaban, S., Kayedpour, N., **Samani, A. E.**, Bozalakov, D., De Kooning, J. D. M., Crevecoeur, G., and Vandevelde, L. (2021). Wind and Solar Intermittency and the Associated Integration Challenges: A Comprehensive Review Including the Status in the Belgian Power System. *Energies*, DOI: 10.3390/en14092630.

8. **Samani, A. E.**, Kayedpour, N., De Kooning, J. D. M., and Vandevelde, L. (2019, November). Performance and Structural Load Analysis

of Small and Medium Wind Turbines Operating with Active Speed Stall Control versus Pitch Control. In *2019 IEEE 2nd International Conference on Renewable Energy and Power Engineering (REPE)*, Toronto, Canada (Reviewed conference proceeding). DOI: 10.1109/REPE48501.2019.9025130.

9. **Samani, A. E.**, D'Amicis, A., De Kooning, J. D. M., Silva, P., and Vandevelde, L. (2019, October). Grid balancing with a large-scale electrolyser providing primary reserve. In *8th Renewable Power Generation Conference (RPG 2019)*, Shanghai, China (Reviewed conference proceeding). DOI: 10.1049/cp.2019.0542.

10. Kayedpour, N., **Samani, A. E.**, De Kooning, J. D. M., Vandevelde, L., and Crevecoeur, G. (2019, November). A data-driven approach using deep learning time series prediction for forecasting power system variables. In *2019 IEEE 2nd International Conference on Renewable Energy and Power Engineering (REPE)*, Toronto, Canada (Reviewed conference proceeding). DOI: 10.1109/REPE48501.2019.9025159.

11. Kayedpour, N., **Samani, A. E.**, De Kooning, J. D. M., Vandevelde, L., and Crevecoeur, G. (2019, October). Robust approximation models for predictive control of a variable pitch wind power drivetrain. In *8th Renewable Power Generation Conference (RPG 2019)*, Shanghai, China (Reviewed conference proceeding). DOI: 10.1049/cp.2019.0591.

12. Kayedpour, N., **Samani, A. E.**, Singh, N., De Kooning, J. D. M., Vandevelde, L., and Crevecoeur, G. (2020). An Optimal Control Strategy to Maximize Power in an Offshore Wind Farm by Reducing Wake Interaction. In *16th EAWE PhD seminar*, Porto, Portugal (Reviewed conference proceeding).

13. De Zutter, S., De Kooning, J. D. M., **Samani, A. E.**, Baetens, J., and Vandevelde, L. (2017, August). Modeling of active yaw systems for small and medium wind turbines. In *2017 52nd International Universities Power Engineering Conference (UPEC)*, Heraklion, Greece (Reviewed conference proceeding). DOI: 10.1109/UPEC.2017.8231885.

Bibliography

[1] "Renewable energy market update 2021." URL: https://www.iea.org/reports/renewable-energy-market-update-2021.

[2] "Global energy review 2021." URL: https://www.iea.org/reports/global-energy-review-2021/renewables.

[3] "Communication from the Commission to the European Parliament, the Council, the European Economic and Social Committee and the Committee of the Regions. delivering the EU's 2030 climate target on the way to climate neutrality." URL: https://eur-lex.europa.eu/legal-content/EN/TXT/?uri=CELEX%3A52021DC0550.

[4] J. Cochran, M. Miller, O. Zinaman, M. Milligan, D. Arent, B. Palmintier, M. O'Malley, S. Mueller, E. Lannoye, A. Tuohy, *et al.*, "Flexibility in 21st century power systems," tech. rep., National Renewable Energy Lab.(NREL), Golden, CO (United States), 2014. DOI: 10.2172/1130630.

[5] P. Denholm and M. Hand, "Grid flexibility and storage required to achieve very high penetration of variable renewable electricity," *Energy Policy*, vol. 39, no. 3, pp. 1817–1830, 2011. DOI: 10.1016/j.enpol.2011.01.019.

[6] P. Denholm, T. Mai, R. W. Kenyon, B. Kroposki, and M. O'Malley, "Inertia and the power grid: A guide without the spin," tech. rep., National Renewable Energy Lab.(NREL), Golden, CO (United States), 2020. DOI: 10.2172/1659820.

[7] K. T. Møller, T. R. Jensen, E. Akiba, and H.-w. Li, "Hydrogen-A sustainable energy carrier," *Progress in Natural Science: Materials International*, vol. 27, no. 1, pp. 34–40, 2017. DOI: 10.1016/j.pnsc.2016.12.014.

[8] B. Dursun and B. Alboyaci, "The contribution of wind-hydro pumped storage systems in meeting turkey's electric energy demand," *Renewable and Sustainable Energy Reviews*, vol. 14, no. 7, pp. 1979–1988, 2010. DOI: 10.1016/j.rser.2010.03.030.

[9] M. K. Chang, J. D. Eichman, F. Mueller, and S. Samuelsen, "Buffering intermittent renewable power with hydroelectric generation: A case study in california," *Applied energy*, vol. 112, pp. 1–11, 2013. DOI: 10.1016/j.apenergy.2013.04.092.

[10] Z. Ming, Z. Kun, and L. Daoxin, "Overall review of pumped-hydro energy storage in china: Status quo, operation mechanism and policy barriers," *Renewable and Sustainable Energy Reviews*, vol. 17, pp. 35–43, 2013. DOI: 10.1016/j.rser.2012.05.024.

[11] F. Díaz-González, A. Sumper, O. Gomis-Bellmunt, and R. Villafáfila-Robles, "A review of energy storage technologies for wind power applications," *Renewable and sustainable energy reviews*, vol. 16, no. 4, pp. 2154–2171, 2012. DOI: 10.1016/j.rser.2012.01.029.

[12] K. M. Tan, T. S. Babu, V. K. Ramachandaramurthy, P. Kasinathan, S. G. Solanki, and S. K. Raveendran, "Empowering smart grid: A comprehensive review of energy storage technology and application with renewable energy integration," *Journal of Energy Storage*, vol. 39, p. 102591, 2021. DOI: 10.1016/j.est.2021.102591.

[13] J. R. Miller and P. Simon, "Electrochemical capacitors for energy management," *Science Magazine*, vol. 321, no. 5889, pp. 651–652, 2008. DOI: 10.1126/science.1158736.

[14] P. G. Bruce, S. A. Freunberger, L. J. Hardwick, and J.-M. Tarascon, "Li–o 2 and li–s batteries with high energy storage," *Nature materials*, vol. 11, no. 1, pp. 19–29, 2012. DOI: 10.1038/nmat3191.

[15] M. R. Lukatskaya, B. Dunn, and Y. Gogotsi, "Multidimensional materials and device architectures for future hybrid energy storage," *Nature communications*, vol. 7, no. 1, pp. 1–13, 2016. DOI: 10.1038/ncomms12647.

[16] N. Xu, X. Li, X. Zhao, J. B. Goodenough, and K. Huang, "A novel solid oxide redox flow battery for grid energy storage," *Energy & Environmental Science*, vol. 4, no. 12, pp. 4942–4946, 2011. DOI: 10.1039/C1EE02489B.

[17] M. Yue, Q. Zheng, F. Xing, H. Zhang, X. Li, and X. Ma, "Flow field design and optimization of high power density vanadium flow batteries: A novel trapezoid flow battery," *AIChE Journal*, vol. 64, no. 2, pp. 782–795, 2018. DOI: 10.1002/aic.15959.

[18] J. B. Von Colbe, J.-R. Ares, J. Barale, M. Baricco, C. Buckley, G. Capurso, N. Gallandat, D. M. Grant, M. N. Guzik, I. Jacob, *et al.*, "Application of hydrides in hydrogen storage and compression: Achievements, outlook and perspectives," *international journal of hydrogen energy*, vol. 44, no. 15, pp. 7780–7808, 2019. DOI: 10.1016/j.ijhydene.2019.01.104.

[19] M. Jehan and D. Fruchart, "Mcphy-energy's proposal for solid state hydrogen storage materials and systems," *Journal of alloys and compounds*, vol. 580, pp. S343–S348, 2013. DOI: 10.1016/j.jallcom.2013.03.266.

[20] W. Liu, C. Webb, and E. M. Gray, "Review of hydrogen storage in ab3 alloys targeting stationary fuel cell applications," *International Journal of Hydrogen Energy*, vol. 41, no. 5, pp. 3485–3507, 2016. DOI: 10.1016/j.ijhydene.2015.12.054.

[21] T. Lohner, A. D'Aveni, Z. Dehouche, and P. Johnson, "Integration of large-scale hydrogen storages in a low-carbon electricity generation system,"

International journal of hydrogen energy, vol. 38, no. 34, pp. 14638–14653, 2013. DOI: 10.1016/j.ijhydene.2013.08.130.

[22] A. T. Thattai, B. Wittebrood, T. Woudstra, J. Geerlings, and P. Aravind, "Thermodynamic system studies for a natural gas combined cycle (ngcc) plant with co2 capture and hydrogen storage with metal hydrides," *Energy Procedia*, vol. 63, pp. 1996–2007, 2014. DOI: 10.1016/j.egypro.2014.11.214.

[23] "Renewables 2021: Analysis and forecast to 2026." URL: https://www.iea.org/reports/renewables-2021.

[24] L. Bird, D. Lew, M. Milligan, E. M. Carlini, A. Estanqueiro, D. Flynn, E. Gomez-Lazaro, H. Holttinen, N. Menemenlis, A. Orths, *et al.*, "Wind and solar energy curtailment: A review of international experience," *Renewable and Sustainable Energy Reviews*, vol. 65, pp. 577–586, 2016. DOI: 10.1016/j.rser.2016.06.082.

[25] H. K. Jacobsen and S. T. Schröder, "Curtailment of renewable generation: Economic optimality and incentives," *Energy Policy*, vol. 49, pp. 663–675, 2012. DOI: 10.1016/j.enpol.2012.07.004.

[26] A. Fernández-Guillamón, E. Gómez-Lázaro, E. Muljadi, and Á. Molina-García, "Power systems with high renewable energy sources: A review of inertia and frequency control strategies over time," *Renewable and Sustainable Energy Reviews*, vol. 115, p. 109369, 2019. DOI: 10.1016/j.rser.2019.109369.

[27] X. Tang, M. Yin, C. Shen, Y. Xu, Z. Y. Dong, and Y. Zou, "Active power control of wind turbine generators via coordinated rotor speed and pitch angle regulation," *IEEE Transactions on Sustainable Energy*, vol. 10, no. 2, pp. 822–832, 2018. DOI: 10.1109/TSTE.2018.2848923.

[28] H. Wang, Z. Chen, and Q. Jiang, "Optimal control method for wind farm to support temporary primary frequency control with minimised wind energy cost," *IET Renewable Power Generation*, vol. 9, no. 4, pp. 350–359, 2015. DOI: 10.1049/iet-rpg.2014.0045.

[29] Z. Li, Z. Cheng, J. Si, S. Zhang, L. Dong, S. Li, and Y. Gao, "Adaptive power point tracking control of pv system for primary frequency regulation of ac microgrid with high pv integration," *IEEE Transactions on Power Systems*, 2021.

[30] "Adequacy and flexibility study for belgium." URL: https://www.elia.be/en/electricity-market-and-system/adequacy/adequacy-studies.

[31] M. Paulus and F. Borggrefe, "The potential of demand-side management in energy-intensive industries for electricity markets in germany," *Applied Energy*, vol. 88, no. 2, pp. 432–441, 2011. DOI: 10.1016/j.apenergy.2010.03.017.

[32] M. Manana, A. Zobaa, A. Vaccaro, A. Arroyo, R. Martinez, P. Castro, A. Laso, and S. Bustamante, "Increase of capacity in electric arc-furnace steel mill factories by means of a demand-side management strategy and ampacity techniques," *International Journal of Electrical Power & Energy Systems*, vol. 124, p. 106337, 2021. DOI: 10.1016/j.ijepes.2020.106337.

[33] M. R. Starke, B. J. Kirby, J. D. Kueck, D. Todd, M. Caulfield, and B. Helms, "Providing reliability services through demand response: A prelimnary evaluation of the demand response capabilities of alcoa inc.," tech. rep., Oak Ridge National Lab.(ORNL), Oak Ridge, TN (United States), 2009. DOI: 10.2172/948544.

[34] C. Tsay, A. Kumar, J. Flores-Cerrillo, and M. Baldea, "Optimal demand response scheduling of an industrial air separation unit using data-driven dynamic models," *Computers & Chemical Engineering*, vol. 126, pp. 22–34, 2019. DOI: 10.1016/j.compchemeng.2019.03.022.

[35] A. Caspari, C. Tsay, A. Mhamdi, M. Baldea, and A. Mitsos, "The integration of scheduling and control: Top-down vs. bottom-up," *Journal of Process Control*, vol. 91, pp. 50–62, 2020. DOI: 10.1016/j.jprocont.2020.05.008.

[36] D. L. Summerbell, D. Khripko, C. Barlow, and J. Hesselbach, "Cost and carbon reductions from industrial demand-side management: Study of potential savings at a cement plant," *Applied Energy*, vol. 197, pp. 100–113, 2017. DOI: 10.1016/j.apenergy.2017.03.083.

[37] X. Xu, M. Abeysekera, C. Gutschi, M. Qadrdan, K. Rittmannsberger, W. Markus, J. Wu, and N. Jenkins, "Quantifying flexibility of industrial steam systems for ancillary services: a case study of an integrated pulp and paper mill," *IET Energy Systems Integration*, vol. 2, no. 2, pp. 124–132, 2020. DOI: 10.1049/iet-esi.2019.0082.

[38] K. Seo, T. F. Edgar, and M. Baldea, "Optimal demand response operation of electric boosting glass furnaces," *Applied Energy*, vol. 269, p. 115077, 2020. DOI: 10.1016/j.apenergy.2020.115077.

[39] S. Zhao, I. E. Grossmann, and L. Tang, "Integrated scheduling of rolling sector in steel production with consideration of energy consumption un-

der time-of-use electricity prices," *Computers & Chemical Engineering*, vol. 111, pp. 55–65, 2018. DOI: 10.1016/j.compchemeng.2017.12.018.

[40] X. Zhang, G. Hug, Z. Kolter, and I. Harjunkoski, "Industrial demand response by steel plants with spinning reserve provision," in *2015 North American Power Symposium (NAPS)*, pp. 1–6, IEEE, 2015. DOI: 10.1109/NAPS.2015.7335115.

[41] Y. Cao, C. L. Swartz, M. Baldea, and S. Blouin, "Optimization-based assessment of design limitations to air separation plant agility in demand response scenarios," *Journal of Process Control*, vol. 33, pp. 37–48, 2015. DOI: 10.1016/j.jprocont.2015.05.002.

[42] R. Adamson, M. Hobbs, A. Silcock, and M. J. Willis, "Integrated real-time production scheduling of a multiple cryogenic air separation unit and compressor plant," *Computers & Chemical Engineering*, vol. 104, pp. 25–37, 2017. DOI: 10.1016/j.compchemeng.2017.04.001.

[43] B. Hayes, I. Melatti, T. Mancini, M. Prodanovic, and E. Tronci, "Residential demand management using individualized demand aware price policies," *IEEE Transactions on Smart Grid*, vol. 8, no. 3, pp. 1284–1294, 2016. DOI: 10.1109/TSG.2016.2596790.

[44] M. Muratori and G. Rizzoni, "Residential demand response: Dynamic energy management and time-varying electricity pricing," *IEEE Transactions on Power systems*, vol. 31, no. 2, pp. 1108–1117, 2015. DOI: 10.1109/TPWRS.2015.2414880.

[45] D. Fabozzi, N. F. Thornhill, and B. C. Pal, "Frequency restoration reserve control scheme with participation of industrial loads," in *2013 IEEE Conference*, (Grenoble, France), 2013. DOI: 10.1109/PTC.2013.6652104.

[46] K. Arnold and T. Janöen, "Demand side management in industry : necessary for a sustainable energy system or a backward step in terms of improving efficiency?," in *Going beyond energy efficiency to deliver savings, competitiveness and a circular economy : ECEEE Industrial Summer Study proceedings ; 12-14 September 2016, Die Kalkscheune, Berlin, Germany*, (Stockholm), pp. 339 – 350, Europ. Council for an Energy Efficient Economy, 2018. URL: https://nbn-resolving.org/urn:nbn:de:bsz:wup4-opus-69405.

[47] M. Cheng, J. Wu, S. J. Galsworthy, C. E. Ugalde-Loo, N. Gargov, W. W. Hung, and N. Jenkins, "Power system frequency response from the control of bitumen tanks," *IEEE Transactions on Power Systems*, vol. 31, no. 3, pp. 1769–1778, 2015. DOI: 10.1109/TPWRS.2015.2440336.

[48] X. Zhang, G. Hug, J. Z. Kolter, and I. Harjunkoski, "Demand response of ancillary service from industrial loads coordinated with energy storage," *IEEE Transactions on Power Systems*, vol. 33, no. 1, pp. 951–961, 2017. DOI: 10.1109/TPWRS.2017.2704524.

[49] T. K. Chau, S. S. Yu, T. Fernando, and H. H.-C. Iu, "Demand-side regulation provision from industrial loads integrated with solar pv panels and energy storage system for ancillary services," *IEEE Transactions on Industrial Informatics*, vol. 14, no. 11, pp. 5038–5049, 2017. DOI: 10.1109/TII.2017.2782244.

[50] M. Cheng, J. Wu, S. J. Galsworthy, N. Gargov, W. H. Hung, and Y. Zhou, "Performance of industrial melting pots in the provision of dynamic frequency response in the great britain power system," *Applied Energy*, vol. 201, pp. 245–256, 2017. DOI: 10.1016/j.apenergy.2016.12.014.

[51] D. Todd, M. Caufield, B. Helms, A. P. Generating, I. M. Starke, B. Kirby, and J. Kueck, "Providing reliability services through demand response: A preliminary evaluation of the demand response capabilities of alcoa inc," *ORNL/TM*, vol. 233, 2008. DOI: 10.2172/948544.

[52] X. Zhang and G. Hug, "Optimal regulation provision by aluminum smelters," in *2014 IEEE PES General Meeting| Conference & Exposition*, pp. 1–5, IEEE, 2014. DOI: 10.1109/PESGM.2014.6939343.

[53] A. W. Dowling and V. M. Zavala, "Economic opportunities for industrial systems from frequency regulation markets," *Computers & Chemical Engineering*, vol. 114, pp. 254–264, 2018. DOI: 10.1016/j.compchemeng.2017.09.018.

[54] A. E. Samani, A. D'Amicis, J. D. M. De Kooning, D. Bozalakov, P. Silva, and L. Vandevelde, "Grid balancing with a large-scale electrolyser providing primary reserve," *IET Renewable Power Generation*, vol. 14, no. 16, pp. 3070–3078, 2020. DOI: 10.1049/iet-rpg.2020.0453.

[55] A. E. Samani, J. D. M. De Kooning, C. A. Urbina Blanco, and L. Vandevelde, "Flexible operation strategy for formic acid synthesis providing frequency containment reserve in smart grids," *International Journal of Electrical Power & Energy Systems*, vol. 139, p. 107969, 2022. DOI: 10.1016/j.ijepes.2022.107969.

[56] A. E. Samani, J. D. De Kooning, N. Kayedpour, N. Singh, and L. Vandevelde, "The impact of pitch-to-stall and pitch-to-feather control on the structural loads and the pitch mechanism of a wind turbine," *Energies*, vol. 13, no. 17, p. 4503, 2020.

[57] N. Kayedpour, A. E. Samani, J. D. M. De Kooning, L. Vandevelde, and G. Crevecoeur, "Model predictive control with a cascaded hammerstein neural network of a wind turbine providing frequency containment reserve," *IEEE Transactions on Energy Conversion*, 2021. DOI: 10.1109/TEC.2021.3093010.

Chapter 2

Opportunities of Power-to-Gas Technology for Offering Flexibility to the Grid

As the integration of renewable energy sources is becoming increasingly important to meet the net-zero emissions target, novel energy solutions are needed to compensate for the variability of renewable power generation, e.g., wind and solar photovoltaics, and offset the supply and demand mismatches. In this context, power-to-gas technology can provide flexibility for the grid by the direct conversion of excess renewable power generation into hydrogen through Polymer Electrolyte Membrane (PEM) electrolysis. The generated hydrogen can be blended into the natural gas network to make a more 'green' natural gas mix for heating, electricity and mobility applications. Therefore, injecting hydrogen as a green energy vector into existing gas infrastructure can boost or even replace natural gas, mitigating greenhouse gas emissions. Furthermore, it can offer flexibility to the grid by utilising surplus renewable electricity.

This chapter studies the technical requirements for primary reserve provision with a large hydrogen PEM stack electrolyser of 25 MW. A dynamic study is performed to analyse the technical capability of providing primary reserve with this system. A techno-economic model is suggested to analyse the revenue of the Frequency Containment Reserve (FCR) provision, including capital costs, operational costs, the revenue of the generated hydrogen and oxygen products and the ancillary service income. The specific case of the Belgian transmission system is considered for inclusion of electricity prices, grid frequency changes and other technical limitations.

The contents of this chapter are published in [1, 2].

Grid Balancing with a Large-Scale Electrolyser Providing Primary Reserve

Arash E. Samani, Anna D'Amicis, Jeroen D. M. De Kooning, Dimitar Bozalakov, Paolo Silva, Lieven Vandevelde

Published in "IET Renewable Power Generation", 2020

Abstract: *As the share of renewable energy sources increases, the grid frequency becomes more unstable. Therefore, grid balancing services will become more important in the future. Dedicated devices can be installed close to the point where off-shore wind farms are connected to the transmission grid on land. There, they can be used to attenuate power variations, reduce congestion and offer grid balancing. The provision of these ancillary services can create a considerable additional economic revenue. In this study, the provision of primary reserve by means of a large hydrogen electrolyser of 25 MW is investigated for the specific case of the Belgian transmission system. The revenue of the provision of the Frequency Containment Reserve (FCR) is analysed on a techno-economic model, including capital costs, operational costs, the revenue of the generated hydrogen and oxygen products and the ancillary service income. The revenue depends strongly on the contracted power-band. Therefore, it is optimised to yield maximum revenue. The results show that providing FCR creates a considerable additional revenue. Therefore, a large electrolyser can be a good candidate to buffer excess renewable energy into green gas while simultaneously providing grid support.*

2.1 Introduction

The electric power industry is changing continuously due to a growing diversity in the energy mix. This is mainly caused by the increasing share of renewable energy sources. Global warming and climate change are the main reasons for a rapid global transition towards renewable energy generation. Furthermore, fossil fuel reserves are being depleted progressively while the demand for energy keeps increasing. Also, the Levelised Cost Of Energy (LCOE) of renewables has decreased drastically to a level where it is cheaper than classical energy sources, e.g., natural gas or nuclear energy. Clearly, a more diverse energy mix is needed, which requires a change in the structure and operation of the conventional power system.

Besides the positive aspects of increasing the share of renewables in the energy mix, the technical feasibility of integrating variable renewable sources should be considered. Due to the intermittent nature of these sources, they bring

more fluctuations and uncertainty into the grid and complicate its operational management. However, as wind and solar power are the fastest growing sources of electricity, their effects must be taken into account [3, 4]. For example, the inertial response of the grid on power imbalances is determined by all rotating masses of the turbo-generators in the system. However, renewable power sources such as wind turbines and photovoltaics do not possess directly-coupled rotating inertia, which reduces the robustness and stability of the power system [5–7].

Different solutions such as Energy Storage Systems (ESS), Demand-Side Response (DSR), and curtailment of variable renewable energy sources have been suggested to manage the energy flows and increase the flexibility of the grid [8–11]. ESS with a certain degree of flexibility can be used to charge, hold and discharge the electricity according to the condition of the grid. Storage technologies with different characteristics have been developed to provide electrical storage for a wide range of power, i.e., Pumped Hydroelectric Storage (PHS), batteries, flywheels and hydrogen technologies. Pumped hydroelectric storage has a long discharge time and a large power storage capacity is counted as utility-scale energy storage. Though pumped hydroelectric energy storage is well suited for bulk power management, specific geographic conditions are required, i.e., geologic and hydrologic constraints. Batteries with a fast response have the potential advantage to be used for frequency regulation [12]. However, this technology, with its low energy density (energy per unit volume), is not able to store a large amount of energy. Therefore, for a grid-scale battery system, a large number of cells is required to store the excess electricity production. Flywheel energy storage systems can provide immediate active power to support the grid. Their main advantage is the fast response time, which makes them suitable for frequency regulation. However, compared to other storage systems, they have a shorter discharge time and power storage, i.e., up to 1 MW for less than an hour. hydrogen storage systems have higher performance in terms of energy storage, i.e., 1 GWh up to 1 TWh, and a discharge time compared to the aforementioned storage systems. Therefore, hydrogen, as an energy carrier, can be one of the possible options for voltage and frequency stabilisation [13–15]. Despite the advantages of hydrogen storage systems, the direct conversion of electrical energy to hydrogen is not economically viable due to the high electrolyser costs and relatively low hydrogen price. Nevertheless, hydrogen storage systems can play a fundamental role where a high amount of renewable energy is available, and more grid support is required.

Studies show that electricity-based hydrogen plays a key role in reducing greenhouse gas (GHG) emissions in the future of the European Union (EU). hydrogen, as a clean vector, is used in fuel cell based electric vehicles which leads to a de-carbonisation of the transport sector. Moreover, hydrogen can contribute in the energy market as a provider of flexibility [16, 17]. The results

of a recent techno-economic assessment of the hydrogen production mix for road transport explains that the electrolyser could act as a key technology to fulfil its hydrogen demand in the medium and long term [16]. It is found in [17] that the most important techno-economic properties of electrolysers are their ability to operate flexibly and the efficient conversion of electricity into hydrogen. These studies show that electrolysers have a positive effect on frequency stability, as electrolysers are able to respond faster to frequency deviations than conventional generators [18].

Large-scale electrolysers are an energy-intensive technology that can be operated to support the grid by regulating the input power based on the grid's condition, i.e., to deliver ancillary services. Therefore, additional revenue can be generated by participating in the ancillary markets. In the recent research conducted by Mohanpurkar et al., the performance of electrolyser systems in providing grid support was investigated. The dynamic response of an electrolyser participating in demand response, local voltage support, and frequency support was tested by utilising the fast response of the electrolyser, i.e., subsecond level. The results verified that electrolysers can be utilized as controllable loads without negatively impacting their lifetime. However, the economic analysis and exact economic benefits due to participating in the demand side response were not covered in [19]. Based on the findings of Allidières et al., PEM water electrolysis stacks/plants represent sufficient flexibility and reactivity to provide primary and secondary power reserves. However, it was concluded that the existing technology requires further developments to reduce efficiency losses and degraded power responses in the conditions of interest for grid services [20]. Matute et al. [21] performed a techno-economic analysis of multi-MW electrolysis plants designed to provide grid services while producing hydrogen for different end uses. The results showed that combining multi-MW electrolysers with the provision of secondary reserve in Spain is a valid option to obtain cost-competitive hydrogen for different applications. However, a sufficient hydrogen demand is required for the profitability of a hydrogen refueling station network [21].

In this article, a techno-economic analysis is performed of a 25 MW PEM electrolyser installation in Belgium, planned to provide grid services while injecting hydrogen into the natural gas pipeline. Different electrolyser operational strategies are investigated to find the optimal method of running the electrolyser, which maximises the economic return. Later, an electrolyser system, i.e., cell stack and controller, is developed to examine the controllability and reactivity of the electrolyser operating with the proposed strategy. A numerical model is developed in Matlab to assess the economic benefits of running a large-scale electrolyser with two different strategies. In the first strategy, the power consumption is varied based on the electricity price variations on the Epex Spot market. As price variations are correlated with the balance of the

grid through the supply and demand principle, this operating strategy is a form of grid balancing. In the second strategy, the economic return is maximised by providing FCR as an ancillary service. Once the optimal operating strategy is determined, an electrochemical model of the electrolyser is developed to test the system response under the most extreme variation in the grid frequency. In this article, we propose an optimal strategy for operating a large-scale electrolyser in Belgium. The main contribution are:

- Maximising the economic efficiency of a large-scale electrolyser installation
- Optimal contribution of an electrolyser in the Belgian ancillary service market
- Technical validation of the proposed strategy for providing symmetric 100 mHz frequency containment reserve
- Monitoring the response of the dynamic model to the maximum frequency variation in the year 2017
- Suggesting a generic techno-economic model which can offer useful and incentive information for the hydrogen sector to improve the economic viability of electrolysers by providing grid balancing services

This article is organised as follows: § 2.2 describes the business case and methodology. The optimisation of the electrolysers power consumption is described in § 2.2.1. § 2.2.2 explains the strategy of providing ancillary services to the grid. The electrolyser degradation and modelling is discussed in § 2.2.3. The optimisation and simulation results of each strategy are presented in § 2.3.1 and § 2.3.2. The PEM electrolysers dynamic response to the grids condition is discussed in § 2.3.3.

2.2 Methodology

Since hydrogen production through electrolysis is an energy-intensive process, the electricity price is of vital importance to the economic viability of the electrolyser. As the first business case, the electrolyser is operated to follow the variations in the electricity price. As mentioned before, these variations are linked to the grid balance through the supply and demand principle. hydrogen storage is not foreseen in the model, assuming that all the produced hydrogen can be injected into the conventional natural gas grid as long as a limit of 2% volume hydrogen is not exceeded. This limit is imposed to avoid exceeding flame temperature limits in natural gas consumers. To inject the hydrogen into

the existing natural gas pipeline, it must be compressed from 30 to 70 bar. It is assumed that the compression stages are not costly in comparison to the electrolysis. Therefore, the compression station costs are not included. However, for high-pressure applications such as mobility (pressure level up to 700 bar), the compression cost is not negligible. Injecting hydrogen in the natural gas grid reduces the CO_2 emission with 202 kg/MWh (39 kWh(HHV)/kg_{H_2}) [22]. However, the avoided emission of CO_2 does not generate substantial revenue for the hydrogen supplier. Table 2.1 gives an overview of the assumptions and the main parameters of the electrolyser.

Table 2.1: 25 MW electrolyser parameters and assumptions

25 MW PEM Electrolyser	
Capital expenditure (CAPEX)	1000 €/kW [22]
Operational cost	1% of capital cost
Nominal H_2 output	5000 Nm^3/h
Lifetime	20 years
Availability	98%
Cell stack lifetime	80000 hours
Operating hours	8760 hours/year
Substitution cell	50% of capital cost
Output pressure	30 bar
Connection cost to the power grid	500,000 €
Connection cost to the gas grid	2,250,000 €
Value of generated hydrogen	2.2 €/kg [22]
Value of generated oxygen	24.5 €/ton [23]

The second business case aims to analyse the possible profitability of using the electrolyser to provide demand-side response services. Ancillary services are essential to support the power grid stability in unbalanced situations. Moreover, participating in the ancillary market brings additional economic revenue. The ancillary services can be provided by regulating the power offtake of the electrolyser according to the grid frequency. In this economic model, the power consumption profile of the electrolyser is varied based on the frequency variation of the Belgian grid in 2017, operated by the Transmission System Operator (TSO) Elia.

The additional economic revenue of the provision of each FCR product type (two symmetrical and two asymmetrical products) will be investigated. Symmetrical FCR products are delivered within a frequency deviation of 100 or 200 mHz from the nominal 50 Hz upward or downward. Asymmetrical FCR products are provided if the frequency deviates more than 100 mHz

from nominal, either upward or downward. The power reserve offered by the electrolyser is assumed to be constant for the whole year, though the tendering process is evolving to a shorter period in the future.

The power response of alkaline and Polymer Electrolyte Membrane (PEM) electrolysers to frequency variations of the grid can be easily modulated [19]. The response time from pressurised standby to a full-load operating condition is less than three seconds. A hot-start is even faster, i.e., less than one second. However, it is not recommended to frequently switch the electrolysers entirely on and off in stand-alone systems, from a system frequency control perspective [24]. Therefore, to provide an adequate response to the grid frequency variation and to fulfil the technical specifications, the electrolyser is supposed to be continuously operated in a variable way to avoid the start-up and shut-down time required to purge the nitrogen. Thus, a minimum operating capacity of 10% (2.5 MW) is considered.

The average prices of all primary reserve products in 2017 are given in Table 2.2. The hourly electricity price in the model is equal to the Epex Spot electricity price in 2017 with an average price of 44.6 €/MWh. The same assumptions as the first business case are considered with a difference that the ancillary service is included in the optimisation algorithm as an end product. Therefore, the algorithm optimises the objective function of producing hydrogen and providing ancillary services as the end products, based on the annual average Epex Spot electricity price. The optimisation aims to find the baseload power and power reserve at which the maximum revenue is generated.

Table 2.2: Annual average price of contracted primary reserves

FCR product	Price (€/MW/h)
Symetric 100 mHz	33
Symetric 200 mHz	15
Asymmetrical	4

The investment profitability of the electrolyser for the lifespan of 20 years is calculated, taking into account both the operational and investment costs. The cash flow is kept identical for each year based on the assumption that both the hydrogen and electricity price will increase by the same amount. According to [22], the hydrogen value for on-site production will reach 2.72 €/Kg in 2030 and 3.59 €/Kg in 2050, with an average yearly increase of 2%. As the electricity prices are also expected to rise in the near future, an annual increase of 2% is assumed. However, by scheduling the power input according to the electricity price, the power consumption decreases, and the influence of the electricity price evolution is cancelled out. The electrolytic cells wear out over

time, and a replacement is required after 10 years (half of the lifetime) with a cost of 50% of the initial investment. This replacement cost is included in the cash flow of the 10th year, and it is weighed with the discounting factor. To analyse the economic feasibility of operating the electrolyser with the first strategy, the Net Present Value (NPV) is calculated as:

$$\mathrm{NPV} = \sum_{k=1}^{N} \frac{\mathrm{CF}(a)}{(1+i)^k} \tag{2.1}$$

where a is the year, $\mathrm{CF}(a)$ is the cash flow in the year a, i is the discount rate, and N is the lifetime. A discount rate of 2% is considered.

2.2.1 Power input optimisation

In the first strategy, the power input of the electrolyser is dynamically modulated to follow the electricity price. No ancillary service provision is considered. The electric power consumption of the electrolyser P_e is regulated as a linear function of the electricity price:

$$P_e = P_0 - KC_{el} \tag{2.2}$$

where K is a constant control factor that determines how strongly the power consumption reacts to price variations. The hourly electricity price is represented by the variable C_{el}. P_0 is the baseload power which can be set between a minimum power $P_{\min}$ of 2.5 MW, to avoid start-up time, and a maximum power P_{Max} of 25 MW. An optimisation algorithm maximises the annual Cash Flow (CF) of the system with an objective function in which electricity expenditure and hydrogen sale are considered as the main cost and revenue drivers, respectively. The objective function of the algorithm is defined as follows:

$$\mathrm{CF} = \sum_{t=1}^{T} \left(H_{2_v} H_{2_p}^t - P_e^t C_{el}^t \right) \Delta T \tag{2.3}$$

where P_e is specified at each time step t, (where $t = 1, 2, \ldots$ 8760 h). The amount of hydrogen produced varies on an hourly basis, as the electricity price also varies hour-by-hour. The value of hydrogen H_{2_v} is a constant, given in Table 2.1. In order to take into account the partial load efficiency of the electrolyser, the produced hydrogen is calculated in function of the relative power $R_p = {}^{P_e}/_{P_{\max}}$ by (2.4) with $0 \leq R_p \leq 1$. The equation is obtained based on experimental data provided by Hydrogenics, a manufacturer of hydrogen generation and fuel cells. Fig. 2.1 illustrate the hydrogen production as function of relative power.

$$H_{2_p} = \left(-5.9 \cdot R_P^2 + 5.07 \cdot R_P + 20.17 \right) \cdot P_e \tag{2.4}$$

where

$$R_P = \frac{P_e}{P_{\max}} \tag{2.5}$$

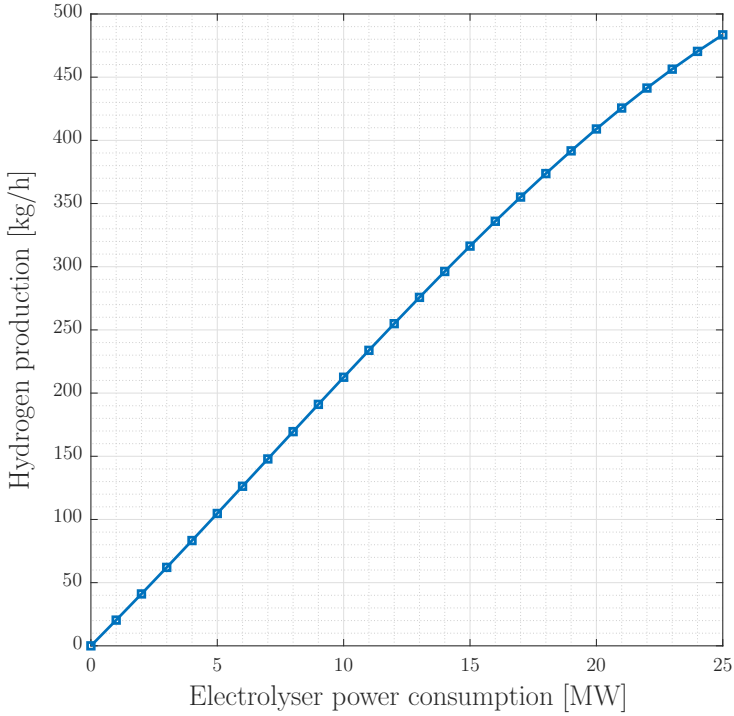

Figure 2.1: Hydrogen production as a function of electrolyser operating power.

Fig. 2.2 shows the annual cash flow of the electrolyser as a function of the baseload P_0 and the control parameter K. The annual cash flow reaches its maximum at $K = 0.29$ and $P_0 = 25$ MW (maximum baseload). Operating the electrolyser at these optimum values generates the maximum revenue for the system, considering the hydrogen production and the electricity expenditure as the main parameters in the cost function.

Operating the electrolyser at its maximum capacity with $K = 0.29$ makes the cash flow mostly positive, giving the possibility to follow the electricity price with considerable hydrogen production.

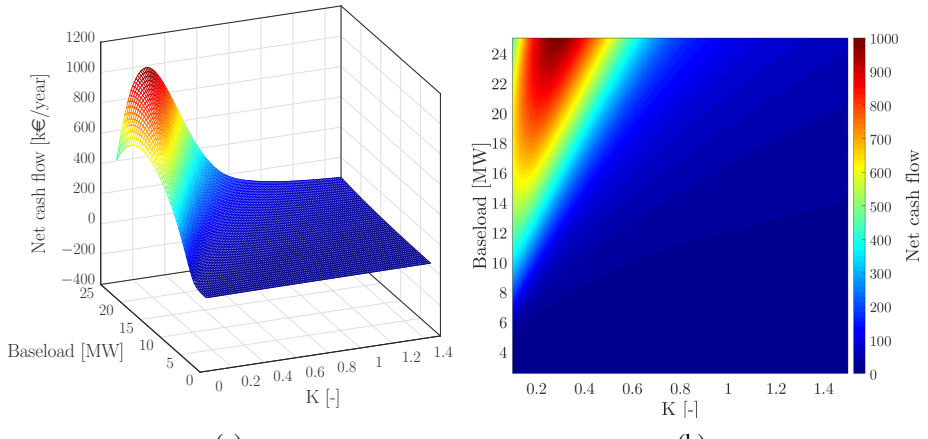

(a) (b)

Figure 2.2: Net cash flow as a function of K and P_0

2.2.2 Providing primary reserve

Symmetric 100 mHz and 200 mHz FCR product

To provide symmetrical 100 mHz and 200 mHz FCR products, the electrolyser is never operated at the maximum or minimum capacity on average, to keep the power reserve available for the positive and negative variation of the grid frequency. Therefore, the baseload power is set between 15% and 95% of the maximum capacity (3.75 MW to 23.75 MW). In theses strategies, the power input responds linearly and proportionally to the frequency variations of the grid. According to the grid operator regulations in Belgium, a deadband of 10 mHz (50 Hz±10 mHz) is considered, in which the primary control is not allowed to react, and the electrolyser operates at its baseload power. The equation used to guarantee such behaviour is:

$$P_e = \begin{cases} \alpha P_{\max} & -0.01 \leq \Delta f \leq 0.01 \\ \alpha P_{\max} + k\Delta f & \text{Otherwise} \end{cases} \tag{2.6}$$

where α is the baseload power as a percentage of the maximum capacity $P_{\max}$. This is the variable that is optimised in the algorithm. The frequency of the grid is represented by f. The parameter Δf is the frequency deviation from 50 Hz ($\Delta f = f$ - 50 Hz). k is the power-frequency characteristic of the electrolyser, defined as:

$$k = \frac{\Delta P}{\Delta f} \tag{2.7}$$

The symmetric mHz FCR product covers the frequency deviation Δf up to

100 mHz. The symmetrical product with respect to the nominal frequency gives an equal chance for downward and upward requests to stabilise the frequency. To provide a symmetrical 200 mHz product, the system reacts to a frequency deviation of 200 mHz from the nominal value. The power input reacts linearly to the frequency variation with a less steep slope compared to the 100 mHz product, because of the less restrictive activation range (48.8 to 50.2 Hz). The equation that expresses the power reserve is as follows:

$$\Delta P = \begin{cases} P_0 - P_{\min}, & \alpha \leq \dfrac{1-\min}{2} + \min \\ P_{\max} - P_0, & \alpha > \dfrac{1-\min}{2} + \min \end{cases} \tag{2.8}$$

The annual cash flow is calculated as:

$$\mathrm{CF} = \sum_{t=1}^{T} \left(H_{2_v} H_{2_p}^t + \Delta P^t \ \lambda_{fcr} \ \beta - P_e^t C_{el} \right) \Delta T \tag{2.9}$$

where λ_{fcr} is the value of the FCR product, H_2^v is the value of hydrogen (2.2 €/kg), t = 1, 2, ... 8760 h, and β is the availability of the electrolyser, i.e., 98%. H_{2_p} is the produced hydrogen which changes linearly with the power input indicated by P_e , and can be calculated using 2.4.

Asymmetrical FCR downwards

To provide the asymmetrical product FCR downwards, the system reacts to frequency deviations above 50.1 Hz. Therefore, if the grid frequency is above 50.1 Hz, the power input of the electrolyser follows the frequency as:

$$P_e = \begin{cases} \alpha P_{\max} + k\Delta f & \delta > 0 \\ \alpha P_{\max} & \text{Otherwise} \end{cases} \tag{2.10}$$

where $\Delta f = f$ - 50.1 Hz, and k is the power frequency characteristic of the electrolyser for a frequency deviation of 0.2 Hz. To keep the power reserve available, the electrolyser cannot be operated at its maximum capacity. Therefore, the baseload varies between a technical minimum of 10% and 95%. The power reserve is given by:

$$\Delta P = P_{\max} - P_0 \tag{2.11}$$

Asymmetrical FCR upwards

In this strategy, the electrolyser reacts to the grid frequency when the frequency is below 49.9 Hz. The power input varies as a function of frequency according

to:

$$P_e = \begin{cases} \alpha P_{\max} + k\Delta f & \Delta f < 0 \\ \alpha P_{\max} & \text{Otherwise} \end{cases} \tag{2.12}$$

where k is the power frequency characteristic of the electrolyser for a frequency deviation of 0.2 Hz, and $\Delta f = f$ - 49.9 Hz. The baseload varies between 15% and 100%. The power reserve is calculated as:

$$\Delta P = P_0 - P_{\min} \tag{2.13}$$

2.2.3 Electrolyser Model

When electrolysers are used as variable loads, both their static and dynamic performance must be considered. During the exploitation of the electrolyser, its static behaviour can vary depending on the accumulated operating hours, which is known as stack degradation. As will be shown, the dynamic behaviour of the PEM stack will be included in the model.

PEM stack degradation

When current is flowing through a PEM cell, a voltage drop is created. According to [25,26] this voltage drop is composed of several components. In addition, this voltage is dependent on the stack output pressure and temperature [27]. The mathematical expression for the cell voltage is given as follows:

$$E_{\text{cell}}(\text{Pa}, T) = E_{\text{th}} + E_{\text{ac,a}} + E_{\text{ac,c}} + E_{\text{ohm}} \tag{2.14}$$

where, E_{cell}, is the PEM cell voltage, Pa is the output pressure, T is the temperature, E_{th} is the thermoneutral voltage, $E_{\text{ac,a}}$ is the activation voltage of the anode, $E_{\text{ac,c}}$ is the activation voltage of the cathode and E_{ohm} is the ohmic voltage drop.

In [25–30], the necessary data to fill in (2.14) and the results are presented in Fig. 2.3 (a). These results are obtained at 25 °C, 30 bar pressure and a current density between 0 and 2.5A/mm^2. The major contributor to the PEM voltage is the thermoneutral voltage, which gives an offset of 1.483V. In practice, a typical value used for the current density is 1A/mm^2. At this point, the next more dominant component is the anode activation voltage and finally the ohmic voltage drop. By using these parameters, the resultant voltage drop is obtained to be $E_{\text{cell}}(\text{Pa}, T) = 1.8V$.

In this article, it is assumed that the lifespan of the PEM stack is 80000 hours (see Table 2.1). In literature, it was found out that the major contributor for the stack degradation is the increased ohmic resistance of the electrodes and membrane. A typical degradation rate of the stack is considered to be about

1mV per cell for 1000 hour operating at full load [31]. Therefore, the total cell voltage increase is 80 mV, i.e., 1.880 V after 80000 hours of operation. Fig. 2.3 (b) shows the curves of new and degraded cells. In this particular case, the degraded cell has 82.7 % more ohmic resistance compared to a new cell. If a constant cell voltage is applied at the cell terminals, then the current density drops from 1A/mm^2 to 0.7A/mm^2, which will result in a decreased hydrogen production. However, these results are obtained at 25 °C (298K). Usually, the PEM stack temperature is higher than that, as it reaches 80 °C (353K). Fig. 2.3 (b) also shows the curves of new and degraded cells at 80 °C. It can be seen that the degraded cell voltage decreases at higher temperature, and at 1A/mm^2 it is close to a new cell voltage. The voltage of the new cell decreases even further down to 1.72V at high temperatures for the same current density.

The conducted analysis shows that cell degradation does not have a severe impact on the PEM stack consumption and power supply performance. Indeed, with a new stack and high temperatures, the PEM power will be slightly lower and gradually increasing with the degradation. Nevertheless, the maximum power at a new stack is known, and it can be used as a contracted power for ancillary services. With the degradation of the stack, the power will increase, but the contracted power will be intact, and the electrolyser will continue to provide FCR as expected. From (2.14), it is evident that the cell voltage is dependent on pressure and temperature. The additional 'Balance of Plant' (BoP) components in the system, i.e., chillers, compressors, etc, are assumed to regulate the pressure and PEM stack temperature such that the total power can be controlled.

Dynamic model of the PEM stack

The electrochemical model of the PEM electrolyser can be described with Randles circuits connected in series. The electrolyser impedance can be calculated from the difference of the standard electrode potential E_0 and the measured output voltage e_t, which is given by (2.15):

$$Z_{el} = \frac{V_{el}}{I_{in}} \tag{2.15}$$

The voltage drop across the electrolyser is the sum of the over-voltages of the anode, the cathode and the membrane. Therefore, the equivalent impedance of a PEM is composed of the cathode and anode impedance in series with the ohmic losses in the membrane R_m [32]. The total impedance Z_{el} of the PEM cell is then given by:

$$Z_{el} = Z_a + R_m + Z_c \tag{2.16}$$

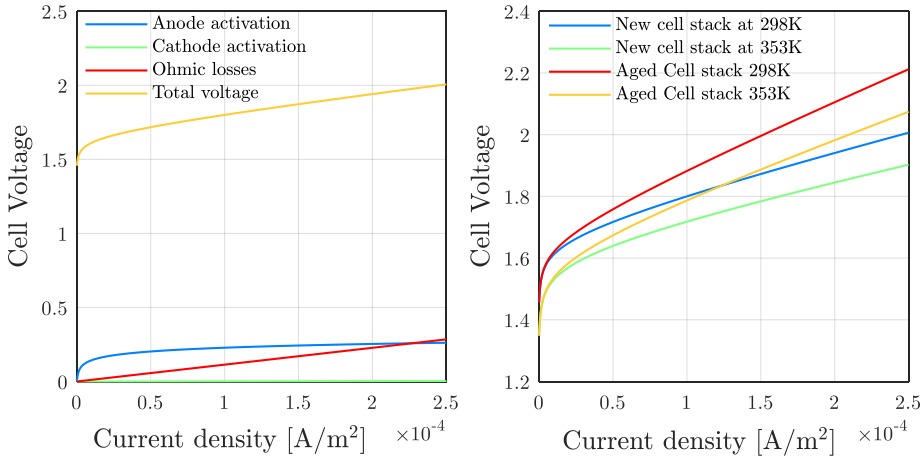

Figure 2.3: V-I characteristics of a degraded PEM cell (after 80000 operations) at 353 K (80°C) and 298 K (25°C)

As illustrated in Fig. 2.4 (a), the impedances of anode and cathode are composed of the double-layer capacitance, the resistance of the charge transfer to the electrode, and the Warburg impedance ($C_{dl} \,||\, [R_t + Z_w]$) [33, 34]. The electrical model can be simplified to the Randles-Warburg (RW) model, in which The RW cell represents the PEM impedance Z_{el} [34–36]. The equivalent electrical circuit of the RW can be used to model the impedance response of electrochemical systems such as a galvanic cell or an electrolytic cell [37]. The electrochemical model of the PEM electrolyser based on the RW cell is illustrated in Fig. 2.4 (b). The equation of the Warburg impedance Z_{wbg} in the Laplace domain is given by:

$$Z_{wbg}(s) = \frac{R_{d1}}{1 + R_{d1}C_{d1}s} + \frac{R_{d2}}{1 + R_{d2}C_{d2}s} \tag{2.17}$$

The parameters values of the RW model are estimated based on the physical characteristics of the system. The parameters in [38] are upscaled with different factors to give the desired impedance behaviour of the 25 MW PEM electrolyser. The values of these parameters are given in Table 2.3.

Up to this point the dynamic behaviour was presented under the assumption of a new stack. Nevertheless, with the degraded stack, the ohmic resistance increases, while the capacitance remains the same. This will increase the time constant of the PEM stack. However, the change will not be greater than the time constant of the BoP equipment. Therefore, even if the stack is degraded, the whole system will be able to provide a fast response which is suitable for

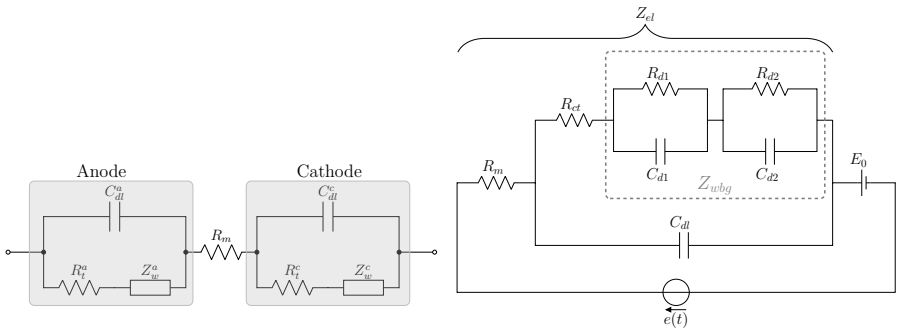

Figure 2.4: (a) Electrical model of PEM stack (b) PEM stack electrochemical model with Randles-Warburg cell

ancillary services provision.

The dynamic performance of the model based on the approximated parameters is monitored by applying an ideal current source, which is shown in Fig. 2.5. The PEM model reacts to the current changes, and the power signal settles down within one second at maximum, while the PEM voltage reaches 0.9 kV at the rated power.

Table 2.3: Randles-Warburg model parameters

R_{ct} (Ω)	C_{dl}(F)	R_{d1} (Ω)	C_{d1} (F)	R_m (Ω)	R_{d2} (Ω)	C_{d2} (F)
0.331	0.545	0.013	1080	0.381	0.121	14400

2.3 Optimisation and simulation results

2.3.1 Power input optimisation

Fig. 2.6 shows the electrolyser performance running with an power input optimisation strategy. As illustrated, the electrolyser power consumption follows the electricity price variations. Therefore, in the coldest months of the year (Oct., Nov., Dec., Jan., Feb.), when electricity prices are high, the power input is accordingly reduced to its minimum, and less hydrogen is produced. In contrast, in warmer months of the year, the input power and consequently the hydrogen production rise due to the low electricity price.

Fig. 2.7 and Fig. 2.8 give a detailed overview of the power consumption, electricity price, and produced hydrogen in the whole month of January and

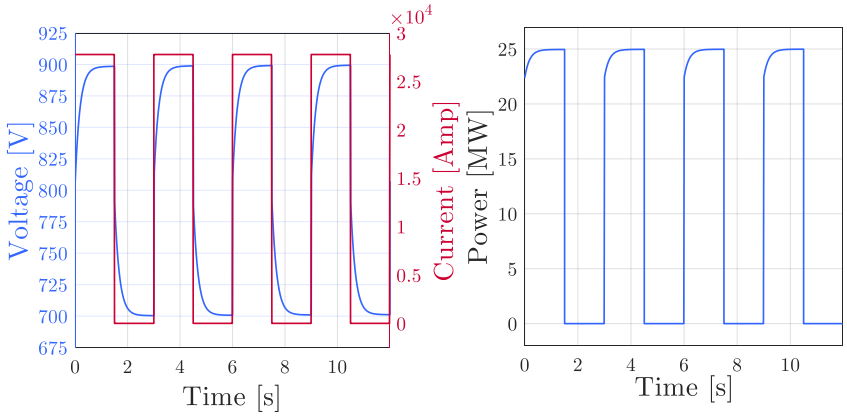

Figure 2.5: The dynamic response of the PEM stack to the ideal current source

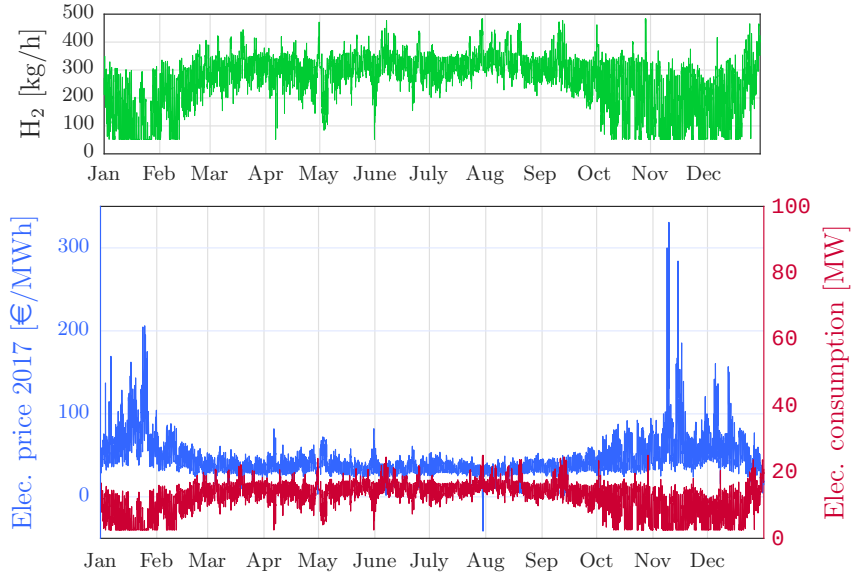

Figure 2.6: Electrolyser power consumption in one year

the first day of the year, respectively. As it can be seen, the electrolyser power consumption is scheduled based on the electricity price. This dynamical operation of the electrolyser maximises the cash flow as the cost function is minimised. As a result, despite the positive net cash flow, the calculated NPV is negative. The economic parameters and generated incomes from selling hydrogen are given in Table 2.4.

The results show that the electrolyser is only operated at its maximum

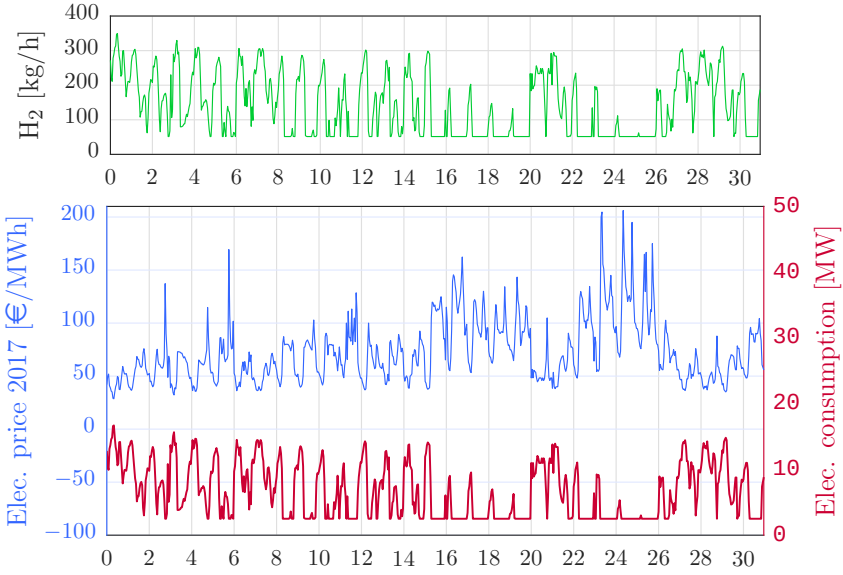

Figure 2.7: Electrolyser power input in first day of the year

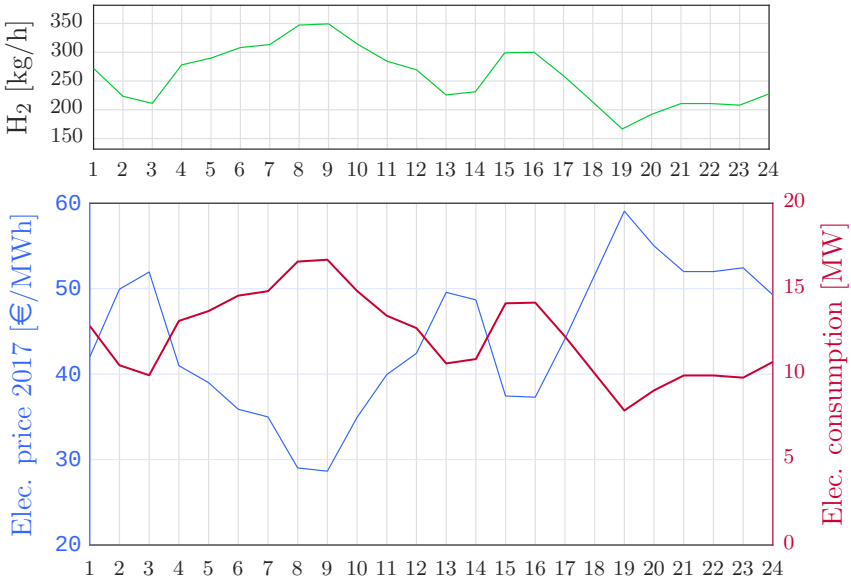

Figure 2.8: Electrolyser power consumption in January

capacity on moments with a very low electricity price, particularly when the price becomes negative. As shown in Fig. 2.9, the electrolyser runs up to

25 MW on the 30th of July due to the negative electricity price.

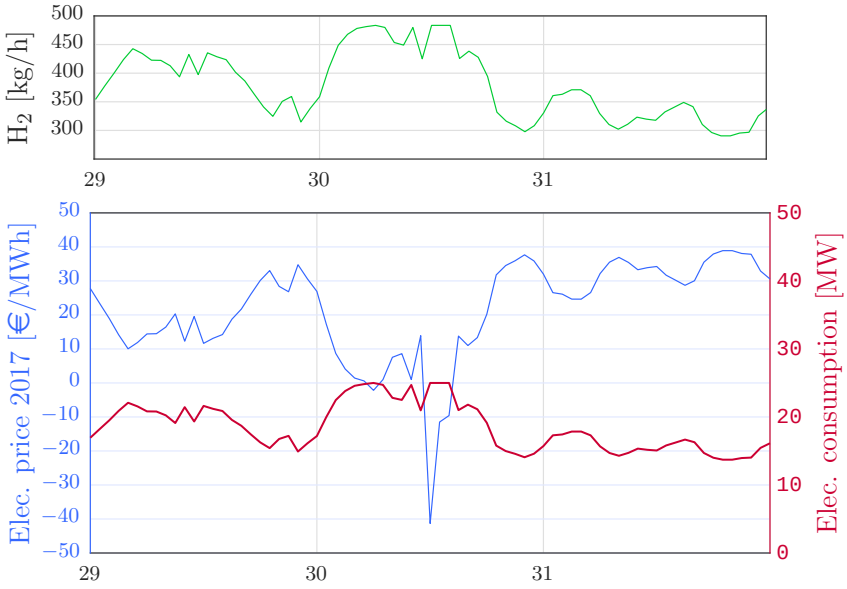

Figure 2.9: Electrolyser power consumption in July

2.3.2 Providing primary reserve

Fig. 2.11 shows the power-frequency chart of symmetric 100 mHz product. The power input follows the frequency variation with the optimum baseload of 13.75 MW with a reserve of 11.25 MW. However, the primary reserve does not react within the first 10 mHz deviations from 50 Hz. As illustrated in Fig. 2.10, offering the 100 mHz product as the primary reserve and operating the electrolyser with a baseload of 55% of its capacity, maximises the annual cash flow with a yearly income of 3.18 M€ by providing ancillary services. The profitability of the investment is estimated, considering a lifespan of 20 years. The power-frequency chart of symmetric 200 mHz product is shown in Fig. 2.11. The maximum annual cash flow is achieved for the electrolyser operating at 55% baseload and providing 11.25 MW power reserve (Fig. 2.10). As a result, running the electrolyser at its optimum baseload generates an income of 1.44 M€ from providing primary reserve and 5.39 M€ from the hydrogen production. The response of the electrolyser in function of time, delivering the symmetrical 100 mHz and the 200 mHz products, is represented in Fig. 2.12. The power input variation of the electrolyser providing the 100 mHz product is twice as high compared to the 200 mHz product. This is because of the fact that the system reacts to the frequency deviation within a different frequency

range but with the same available power reserve.

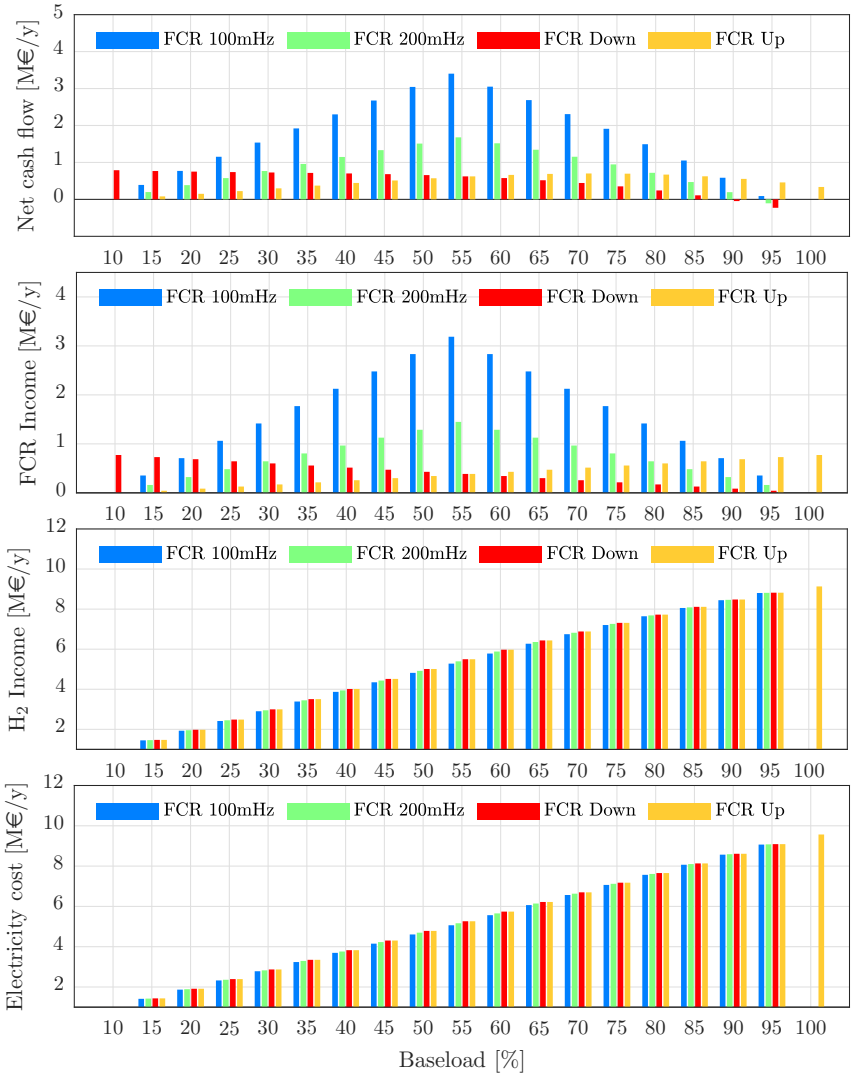

Figure 2.10: Economics for the FCR products varying the baseload

The power-frequency of the electrolyser operating at its optimum point providing the asymmetric downward product is presented in Fig. 2.11. The maximum net cash flow is obtained by running the electrolyser at the minimum technical capacity as baseload and providing 22.25 MW of power reserve. The optimal economic solution yields an income of 770 k€/y from offering primary reserve and 970 k€/y from the hydrogen sale.

Fig. 2.11 illustrates the power-frequency chart of the electrolyser offering the asymmetric upward product. The income of 510 k€/y from offering primary reserve and 6.8 M€/y from the hydrogen sale are not enough to cover the electricity cost. Therefore, the NPV becomes negative (-20.6 M€/MW/h). The dynamic response of the electrolyser delivering FCR down and FCR up are shown in Fig. 2.12. The power input is adjusted either with increasing of frequency (FCR down) or with the frequency drop (FCR up). As shown, the electrolyser mostly operates at a very low capacity which gives rise to the poor economic viability. The optimised economic parameters and generated incomes from selling hydrogen and providing ancillary services for each ancillary product are listed in table 2.4.

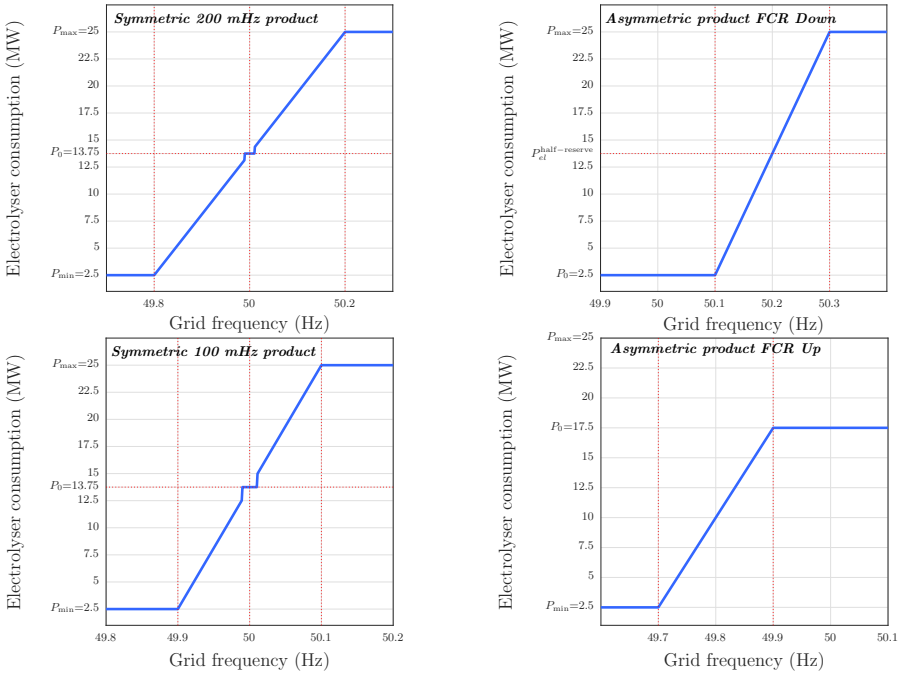

Figure 2.11: Power-Frequency chart in the optimal technical condition for FCR products

A sensitivity analysis is performed to determine the impact of market price variations on baseload and profit, considering the changes in electricity, FCR and hydrogen prices. The sensitivity analysis is conducted for electricity and FCR prices for 2017 and 2021. Fig. 2.13 illustrates the sensitivity analysis based on the market price in 2017. Fig. 2.13(a) depicts the sensitivity of the cash flow and baseload to electricity price, considering a fixed FCR price of 33 €/MW/h. Fig. 2.13(b) shows the sensitivity analysis for a range of FCR prices

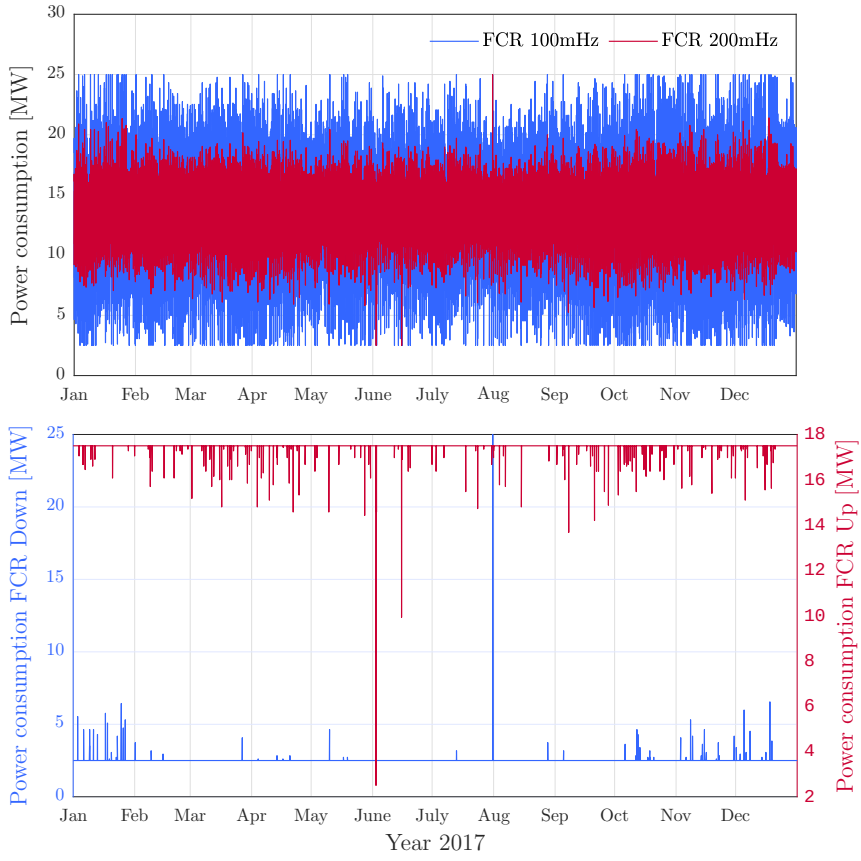

Figure 2.12: Comparison of the dynamic power consumption for FCR products

Table 2.4: Economic parameters for different ancillary services and operating strategies based on the optimal operating point

	Power input optimisation	100 mHz FCR	200 mHz FCR	FCR downwards	FCR upwards
NPV [M€]	-18.55	21.23	-6.78	-27.76	-20.6
IRR [%]	-6	9	-0.7	-13	-7
FCR income [M€]	-	3.18	1.44	0.77	0.51
H_2 income [M€]	5	5.3	5.39	0.97	6.88

with a fixed electricity price of 44.6 €/MWh. Fig. 2.13(c) illustrates the optimal baseload sensitivity to the hydrogen price variation. The calculations are based on an average selling price of hydrogen of 2 to 3 €/kg (onsite production and

pipeline delivery). The results show that, at a hydrogen price of 2.2 €/kg, it is worthwhile to offer the maximum reserve capacity to the power grid for a wide range of electricity and FCR prices. This is mainly due to the low selling price of hydrogen and the high yield generated from ancillary services, which maximises the cash flow. However, for the hydrogen price higher than 3.5 €/kg, the cash flow is maximised by lowering the power reserve and producing a higher amount of hydrogen. As illustrated in Fig. 2.13(c), despite the high ancillary service price, it is more profitable to run at full load for hydrogen prices above 6 €/kg.

Fig. 2.14 shows the impact of market prices in 2021 on baseload and cash flow. The sensitivity analysis is performed, assuming an FCR price of 19.6 €/MW/h and an electricity price of 62.2 €/MWh. As illustrated in Fig. 2.14 (a) and (b), the maximum power reserve provision is a valid option for the limited range of electricity and FCR prices. This is due to a decline in the ancillary service value and relatively higher electricity prices in 2021. Fig. 2.14 (c) shows the impact of hydrogen price on the baseload. As can be seen, providing maximum power reserve maximises the profit within the hydrogen price range of 2.5-3.5 €/Kg. With the price of hydrogen growing, it is more efficient to reduce reserves while increasing production.

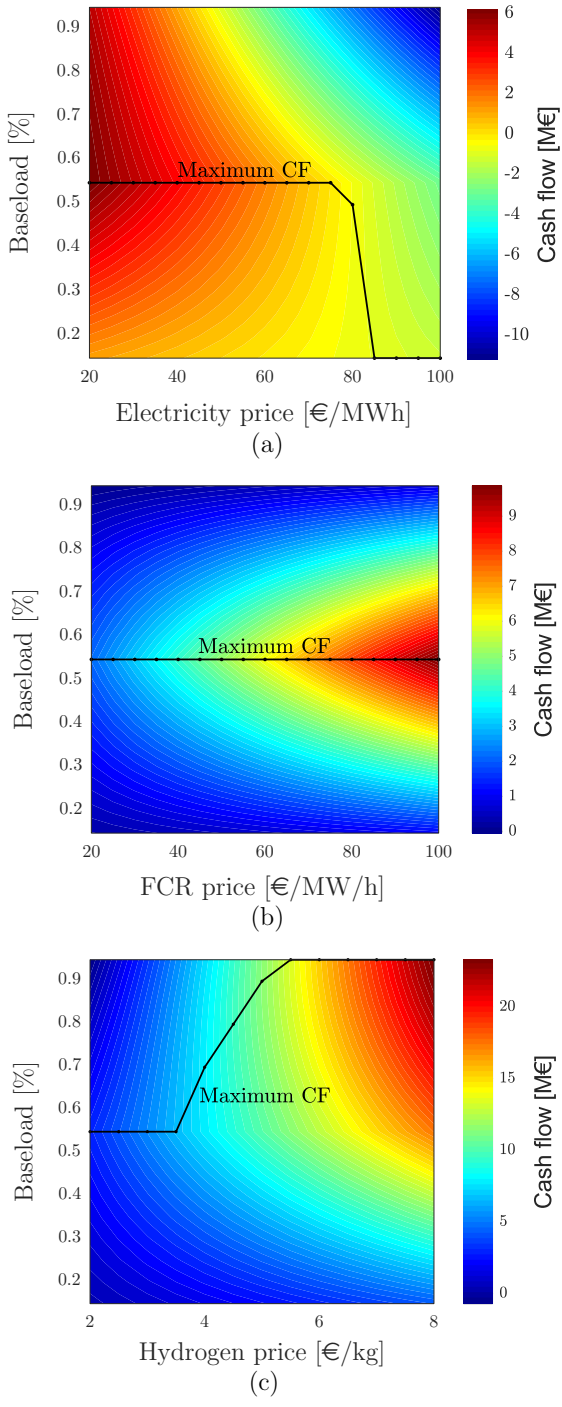

Figure 2.13: Sensitivity of profit to (a) electricity price, (b) FCR price and (c) hydrogen price

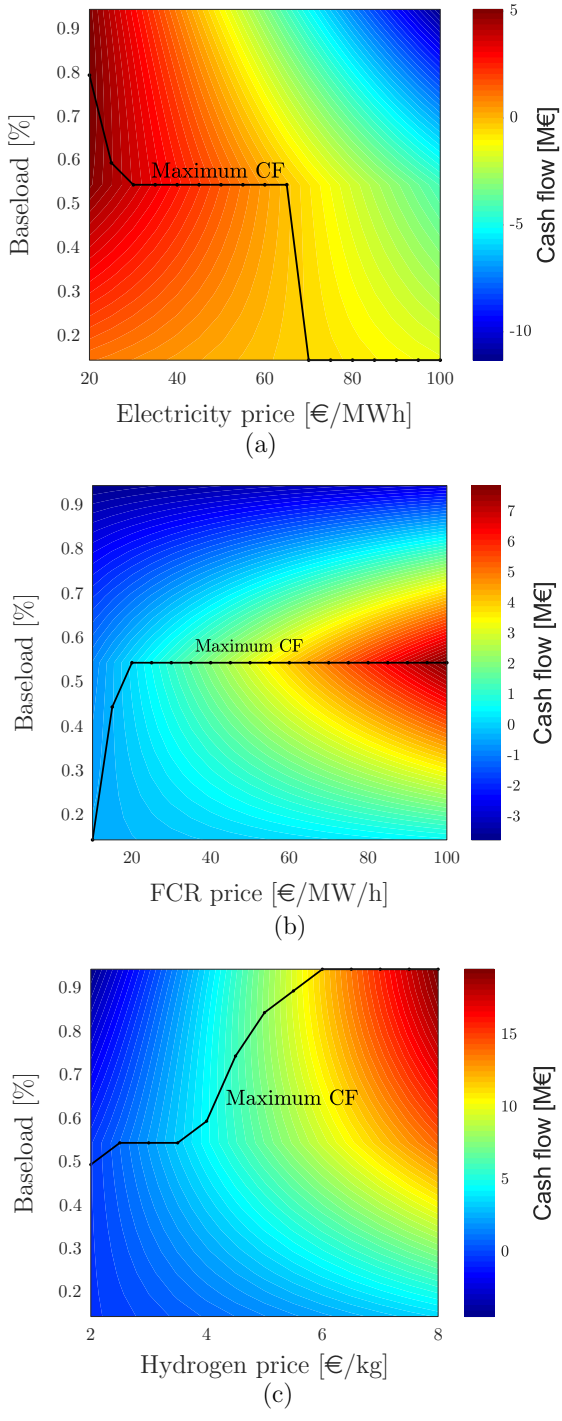

Figure 2.14: Sensitivity of profit to (a) electricity price, (b) FCR price and (c) hydrogen price

2.3.3 Electrolyser dynamic simulation

To test the dynamic performance of the PEM electrolyser in providing ancillary services, a cascaded control system is designed to regulate power consumption. The power reference signal reacts linearly and proportionally to the grid frequency deviation according to (2.6). In this control scheme, the Proportional Integral (PI) controller (slow outer controller) reacts to the frequency deviation and provides the reference signal to the current controller (fast inner controller). Therefore, the cascade controller adjusts the power consumption of the electrolyser by regulating the PEM stack current. Fig. 2.15 illustrates the control diagram. The proportional and integral gains of the control system are given in Table 2.5. The output signal of the ramping block is passed to the BoP equipment as well as the cascaded loops of the electrolyser control. Since the BoP reacts within 3s [19], a time delay block is included in the forward path to match the responses of BoP and electrolyser stack.

Table 2.5: The proportional and integral gains of the cascaded controller

Controller	Proportional gain (P)	Integral gain (I)
Power (outer loop)	20	10
Current (inner loop)	10	10

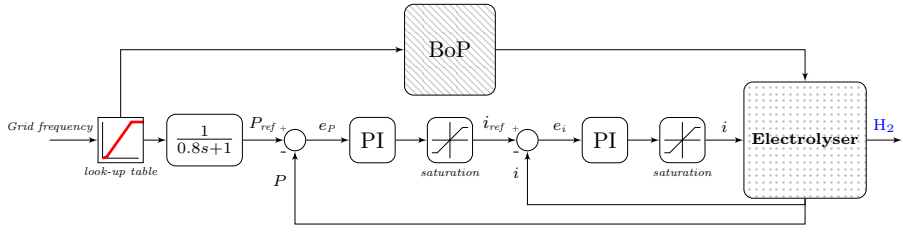

Figure 2.15: Control diagram of PEM electrolyser

Fig. 2.16 shows the flexible operation of the electrolyser providing 100 mHz FCR. The performance of the electrolyser is monitored for ten minutes on the first day of January 2017. The grid frequency varies every ten seconds, and the electrolysers power consumption is regulated based on the grid frequency. The 25 MW electrolyser is operated at its optimum operating point obtained in section 2.3.2. Therefore, the electrolyser operates at 55% of its full capacity while providing 11.25 MW of the primary reserve. The power offtake is regulated with a cascade controller by regulating the current input. As illustrated in Fig. 2.16, the dynamics of the PEM electrolyser are considerably fast during

the operation, and it can react to the grid frequency deviations within five seconds. Therefore, the PEM electrolysis can be operated at different power values with a high degree of flexibility. Also, the hydrogen production obtained from (2.4) and the current input variation of the electrolyser running with the grid balancing strategy is represented in Fig. 2.16.

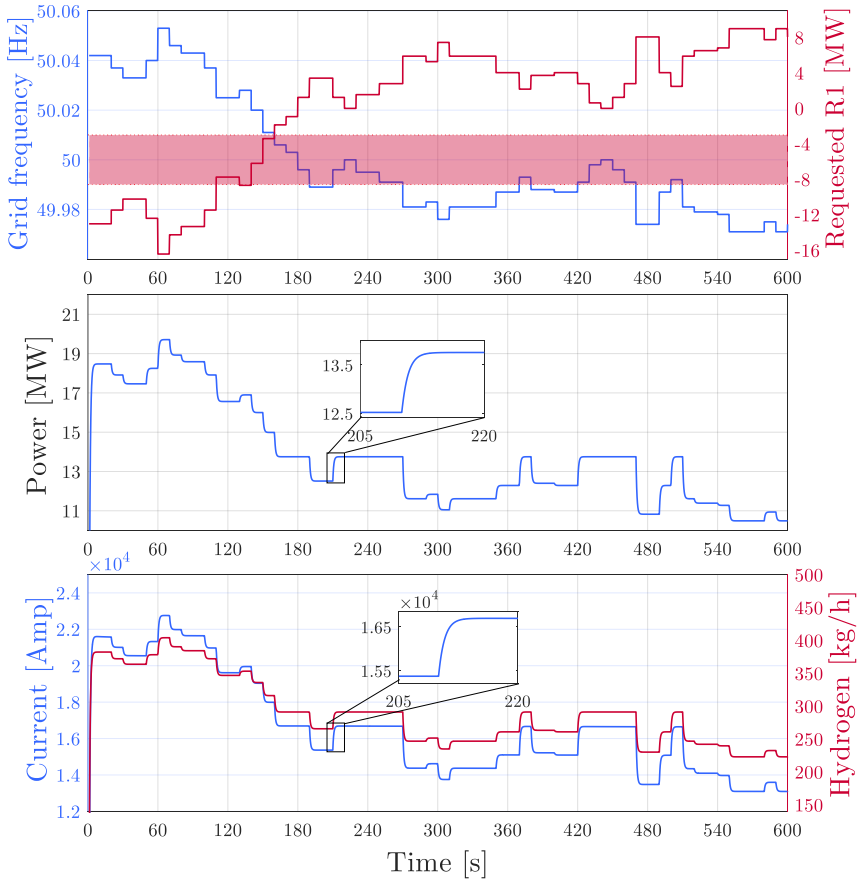

Figure 2.16: Dynamics of PEM Electrolyser providing FCR 100 mHz

Fig. 2.17 demonstrates the dynamics of the 25 MW PEM electrolyser reacting to the maximal frequency deviation that occurred in the year 2017. The maximum frequency deviation is obtained for the reaction zone of FCR 100 mHz (49.9 to 50.1 Hz). In this frequency event, the frequency increased from 49.978 to 50.1 Hz. The controllability of the electrolyser is tested in this region to regulate power consumption for the desired response time within a maximum of 30 seconds. As shown in Fig. 2.17, the electrolyser responds to

the 0.125 Hz frequency variation with an abrupt load change of 13.725 MW (11.275 MW to 25 MW and back) in less than five seconds. This shows that the PEM stack has sufficiently fast dynamic behaviour to react to realistic frequency changes and provide services to the power grid.

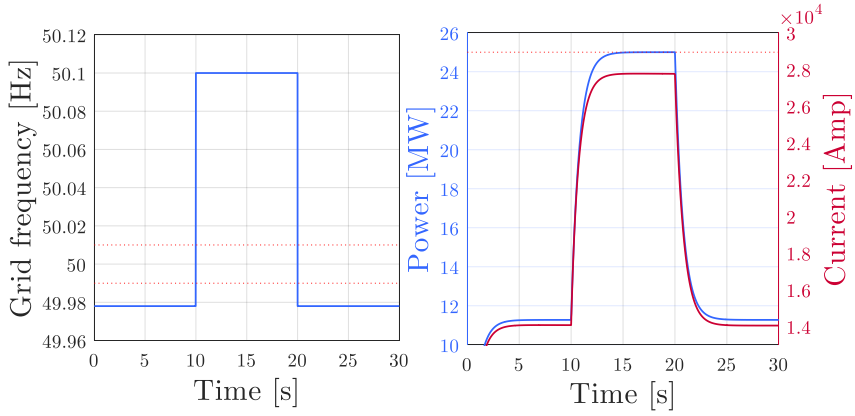

Figure 2.17: Step response of PEM electrolyser to the maximum frequency variation of year 2017 occurred in Belgium

2.4 Conclusion

The main goal of this study is to investigate an optimal strategy for operating a large-scale electrolyser in Belgium to maximise economic efficiency by providing FCR. Therefore, we have assessed the techno-economic performance of two operational strategies for power-to-hydrogen technology. In the first strategy, the electricity consumption of the electrolyser was modulated according to the electricity price. Later, the electrolyser was operated to participate in the ancillary market, by adjusting the power offtake according to the grid frequency. Four possible ancillary service products have been investigated, and technical validation is performed for the optimal operating strategy.

The results demonstrate that operating the electrolyser to follow the electricity price would not be economically viable. This is due to the high investment cost and low hydrogen selling price. It was found that offering the symmetric primary reserve (FCR 100 mHz) is a valid option to generate additional revenue from ancillary services. The optimal economic strategy is to run the electrolyser at a baseload of 55% while providing the remaining capacity as a power reserve. Moreover, the Randles-Warburg electrochemical model is used to represent the dynamic behaviour of the PEM stack of the electrolyser. The electrolyser response to the maximum frequency variation has been tested to

verify the controllability of the power offtake. Simulation results show that the fast dynamics of the PEM electrolyser provide a high degree of flexibility, which provides the opportunity to participate in the ancillary market.

Bibliography

[1] A. E. Samani, A. D'Amicis, J. D. De Kooning, P. Silva, and L. Vandevelde, "Grid balancing with a large-scale electrolyser providing primary reserve," 2019. DOI: 10.1049/cp.2019.0542.

[2] A. E. Samani, A. D'Amicis, J. D. De Kooning, D. Bozalakov, P. Silva, and L. Vandevelde, "Grid balancing with a large-scale electrolyser providing primary reserve," *IET Renewable Power Generation*, vol. 14, no. 16, pp. 3070–3078, 2020. DOI: 10.1049/iet-rpg.2020.0453.

[3] M. Antonelli, U. Desideri, and A. Franco, "Effects of large scale penetration of renewables: The italian case in the years 2008–2015," *Renewable and Sustainable Energy Reviews*, vol. 81, pp. 3090–3100, 2018. DOI: 10.1016/j.rser.2017.08.081.

[4] A. Gerber, M. Qadrdan, M. Chaudry, J. Ekanayake, and N. Jenkins, "A 2020 gb transmission network study using dispersed wind farm power output," *Renewable Energy*, vol. 37, no. 1, pp. 124–132, 2012. DOI: 10.1016/j.renene.2011.06.004.

[5] S. C. Johnson, D. J. Papageorgiou, D. S. Mallapragada, T. A. Deetjen, J. D. Rhodes, and M. E. Webber, "Evaluating rotational inertia as a component of grid reliability with high penetrations of variable renewable energy," *Energy*, vol. 180, pp. 258–271, 2019. DOI: 10.1016/j.energy.2019.04.216.

[6] A. Ulbig, T. S. Borsche, and G. Andersson, "Analyzing rotational inertia, grid topology and their role for power system stability," *IFAC-PapersOnLine*, vol. 48, no. 30, pp. 541–547, 2015. DOI: 10.1016/j.ifacol.2015.12.436.

[7] J. Jomaux, T. Mercier, and E. De Jaeger, "A methodology for sizing primary frequency control in function of grid inertia," in *2016 IEEE International Energy Conference (ENERGYCON)*, 2016. DOI: 10.1109/ENERGYCON.2016.7513886.

[8] Z. Lu, H. Li, and Y. Qiao, "Probabilistic flexibility evaluation for power system planning considering its association with renewable power curtailment," *IEEE Transactions on Power Systems*, vol. 33, no. 3, pp. 3285–3295, 2018. DOI: 10.1109/TPWRS.2018.2810091.

[9] J. Gao, Z. Ma, and F. Guo, "The influence of demand response on wind-integrated power system considering participation of the demand side," *Energy*, vol. 178, pp. 723–738, 2019. DOI: 10.1016/j.energy.2019.04.104.

[10] T. M. Gür, "Review of electrical energy storage technologies, materials and systems: challenges and prospects for large-scale grid storage," *Energy & Environmental Science*, vol. 11, no. 10, pp. 2696–2767, 2018. DOI: 10.1039/C8EE01419A.

[11] Y. Huang, P. Keatley, H. Chen, X. Zhang, A. Rolfe, and N. Hewitt, "Techno-economic study of compressed air energy storage systems for the grid integration of wind power," *International Journal of Energy Research*, vol. 42, no. 2, pp. 559–569, 2018. DOI: 10.1002/er.3840.

[12] H. Zhao, M. Hong, W. Lin, and K. A. Loparo, "Voltage and frequency regulation of microgrid with battery energy storage systems," *IEEE Transactions on Smart Grid*, vol. 10, no. 1, pp. 414–424, 2019. DOI: 10.1109/TSG.2017.2741668.

[13] Y. Zhang, P. E. Campana, A. Lundblad, and J. Yan, "Comparative study of hydrogen storage and battery storage in grid connected photovoltaic system: Storage sizing and rule-based operation," *Applied energy*, vol. 201, pp. 397–411, 2017. DOI: 10.1016/j.apenergy.2017.03.123.

[14] D. F. R. Melo and L.-R. Chang-Chien, "Synergistic control between hydrogen storage system and offshore wind farm for grid operation," *IEEE Transactions on Sustainable Energy*, vol. 5, no. 1, pp. 18–27, 2013. DOI: 10.1109/TSTE.2013.2272332.

[15] F. Díaz-González, A. Sumper, O. Gomis-Bellmunt, and R. Villafáfila-Robles, "A review of energy storage technologies for wind power applications," *Renewable and sustainable energy reviews*, vol. 16, no. 4, pp. 2154–2171, 2012. DOI: 10.1016/j.rser.2012.01.029.

[16] Z. Navas-Anguita, D. García-Gusano, J. Dufour, and D. Iribarren, "Prospective techno-economic and environmental assessment of a national hydrogen production mix for road transport," *Applied Energy*, vol. 259, 2020. DOI: 10.1016/j.apenergy.2019.114121.

[17] B. Lux and B. Pfluger, "A supply curve of electricity-based hydrogen in a decarbonized european energy system in 2050," *Applied Energy*, vol. 269, p. 115011, 2020. DOI: 10.1016/j.apenergy.2020.115011.

[18] B. W. Tuinema, E. Adabi, P. K. Ayivor, V. G. Suárez, L. Liu, A. Perilla, Z. Ahmad, J. L. R. Torres, M. A. van der Meijden, and P. Palensky,

"Modelling of large-sized electrolysers for real-time simulation and study of the possibility of frequency support by electrolysers," *IET Generation, Transmission & Distribution*, vol. 14, no. 10, pp. 1985–1992, 2020. DOI: 10.1049/iet-gtd.2019.1364.

[19] M. Mohanpurkar, Y. Luo, D. Terlip, F. Dias, K. Harrison, J. Eichman, R. Hovsapian, and J. Kurtz, "Electrolyzers enhancing flexibility in electric grids," *Energies*, vol. 10, no. 11, p. 1836, 2017. DOI: 10.3390/en10111836.

[20] L. Allidières, A. Brisse, P. Millet, S. Valentin, and M. Zeller, "On the ability of pem water electrolysers to provide power grid services," *International Journal of Hydrogen Energy*, vol. 44, no. 20, pp. 9690–9700, 2019. DOI: 10.1016/j.ijhydene.2018.11.186.

[21] G. Matute, J. Yusta, and L. Correas, "Techno-economic modelling of water electrolysers in the range of several mw to provide grid services while generating hydrogen for different applications: A case study in spain applied to mobility with fcevs," *International Journal of Hydrogen Energy*, vol. 44, no. 33, pp. 17431–17442, 2019. DOI: 10.1016/j.ijhydene.2019.05.092.

[22] D. Thomas, D. Mertens, M. Meeus, W. Van der Laak, and I. Francois, "Power-to-gas roadmap for flanders," *WaterstofNet vzw*, 2016. URL: https://www.waterstofnet.eu/nl/waterstof-industrie-cluster-netwerk/about-the-cluster.

[23] B. Rashford, "How to determine if that renewable energy project makes economic sense," *Barnyards & backyards*, 2010. URL: http://www.uwyo.edu/barnbackyard.

[24] M. Kiaee, A. Cruden, D. Infield, and P. Chladek, "Utilisation of alkaline electrolysers to improve power system frequency stability with a high penetration of wind power," *IET Renewable Power Generation*, vol. 8, no. 5, pp. 529–536, 2013. DOI: 10.1049/iet-rpg.2012.0190.

[25] V. Liso, G. Savoia, S. Araya, G. Cinti, and S. K. Kær, "Modelling and experimental analysis of a polymer electrolyte membrane water electrolysis cell at different operating temperatures," *Energies*, vol. 11, no. 12, 2018. DOI: 10.3390/en11123273.

[26] H. Zhang, S. Su, G. Lin, and J. Chen, "Efficiency calculationand configuration design of a pem electrolyzer system for hydrogen production," *International Journal of Electrochemical Science*, vol. 7, pp. 4143–4157, 2012. URL: http://www.electrochemsci.org.

[27] O. Atlam and M. Kolhe, "Equivalent electrical model for a proton exchange membrane (pem) electrolyser," *Energy Conversion and Management*, vol. 52, no. 8, pp. 2952 – 2957, 2011. DOI: 10.1016/j.enconman.2011.04.007.

[28] T. Yigit and O. F. Selamet, "Mathematical modeling and dynamic simulink simulation of high-pressure pem electrolyzer system," *International Journal of Hydrogen Energy*, vol. 41, no. 32, pp. 13901 – 13914, 2016.

[29] N. Dale, M. Mann, and H. Salehfar, "Semiempirical model based on thermodynamic principles for determining 6kw proton exchange membrane electrolyzer stack characteristics," *Journal of Power Sources*, vol. 185, no. 2, pp. 1348 – 1353, 2008. DOI: 10.1016/j.jpowsour.2008.08.054.

[30] A. Awasthi, K. Scott, and S. Basu, "Dynamic modeling and simulation of a proton exchange membrane electrolyzer for hydrogen production," *International Journal of Hydrogen Energy*, vol. 36, no. 22, pp. 14779 – 14786, 2011. Fuel Cell Technologies: FUCETECH 2009.

[31] L. Bertuccioli, A. Chan, D. Hart, F. Lehner, B. Madden, and E. Standen, "Study on development of water electrolysis in the eu," *Fuel cells and hydrogen joint undertaking*, 2014. URL: https://www.fch.europa.eu.

[32] D. Guilbert and G. Vitale, "Dynamic emulation of a pem electrolyzer by time constant based exponential model," *Energies*, vol. 12, no. 4, p. 750, 2019. DOI: 10.3390/en12040750.

[33] J. C. Garcia-Navarro, M. Schulze, and K. A. Friedrich, "Measuring and modeling mass transport losses in proton exchange membrane water electrolyzers using electrochemical impedance spectroscopy," *Journal of Power Sources*, vol. 431, pp. 189–204, 2019. DOI: 10.1016/j.jpowsour.2019.05.027.

[34] A. Saadi, M. Becherif, D. Hissel, and H. S. Ramadan, "Dynamic modeling and experimental analysis of pemfcs: A comparative study," *International Journal of Hydrogen Energy*, vol. 42, no. 2, pp. 1544–1557, 2017. DOI: 10.1016/j.ijhydene.2016.07.180.

[35] M. Rubio, A. Urquia, and S. Dormido, "Diagnosis of pem fuel cells through current interruption," *Journal of Power Sources*, vol. 171, no. 2, pp. 670–677, 2007. DOI: 10.1016/j.jpowsour.2007.06.072.

[36] C. Martinson, G. Van Schoor, K. Uren, and D. Bessarabov, "Equivalent electrical circuit modelling of a proton exchange membrane electrolyser based on current interruption," in *2013 IEEE International*

Conference on Industrial Technology (ICIT), pp. 716–721, IEEE, 2013. DOI: 10.1109/ICIT.2013.6505760.

[37] K. Darowicki and L. Gawel, "Impedance measurement and selection of electrochemical equivalent circuit of a working pem fuel cell cathode," *Electrocatalysis*, vol. 8, no. 3, pp. 235–244, 2017. DOI: 10.1007/s12678-017-0363-0.

[38] C. A. Martinson, G. Van Schoor, K. Uren, and D. Bessarabov, "Characterisation of a pem electrolyser using the current interrupt method," *International journal of hydrogen energy*, vol. 39, no. 36, pp. 20865–20878, 2014. DOI: 10.1016/j.ijhydene.2014.09.153.

Chapter 3

Demand response operation of CCU based processes

Novel CO_2-based technologies are emerging to respond to the global challenge of decreasing greenhouse gas emissions. These processes, referred to as Carbon Capture and Utilisation (CCU), allow the direct conversion of carbon dioxide into more valuable chemical products such as formic acid, methanol, and methane. Despite the remarkable advantages of CCU based technologies, a few challenges need to be addressed to take these forward on an industrial scale. These processes require a high amount of energy for production, leading to low economic performance. In this context, energy-intensive CO_2-based processes can offer flexibility to the electrical grid and generate extra revenue through participating in the ancillary market and thus improving economic viability. Therefore, a new operating strategy is required for the flexible operation of these processes to facilitate the integration of these processes into the power grid.

This chapter studies an energy-intensive industrial load with a high potential to offer grid balancing services, i.e., a carbon capture utilization-based chemical plant synthesizing formic acid. The designed control architecture uses the infrastructure and storage capabilities to address the challenges of applying fast ramp rates and conditions of time-critical grid services. This is not straightforward due to strict technical constraints and the nonlinear dynamics of chemical systems. The adaptive operating approach increases the process's flexibility and facilitates a fast demand response operation. A flexible operating strategy is suggested for the cooperative operation of a Polymer Electrolyte Membrane (PEM) electrolyser and multi-stage compression system in a chemical process to provide Frequency Containment Reserve (FCR). This strategy aims to realise the desired power regulation dynamics on the grid side while maintaining the reactor's optimal operating conditions, i.e.,

temperature, pressure and flow rate ratio. Furthermore, a techno-economic analysis is performed to obtain optimal operating points and baseloads to achieve the most favourable contribution in the ancillary market. The proposed approach is validated by dynamic simulations taking into account the impact of flexible operation and FCR provision on a.o. the reactor efficiency.

The contents of this chapter have been accepted for publication in the International Journal of Electrical Power & Energy Systems [1].

Flexible operation strategy for formic acid synthesis providing frequency containment reserve in smart grids

Arash E. Samani, Jeroen D. M. De Kooning, Cesar A. Urbina Blanco, Dimitar Bozalakov, Lieven Vandevelde

Published in "International Journal of Electrical Power & Energy Systems", 2022

Abstract*The demand-side contribution to grid frequency regulation is becoming increasingly important due to the growing penetration of renewable energy in the power system. Among energy-intensive industrial loads, chemical plants have a high potential to offer grid balancing services due to their existing control infrastructure and storage capabilities. However, applying fast ramp rates and providing time-critical grid services is not straightforward due to strict constraints and the nonlinear dynamics of chemical systems. Therefore, adaptive operating approaches are required to increase the process's flexibility and facilitate the fast demand response operation. This work proposes a flexible operating strategy for the cooperative operation of a Polymer Electrolyte Membrane (PEM) electrolyser and multi-stage compression systems in a chemical process to provide Frequency Containment Reserve (FCR). This strategy aims to realise the desired power regulation dynamics on the grid side while maintaining the reactor's optimal operating conditions, i.e., temperature, pressure and flow rate ratio. A techno-economic analysis is performed to obtain optimal operating points. The techno-economic analysis shows that operating the process at a baseload of 73% while offering the remaining capacity as a power reserve can create additional revenue and improve the economic profit by around 10%. The proposed approach is validated by dynamic simulations of a Carbon Capture and Utilisation (CCU) process for formic acid production. The results show that the proposed strategy can enhance the process's operational flexibility and enable FCR provision with a limited impact on reactor efficiency (<1%).*

3.1 Introduction

The transition towards a low carbon future has led to a higher integration of renewable energy sources into the power system. According to the European Green Deal, in line with the Paris Agreement, the EU aims to increase the share of renewable energy by at least 32% and reduce greenhouse gas emissions by at least 40% (compared to 1990 levels) by 2030 [2]. Although the increased share of renewable energy sources in the energy system mitigates the CO_2

emissions, it introduces new challenges to the power system management due to the intermittent, non-dispatchable nature of renewable energy [3, 4]. The higher dependency on renewables reduces the system reliability, i.e., stability and security, and increases the load on fossil-based power plants to balance the supply-demand mismatches [5]. Therefore, a new dynamic equilibrium with a higher degree of flexibility is required to ensure the power grid robustness and accommodate higher levels of renewable power generation.

The electrical demand side can provide flexibility by adjusting the load pattern based on grid requirements. Energy-intensive industrial processes with high specific electricity costs, i.e., electricity costs per gross value added [6], are the prime candidates for demand-side integration. The industrial sector flexibility has been primarily studied for the price-based demand response programs, in which the plant operation is scheduled based on the electricity price variation. The price-based demand response has been applied in different industrial applications such as steel furnaces [7], chlorine production [8], ethylene oxide production [9], air separation units [10, 11], cement plants [12], pulp mills [13], and glass furnaces [14]. Although the price-based demand response indirectly helps the Transmission System Operator (TSO) to maintain the balance between supply and demand, there is an increasing need for fast demand response programs such as frequency regulation. Therefore, a continuous response of the industrial loads is needed on a time scale of tens of seconds to tens of minutes to actively support the power system. In Europe, the TSOs offer a full spectrum of frequency ancillary services, including inertial response, Frequency Containment Reserve (FCR), automated Frequency Restoration Reserve (aFRR), and manual Frequency Restoration Reserve (mFRR). These services can be provided by a major electricity consumer, supplier, or trader known as Balancing Service Providers (BSPs) or Flexibility Service Providers (FSPs).

In [15], it is shown that aluminium smelters, Liquefied Natural Gas (LNG) plants, cement processing plants, and greenhouses could be successfully integrated into the power system by providing aFRR. In [6, 16], the technical potential of energy-intensive industries is studied for mFRR provision in Germany. It is shown that electric arc furnaces, chlor-alkali electrolysis, aluminium electrolysis, and cross-sectional technologies such as mills, pumps and compressors can provide an adequate flexibility margin for demand response. In [17], a decentralised control algorithm is developed and tested to regulate the power input of bitumen tanks based on grid frequency variations. A dynamic load control system is implemented for the even distribution of on/off switch actions amongst all tanks. Therefore, the flexible operation of the bitumen tanks is achieved with a limited impact on the temperature of the tanks. In [18], a strategy for providing ancillary services is suggested by switching on/off units with the capability of discrete power changes, e.g., cement crushers or paper mills. It is shown that continuous power regulation can be achieved by

combining on/off switching of cement crushers with an on-site energy storage system. Also, Model Predictive Control (MPC) and optimal scheduling are implemented to follow the command load and minimise the switching actions without disturbing the cement kiln. Though the industry's potential for frequency regulation is investigated in literature, the FCR provision has not been taken forward in most industrial loads due to the time-critical requirement of this service and the operational complexities, i.e., process constraints, ramp rate, safety and efficiency losses. Therefore, further research needs to be carried out to enable the industrial loads to offer FCR.

In the chemical industry, demand response can be provided by exploiting energy systems with a fast dynamic response, i.e., compressors, pumps, fans, electric heaters. In this context, electrolysis processes have been identified early on as potential balancing service providers due to their large electricity consumption and fast dynamics [6, 16]. The flexible operation of a membrane electrolyser in chlor-alkali processes has been investigated in literature [19, 20] for FCR provision. Several chlor-alkali and aluminium smelter plants have already been integrated into the grid through providing fast demand response [21]. In recent years, Polymer Electrolyte Membrane (PEM) electrolysis have received extensive attention to providing ancillary services for the power grid due to their high electricity consumption, flexibility and reactivity [22–24]. Moreover, PEM electrolyser is an enabling technology for CO_2 hydrogenation and can play a key role for direct conversion of CO_2 value-added chemicals.

In the transition towards a circular economy, novel chemical processes are being developed for the direct conversion of CO_2 to value-added chemicals, such as formic acid, methanol, and methane. Among these processes, formic acid is one of the most promising routes for CO_2 utilisation with widespread applications [25]. Formic acid is a basic chemical that finds use in a variety of applications such as leather and rubber production, textiles, pharmaceuticals, preservatives and antibacterial agents in livestock feed. It can also be used as a building block for the bio-catalytic production of value-added chemicals such as Single-Cell Protein (SCP) to support livestock production. Moreover, formic acid can be used as a hydrogen carrier (53 g H_2/L) [26, 27] and as fuel for fuel cells, and it is much less expensive to store than hydrogen. The global production of formic acid has increased from 390 kton/year in 1995 to 762 kton/year in 2019 with a firm growth rate of over 3.8% from 2014 to 2019, mainly produced by hydrolysis of methyl formate [28, 29]. The total trade value of formic acid in 2019 was 290 million US$ [30]. The formic acid market is expected to grow in the near future due to health and environmental concerns, e.g., the ban on using antibiotics in animal feed and silage preservation, and emerging applications, e.g., formic acid fuel cells and hydrogen-based storage systems [29, 31]. According to [25], the direct synthesis of formic acid from CO_2 has a Technology Readiness Level (TRL)

of 3-5. However, several processes have been patented, and some of them were tested on a pilot scale by BASF and Reactwel for the continuous hydrogenation of CO_2 to pure formic acid [28].

These processes, which are referred to as Carbon dioxide Capture and Utilisation (CCU), can utilise the PEM electrolyser flexibility and provide ancillary services for the grid. In this context, the approaches that facilitate the integration of CCU based processes into the power system can tackle two problems at the same time. Firstly, utilising the CCU based processes will reduce carbon dioxide emissions. Secondly, the chemical process as an ancillary service provider can support the power grid, which leads to the further integration of renewable energy sources into the power system. Given these advantages, the chemical industry can play a key role in accelerating a low carbon future transition.

Active participation of large electricity consumers in the FCR market is crucial to maintain the power balance in the future grid with a high integration of renewable energy sources. Although several energy-intensive industries already have the potential capacity to provide frequency regulation services, the following challenges should be addressed to ensure the secure and cost-efficient provision of fast-paced ancillary services:

- Chemical processes have difficulty operating flexibly as BSPs or FSPs since they are planned to run continuously at their nominal capacities with predetermined setpoints.
- Applying fast ramp rates, i.e., the rate of change in power demand, is not straightforward due to their nonlinear dynamics and operational constraints, e.g., safety, product quality and wear.
- The lack of an adaptive control architecture for the flexible operation in chemical processes makes it challenging to satisfy grid services requirements while maintaining process efficiency.
- The economic profit of chemical plants is questioned under flexible operation dealing with grid and market uncertainties.

Motivated by the above, this article investigates the feasibility of providing grid balancing with FCR while capturing CO_2 with a thermo-catalytic formic acid synthesis process. An operating strategy is proposed for flexible operation of the process by dynamically regulating process components. For the methodology followed in this research, firstly, the dynamic model of the process elements is developed. The compression stages are modelled in Aspen HYSYS, and simulation results are used to make an integrated model in Matlab/Simulink, including the PEM electrolyser, compressors and the reactor.

Then, a control algorithm is designed to operate the electrolyser and compressors flexibly to provide ancillary services while maintaining the desired reactor pressure and temperature, resulting in an optimal efficiency and supporting the downstream processes. Finally, an industry scale formic acid process is used to validate the methodology under these dynamic conditions.

The key contribution is the proposed operating strategy to increase the process's operational flexibility and facilitate the integration of chemical processes into the electrical grid, addressing the main challenges of chemical plants for FCR provision. The main deltas of this research with respect to the state of the art are:

- FCR is provided while ensuring the continuous operation of the process without using additional equipment (e.g. additional storage devices).
- Applying fast ramp rates are enabled by exploiting elements with fast dynamics and implementing a control algorithm based on the cooperative operation of its components, i.e., PEM electrolyser and multi-stage compression units.
- Critical values of the process, i.e., pressure and temperature limits and reaction efficiency, are respected by maintaining the optimal operating condition at the reactor.
- The optimal contribution of the process in the European ancillary market is obtained, which generates additional revenue and improves the economic profit.

The methodology applied in this research is also applicable to different CCU based processes for direct conversion of CO_2 to chemical synthesis such as methane or methanol where CO_2 and hydrogen are used as raw materials, and the reaction takes place under high pressure. Therefore, the proposed techno-economic model and control architecture offers useful and incentive information for chemical industries to provide grid balancing services and improve the economic viability of CCU based processes.

The remainder of the article is structured as follows: The dynamic model of the CCU based process for formic acid production is described in section 3.2. The proposed control algorithm for providing FCR is presented in section 3.3. The techno-economic performance is assessed in section 3.4. The effectiveness of the control performance is examined in section 3.5. Finally, the outcomes of the proposed approach are summarised in section 3.6.

3.2 Process model for formic acid synthesis

A dynamic model is developed for a CCU based process for formic acid production via thermo-catalysis through heterogenisation of ruthenium catalysts, as described in [32]. The model objectives are to simulate the process dynamics under flexible operation and to control the operating condition at the reaction stage. Fig. 3.1 shows the process flow diagram for conversion of CO_2 and H_2 to formic acid based on the process developed in [32]. The process consists of five stages: (I) the compression stage, (II) the reaction stage, (III) the formic acid enrichment stage, (IV) the amine exchange stage and (V) the formic acid formation and purification. The process is upscaled to produce 1100 kg/h (10 kt/yr) formic acid using 2464 kg/h of CO_2 and 112 kg/h of H_2. In the first stage, CO_2 and H_2 are compressed to reach the required pressure level for the reaction. In the second stage, CO_2 is hydrogenated in the presence of a base, triethylamine (Et_3N). The function of the base during the hydrogenation is to drive the severely thermodynamically limited equilibrium of CO_2 hydrogenation to formic acid ($\Delta G_1 = 22$ kJ.mol^{-1}) (3.1) via the formation of a stable adduct with formic acid ($\Delta G_2 = -19$ kJ.mol^{-1}), Et_3NH^+:$HCOO^-$ [33, 34]:

$$CO_2(g) + H_2(g) \rightarrow HCOOH(aq) \tag{3.1}$$

$$CO_2(g) + H_2(g) + Et_3N(aq) \rightleftharpoons Et_3NH^+{:}HCOO^-(aq) \tag{3.2}$$

In the next stage, water and excess triethylamine are removed from the liquid stream from the catalytic reactor to afford the Et_3NH^+:$HCOO^-$ adduct at an Acid to Amine Ratio (AAR) of 2.3 to allow the amine exchange in the next stage. Direct separation of the Et_3NH^+:$HCOO^-$ adduct into formic acid and triethylamine is not possible. However, the n-butyl imidazole (*n*BIM) adduct, *n*BIMH^+:$HCOO^-$, readily decomposes by heat into formic acid and *n*BIM [35]. Thus, the concentrated Et_3NH^+:$HCOO^-$ is combined with n-butyl imidazole (*n*BIM) to form *n*BIMH^+ : $HCOO^-$. Then, it is fed into a separation column from which pure formic acid can be obtained as the overhead product according to reactions (3.3) and (3.4):

$$Et_3NH^+{:}HCOO^-(l) + n\text{BIM}(l) \rightleftharpoons n\text{BIM}H^+{:}HCOO^-(l) + Et_3N(l) \tag{3.3}$$

$$n\text{BIM}H^+{:}HCOO^-(l) \rightarrow HCOOH(l) + n\text{BIM}(l) \tag{3.4}$$

This article focuses on the flexible operation of the process components with fast dynamics, i.e., the PEM electrolyser and compressors, and the impact of this flexible operation on the reaction stage. Though the separation and purification stages are important to produce formic acid, their dynamic behaviour is not included in the simulations. These stages do not interrupt the dynamic response

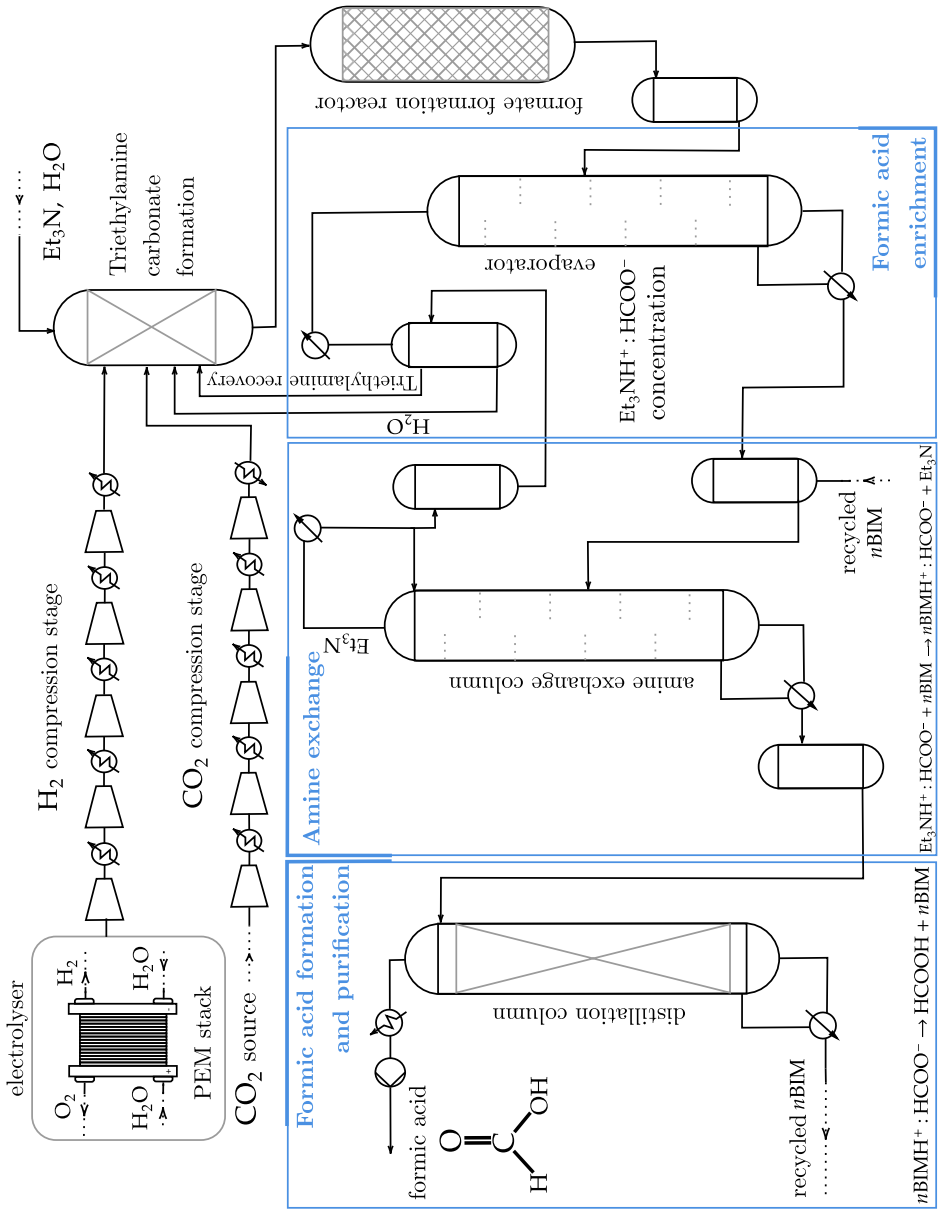

Figure 3.1: Process flow diagram of formic acid synthesis from CO_2 and H_2 from PEM electrolyser.

of the electrolyser and compressors, and their slow dynamics dampen the fast variations. However, the parameters such as AAR, reactor productivity, and CO_2 conversion are included in the reactor model. Therefore, the reactor output data under the flexible operation can be used to assess the influence on the subsequent process stages. Therefore, the main focus remains on the first three stages of the process, and performance analysis of separation and purification stages are out of scope for this study.

The process is comprised of two main input streams, i.e., CO_2 and H_2, which are pressurised before feeding into the reactor. The purity of the CO_2 source depends on the availability of the captured CO_2, and it may come from different sources, i.e., atmosphere, power plant combustion exhaust gasses or waste streams of other processes. This model assumes that the captured CO_2 is available at atmospheric pressure and ambient temperature. Therefore, a compression stage is modelled to increase the pressure up to the optimal operating pressure for CO_2 hydrogenation. On condition that CO_2 is compressed in the upstream process, and it is available at the desired pressure, the compression stage in the preceding process is considered for flexible operation. The compression stage with intermediate cooling stages is modelled in Aspen HYSYS. The CO_2 stream is cooled down to 25 °C through intermediate cooling stages to maintain a semi-isothermal compression of compressors, resulting in a high compression efficiency. Based on the simulation results, a five-stage compression system is required to reach the pressure of 120 bar at the reactor. A pressure drop of 0.1 bar is assumed at each intermediate cooling stage. After the compression stage, the CO_2 stream is heated to reach 120 °C at the reactor inlet. A 5.79 MW PEM electrolyser generates the required H_2 of the process. The H_2 stream is compressed through a five-stage compression system up to 120 bar with intermediate cooling stages. The compressors of both stages are assumed to operate at an isentropic efficiency of 80%, which leads to the nominal power of 288 kW and 252 kW for H_2 and CO_2 compression, respectively.

All process components are separately modelled and integrated into one complete process model in Matlab/Simulink. Fig. 3.2 illustrates the configuration and connections of electrolyser, Permanent Magnet Synchronous Machine (PMSM) and compressors. The electrochemical model of the PEM stack is developed to represent the impedance behaviour of the PEM electrolyser. The compression stages are first modelled in Aspen HYSYS to identify the specifications, e.g., number of stages and power consumption. Then, each compressor model is built in Simulink and coupled with a PMSM-model to allow variable speed operation. Next, the PEM stack model is connected to the compression stage, taking the hydrogen mass flow rate, pressure and temperature as input signals.

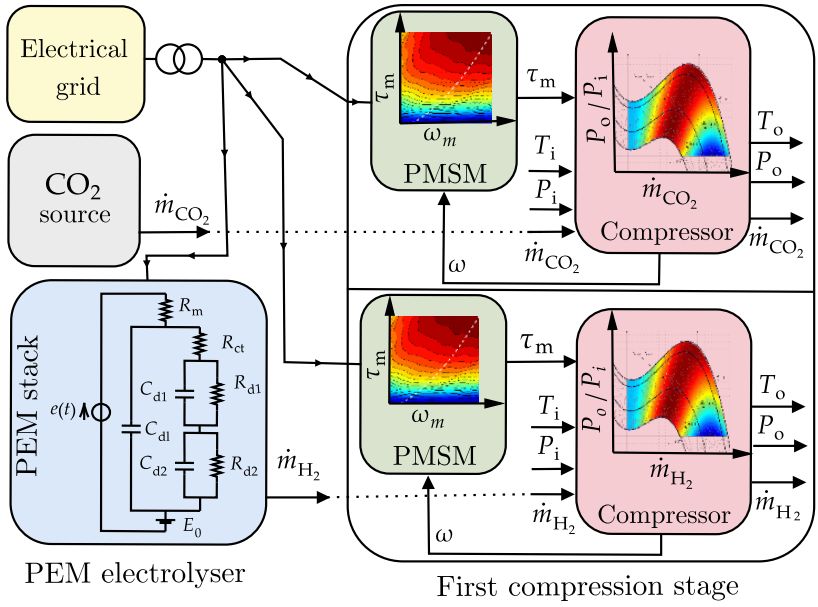

Figure 3.2: Subsystems configuration and connections: electrolyser, compressor and electrical motor.

3.2.1 PEM Electrolyser

The PEM electrolyser is one of the most energy-intensive components in the process of formic acid synthesis. Also, it has adequate flexibility and agility to regulate its power. The response time from pressurised standby to a full-load operating condition is less than three seconds, and it is below one second for a hot-start. These properties make the PEM electrolyser a prime candidate for engaging in fast-paced ancillary services, e.g., FCR. According to [24, 36, 37] electrolysers can effectively respond to the grid frequency variations, as they are able to respond faster to frequency deviations than gas-turbine and steam-turbine driven synchronous generators. Different applications of PEM electrolysers operating as BSPs or FSPs are investigated in [22, 23]. In [24], it is found that the PEM stack mainly dictates reactivity, and to a lesser degree, Balance-Of-Plant (BOP). Therefore, the PEM stack is modelled to represent the electrolyser dynamics in the formic acid process.

As shown in Fig. 3.3(a), the electrochemical model of the PEM stack can be described by Randles equivalent circuits connected in series. In the Randles model, electric components represent the dynamic behaviour of different layers in the PEM stack. The voltage drop across the PEM stack V_{el} can be calculated as the difference between the standard electrode potential E_0 and the voltage losses including the anode activation voltage V_{a}, cathode activation voltage V_{c}

and the ohmic voltage drop of the membrane V_m [38, 39]:

$$V_{el} = E_0 - V_a - V_c - V_m \tag{3.5}$$

The equivalent impedance of a PEM stack can be calculated by measuring the current through the PEM stack I_{in} and the voltage across the PEM stack V_{el}, which is the sum of the cathode impedance Z_c, anode impedance Z_a and the membrane ohmic losses R_m:

$$Z_{el} = \frac{V_{el}}{I_{in}} = Z_a + R_m + Z_c \tag{3.6}$$

As shown in Fig. 3.3(a), the impedance of each electrode is reflected by the double-layer capacitance C_{dl}, the charge transfer resistance R_t, and the Warburg impedance of the electrode Z_w, $(C_{dl} \,||\, [R_t + Z_w])$. The electrical model can be simplified to the Randles-Warburg (RW) model by neglecting the small cathode activation voltage and representing the double layer capacity with a pure, single-frequency theoretical capacity [39, 40]. Fig. 3.3(b) illustrates the PEM stack electrochemical model using the RW cell. The RW equivalent circuit can be used to model the impedance response of electrochemical systems such as a galvanic cell or an electrolytic cell [41]. The RW values identified in [42] are upscaled to achieve the desired impedance behaviour of the 5.79 MW PEM electrolyser. Table 3.1 gives the values of these parameters.

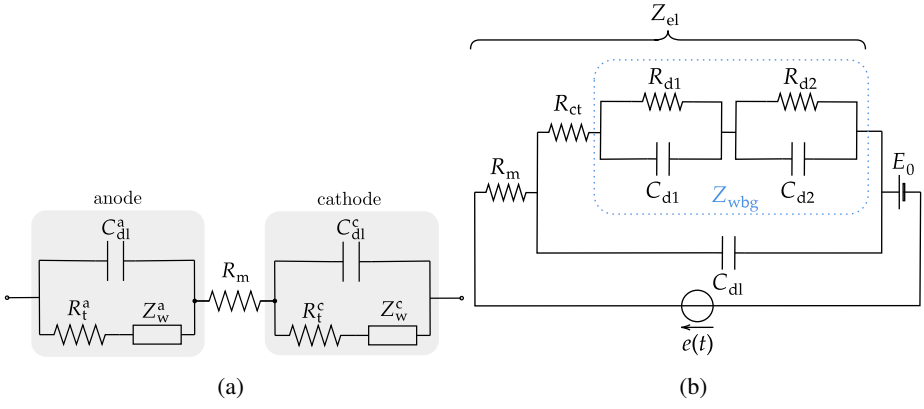

Figure 3.3: (a) Electrical model of the PEM stack (b) PEM stack electrochemical model with Randles-Warburg cell.

Fig. 3.4 shows the dynamic behaviour of the PEM stack model with an ideal current source by means of step responses. The PEM model reacts to the current changes, and the power signal settles down within one second at maximum, while the PEM voltage reaches 900 V at the rated power. The

Table 3.1: Randles-Warburg model parameters.

R_{ct} (mΩ)	C_{dl} (F)	R_{d1} (mΩ)	C_{d1} (F)	R_m (mΩ)	R_{d2} (mΩ)	C_{d2} (F)
31.8	0.09	1.3	1.96	27.2	12.1	26.18

produced hydrogen H_2^p (kg/h) in function of the operating power P_e (MW) is calculated by (3.7), considering the partial load efficiency of the electrolyser $\eta = {}^{P_e}/_{P_{nom}}$ [22, 23].

$$H_2^p = \left(-5.9 \cdot \eta^2 + 5.07 \cdot \eta + 20.17\right) \cdot P_e \tag{3.7}$$

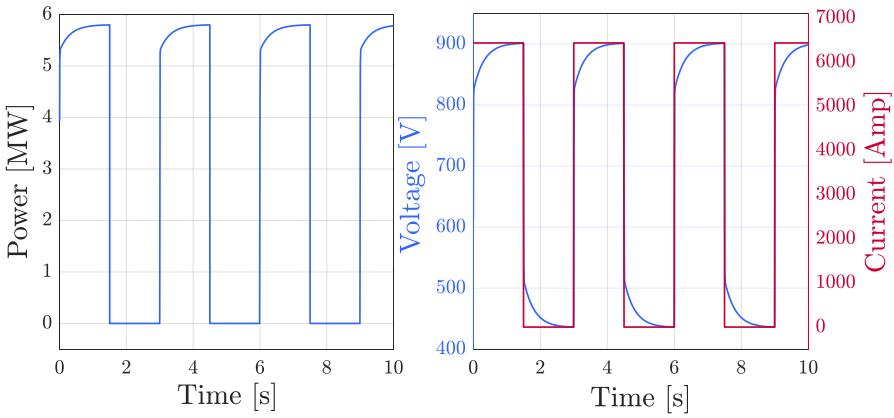

Figure 3.4: The dynamic response of the PEM stack to the ideal current source.

3.2.2 Compression system

Two compression stages are modelled for the process of formic acid synthesis to reach the desired pressure level at the reaction stage. The process feed streams, i.e., H_2 and CO_2, are pressurised up to 120 bar through multi-stage compression systems. The compression stages consist of five centrifugal compressors with intermediate coolers. The multiple-stage compressor trains are first modelled in Aspen HYSYS. The simulation results are used to build up an integrated model including the electrical motors in Simulink.

Under the flexible operating strategy, the process operating condition changes according to the grid frequency variation. Accordingly, the compressors' operating point needs to be adaptively controlled to adjust their operating

point based on process requirements. A variable speed motor control can be used to regulate the operating point of the compressors in an energy-efficient manner. Therefore, each compressor is coupled with a PMSM model to enable the compressors to be operated at different rotational speeds. The dynamic model of the PMSMs is developed in the rotating $d-q$ synchronous reference frame, taking into account the armature reaction effect, copper losses and iron losses [43]. The compressor model includes the compressor's mechanical dynamics by means of a first order equation of motion including rotational inertia and the compressor and motor torques. The variable-speed control is performed by regulating the motor torque by using field-oriented control [44]. The proposed approach is simulated on each PMSM coupled with a compressor model using an approximation of the compressor performance map.

Fig. 3.5 shows the compressor data, including the polynomial approximations for four rotational speeds, i.e., 57%, 67%, 95% and 100% of the nominal speed (solid black lines). In order to simulate the performance of the compression systems, the performance map of the compressors is generated based on the centrifugal compressor data available in Aspen HYSYS. A third-order polynomial approximation of the speed curves is calculated based on the available operating points at each compressor speed. The polynomial of each speed curve can be approximated as:

$$\Psi_c(m_\mathrm{r}, \omega) = c_3(\omega)\, m_\mathrm{r}^3 + c_2(\omega)\, m_\mathrm{r}^2 + c_1(\omega)\, m_\mathrm{r} + c_0(\omega) \tag{3.8}$$

where Ψ_c is the pressure ratio, ω is the compressor speed, and m_r is the relative flow rate which is the ratio of the operating flow rate m_op and the nominal flow rate m_nom ($m_\mathrm{r} = {}^{m_\mathrm{op}}/_{m_\mathrm{nom}}$). In order to simulate the system response accurately, a continuous map of the compressors is required. As the variation of the polynomial coefficients with the rotational speed is approximately linear, the speed curves are interpolated linearly. The third-order polynomial approximations of the speed curves are illustrated with dotted lines in Fig. 3.5. Moreover, the speed curves are approximated in the efficiency map, and the curves are interpolated by using shape-preserving piecewise cubic interpolation to obtain a continuous compressor efficiency map. Fig. 3.5 illustrates the efficiency of the compressor as a function of the relative flow rate and the pressure ratio at different rotational speeds.

3.3 Control design

A flexible control approach is required in order to facilitate the integration of the CCU based process into the power grid. The control system must enable the process flexibility at the operational level to satisfy the grid code requirements.

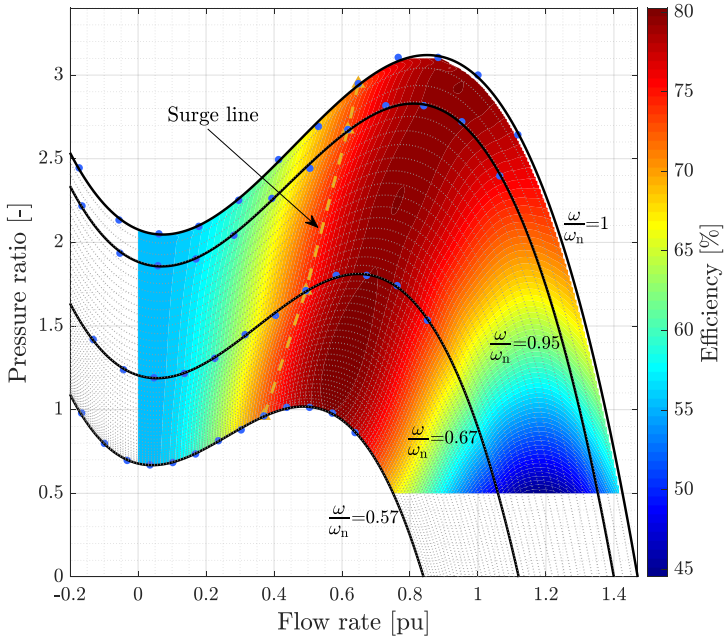

Figure 3.5: The approximated compressor map: speed curves approximated based on data points (solid lines) and interpolated speed curves (dotted lines).

The process components with a high degree of flexibility, e.g., the electrolyser, compressors and pumps, can be operated flexibly while respecting the critical values and safety of the process. Therefore, a control algorithm is designed to fulfil two main objectives:

- Providing ancillary services for the grid in the form of frequency containment reserve.
- Maintaining the required operating conditions for the reaction to ensure the desired process efficiency and product quality.

Fig. 3.6 illustrates the proposed control scheme of the process. The control system of the formic acid synthesis process consists of two main control loops. The primary control loop reacts to the grid frequency variation by regulating the PEM electrolyser power consumption. The secondary and tertiary control loops follow the primary controller and regulate the compressor speeds to maintain the reactor's optimal pressure, temperature, and flow rate. The different control levels are explained in the following subsections.

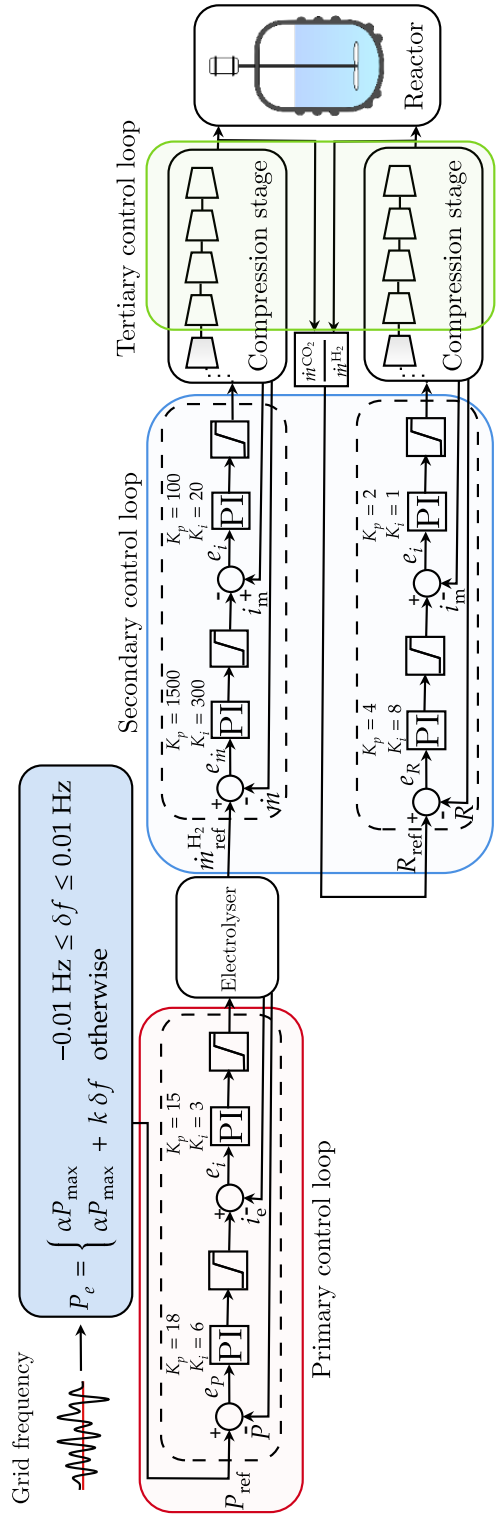

Figure 3.6: Control system for the flexible operation of the formic acid synthesis process based on CO_2 and H_2.

3.3.1 PEM electrolyser control: frequency regulation

In the primary control loop, the PEM electrolyser is regulated to follow the grid frequency. Therefore, when the grid frequency deviates from the nominal value, the controller tracks the frequency deviation and adjusts the electrolyser operating point based on a predefined droop. When the frequency falls below the nominal value, i.e., when there is a shortage of power, the electrolyser's power input is reduced to decrease the load on the grid. Conversely, when the frequency is higher than the nominal value, i.e., there is an excess of power, the power setpoint is increased.

The frequency regulation in this work focusses on the standard 200mHz FCR product on the European ancillary service market [45]. Fig. 3.7 shows the power-frequency chart of the symmetric 200mHz product. In order to provide a symmetrical 200mHz product, the electrolyser reacts to grid frequency deviations within the range of 48.8 to 50.2 Hz. Therefore, the power reserve is fully activated once the frequency deviation reaches 200 mHz. As the FCR product is symmetric, the frequency is stabilised equally for both upward and downward deviations. According to European TSOs' regulations, a deadband of 10 mHz (50 Hz±10 mHz) is considered [46]. In the deadband, the primary control is not allowed to react to the frequency variations, and the electrolyser operates at the baseload power. Therefore, the power setpoint of the electrolyser is calculated as:

$$P_e = \begin{cases} \alpha P_{\max} & -0.01 \text{ Hz} \leq \delta f \leq 0.01 \text{ Hz} \\ \alpha P_{\max} + k\delta f & \text{otherwise} \end{cases} \tag{3.9}$$

where α is the baseload factor as a percentage of the maximum capacity $P_{\max}$. The frequency of the grid is represented by f. The parameter δf is the frequency deviation from 50 Hz ($\delta f = f$ - 50 Hz). The droop constant k is the power-frequency characteristic of the electrolyser calculated based on the contractual power reserve δP_{FCR} and the frequency deviation range of 200 mHz of the FCR product defined as:

$$k = \frac{\delta P_{\text{FCR}}}{\delta f} \tag{3.10}$$

As illustrated in Fig. 3.6, a cascaded control system is designed to track the setpoint signal calculated by (3.9). In the control scheme, the Proportional Integral (PI) controller (outer loop controller) reacts to the grid frequency variation and provides the reference signal to the PEM stack current controller (inner loop controller). Therefore, the cascaded control strategy adjusts the electrolyser power consumption by regulating the PEM stack current.

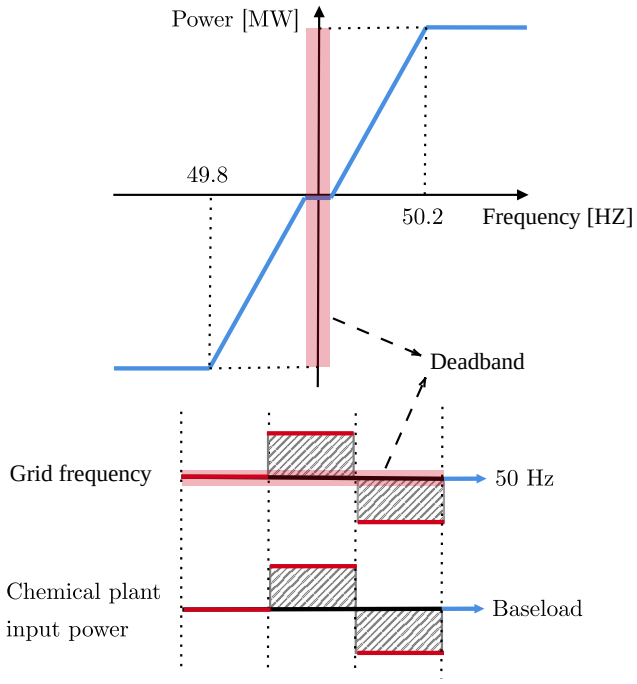

Figure 3.7: Power-Frequency chart for the symmetric 200mHz FCR product and chemical process operation based on the grid frequency.

3.3.2 Compression stages control system

As described in the previous section, the primary control modifies the electrolyser power consumption to provide FCR. Therefore, the flow rate of the generated hydrogen at the process input changes based on the grid frequency variation. In this condition, if the compressors are not controlled adaptively and ignore the H_2 variation, the optimal operating condition of the reactor will be violated. In the worst case, the pressure and temperature exceed the allowed operating range. In the H_2 stream, the compressors' power must be regulated according to the hydrogen generated by the PEM electrolyser. Moreover, the CO_2 flow rate needs to be adjusted based on the hydrogen variation to ensure the desired ratio of H_2 and CO_2 at the reaction stage. Also, the compressors must be controlled to maintain the discharge pressure and temperature at the desired level despite the flow rate variation. Therefore, additional controllers are required to maintain the optimal operating condition of the process. A control system is designed for the H_2 and CO_2 compression stages to control each compressor's power through variable-speed control. In this control ap-

proach, the compressors operate at different rotational speeds by regulating the PMSM torque, using field-oriented control. For instance, if the H_2 flow rate reduces, the pressure ratio across the compressor does not change, enabling the compressor to supply a lower flow rate at a reduced speed.

In the H_2 compression stage, the first compressor is controlled to track the generated hydrogen and supply the desired pressure at a modified speed. As shown in Fig. 3.6, in the cascaded control system, the outer PI control loop reacts to the generated hydrogen and sends the reference signal to the inner loop PI controller, which controls the rotational speed by regulating the motor torque. If the following four compressors in the compression stage operate at their maximum power, their discharge pressure and temperature will change with the flow rate variation, which negatively impacts reaction efficiency. Therefore, the other four compressors are controlled in the tertiary control loop to adjust their rotational speed based on the flow rate dictated by the first compressor. As illustrated in Fig. 3.8, the reference speed signal is generated by a lookup table obtained from the characteristic curve of each compressor (Fig. 3.5), and the speed signal is tracked by regulating the motor torque. Therefore, each compressor pressure's ratio remains at the designed value, allowing the compressors to supply the variable flow rate at the modified speed.

The first compressor in the CO_2 compression stage is controlled to track the generated hydrogen and regulate the CO_2 flow rate to maintain the CO_2 and H_2 ratio at the optimal level. As shown in Fig. 3.6, in the cascaded control system, the outer PI controller reacts to the H_2 and CO_2 ratio and sends the reference signal to the motor torque controller (inner controller). Therefore, the cascaded control regulates the CO_2 flow rate by controlling the compressor speed. The following compressors in the compression stage modify their rotational speed based on the flow rate dictated by the first compressor.

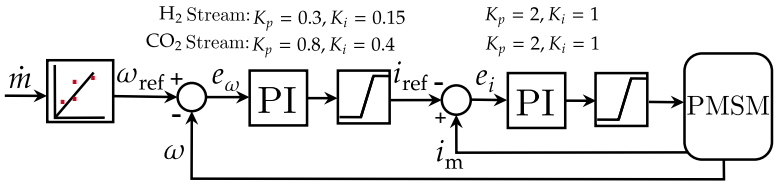

Figure 3.8: The tertiary control diagram for regulating the speed of the last four compressors in the compression stages.

3.4 Techno-economic analysis

Before studying the performance of the proposed control structure, the optimal range of the power reserve and the baseload setpoint need to be determined. Therefore, in this section, a techno-economic analysis is formulated based on market prices, formic acid production and FCR provision.

An industrial-scale CO_2-based formic acid process is energy-intensive. In [47], it is shown that reducing the electricity cost is a driving factor to improve the economic performance of the process. Also, it is shown that hydrogen production consumes around 90% of the total electricity consumption through electrolysis, which is 40% of the required energy for the whole process. In [22,23], it is discussed that participating in the ancillary markets can improve the economic efficiency of hydrogen production. Therefore, offering ancillary services for the grid can generate additional revenues, reducing the formic acid production cost to become competitive with conventional methods.

In order to compare the economic performance of flexible operation with the full-load operation, the profit estimation of the process is formulated by considering the main parameters that vary by the flexible operation, i.e., electricity cost, formic acid production and ancillary service revenue. It is assumed that other cost function parameters, which are slightly disrupted by flexible operation, remain unchanged. Therefore the objective function is defined as:

$$\text{Obj} = \max \sum_{t=1}^{T} (Q_{\text{FA}}(t) \cdot E_{\text{FA}}) - \sum_{t=1}^{T} (P_{\text{e}}(t) \cdot E_{\text{el}}) + \delta P_{\text{FCR}} \cdot E_{\text{FCR}} \cdot T \quad (3.11)$$

The objective function is evaluated over a period T of one year with a time stepping t of 10 s. The first term represents the income from the formic acid production. It is the sum of the formic acid flow rate Q_{FA} in kg/h, which varies by regulating the electrolysers operating point, multiplied by the value of formic acid E_{FA}, which is a fixed value. The second term is the electricity cost, which is the power consumed P_{e} multiplied by the electricity price E_{el}. The operating power P_e is calculated by $P_e = P_b + k\delta f$, where the baseload power $P_b = \alpha P_{\max}$ is a setpoint for the control system responding to the frequency variation. The third term is the revenue from the provision of FCR, which is a product of the reserved power P_{FCR}, the FCR price E_{FCR} and time T. The revenue from FCR is not based on the actual power P_{e}, but only on the contracted reserve P_{FCR}, i.e., it is a standby remuneration, not an activation remuneration. The actual power P_{e} continuously follows the grid frequency f variations. The power P_{e} is calculated using (3.9). Q_{FA} is calculated by a quadratic function for hydrogen production between 2.3 and 112.0 kg/h:

$$Q_{\text{FA}}(t) = -0.06 \cdot H_2^{\text{p}}(t)^2 + 19.42 \cdot H_2^{\text{p}}(t) - 40.44 \quad (3.12)$$

where H_2^p can be calculated by using (3.7).

The objective function (3.11) is subjected to the following constraints:

$$P_b + \delta P_{FCR} \leq P_{max} \tag{3.13}$$

$$-P_b + \delta P_{FCR} \leq -P_{min} \tag{3.14}$$

and the following bounds:

$$P_{min} \leq P_b \leq P_{max}$$

$$0 \leq \delta P_{FCR} \leq \frac{1}{2}(P_{max} - P_{min})$$

where the minimum capacity P_{min} of 10% is considered to ensure the continuous operation of the electrolyser. This avoids the start-up and shut-down time required to purge the nitrogen. Therefore, the baseload power is limited between minimum capacity P_{max} and the maximum capacity P_{max} (0.58 MW to 5.8 MW). In order to provide a symmetrical 200 mHz FCR product and keep the power reserve available for both a positive and a negative variation of the grid frequency, the power reserve δP_{FCR} is defined to not exceed half of the available capacity ($P_{max} - P_{min}$). The power reserve and the market prices are assumed to be constant for the whole year. The FCR price is equal to the average price of the 200mHz FCR product in 2021 (January-August), i.e., 19.6 €/MW/h. The electricity price in the model is equal to the average electricity price in Epex Spot in 2021 (January-August), i.e., 62.2 €/MWh. The formic acid price is considered 0.5 €/kg [47].

The objective function (3.11) finds the optimum operating point in which the profit function is maximised. Fig. 3.9 shows the profit as a function of baseload. Also, the formic acid production, hydrogen and CO_2 consumption are presented at different baseloads. As it can be seen, offering FCR and operating the electrolyser with a baseload of 73% maximises the profit function, which results in the profit improvement of around 10% compared to the full-load operation. Nevertheless, the flexible operation at the optimum baseload reduces the formic acid production by 13%.

Taking into account the importance of FCR and electricity price, the sensitivity analysis is carried out to determine how variations in market prices can alter the profit. Fig. 3.10(a) depicts the sensitivity of the profit to FCR price, considering a fixed electricity price of 62.2 €/MWh. Fig. 3.10(b) shows the sensitivity analysis of profit for a range of electricity prices with a fixed FCR price of 19.6 €/MW/h. The profit variation represents the profit improvement in percentage comparing to the full-load operation. Firstly, the figures show how the profit rises with increasing electricity or FCR prices. Secondly, as either one of these prices goes up, it is worthwhile to offer more primary reserve, consequently lowering the baseload.

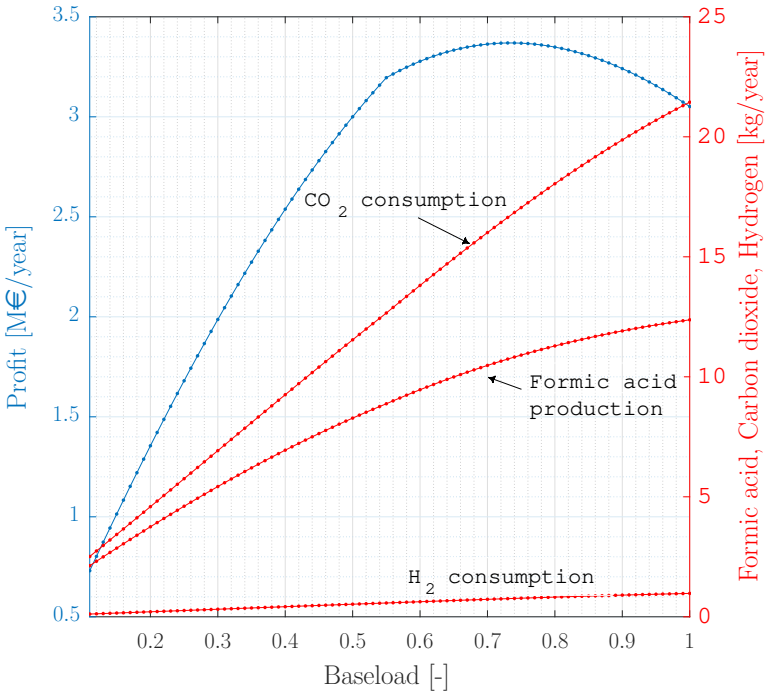

Figure 3.9: Profit, carbon dioxide and hydrogen consumption and formic acid production at different baseloads.

3.5 Dynamic simulation

After having discussed the optimal economic approach and indicating the optimal range of baseload power and power reserve, the dynamic performance of the process is investigated in this section. The power consumption of the PEM electrolyser is regulated to provide FCR by the primary control loop (section 3.3.1). As illustrated in Fig. 3.10, the optimal baseload can vary based on FCR and electricity price. Therefore, the PEM electrolyser operates at a baseload of 70% (4.05 MW), approximately the mean value of the obtained optimal range, while providing the remaining 30% of its capacity (1.74 MW) as power reserve. Fig. 3.12 shows the flexible operation of the electrolyser providing symmetrical 200 mHz FCR. A real 800 s grid frequency dataset is used from the synchronous grid of continental Europe, which includes the significant grid frequency variation [48]. The frequency profile is selected to include frequency variations above and below the nominal frequency (50 Hz), allowing to monitor process dynamics for both upward and downward regulations. As illustrated in Fig. 3.11, the frequency profile represents an accurate estimation of the grid frequency behaviour in one year, respecting the 98%

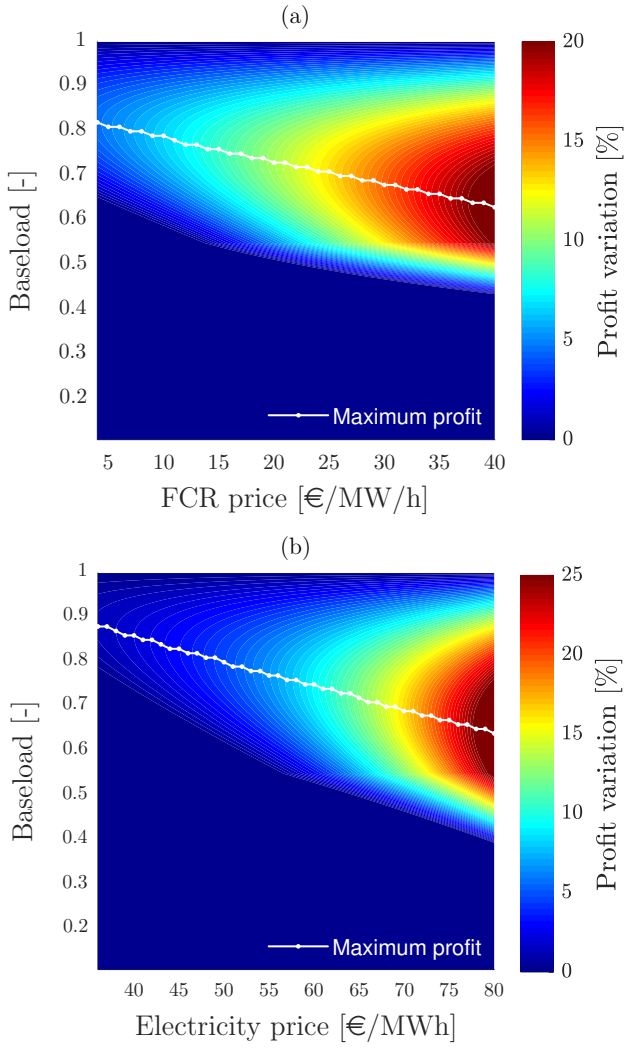

Figure 3.10: Sensitivity of profit to (a) FCR price and (b) electricity price.

confidence interval of the frequency distribution. The data have a sampling period of 10 s, and the electrolyser responds to the grid frequency variation. The power input is regulated using a cascaded control system by controlling the PEM stack current. The electrolyser operates at the baseload when the grid frequency is within the deadband (50 Hz±10 mHz). The reference signal is the electrolyser operating setpoint P_e, which is the sum of baseload and power reserve calculated by $P_e = P_b + \delta P$, where activated power reserve is defined by $\delta P = k\,\delta f$. Therefore, the primary controller reacts proportionally to the

grid frequency variations by regulating the electrolyser power. As illustrated in Fig. 3.12, when the grid frequency drops below 49.99 Hz, the electrolyser operates below the baseload. Contrarily, the electrolyser's power consumption increases above the baseload while the frequency is above 50.01 Hz. Consequently, the generated hydrogen varies based on the grid frequency variation as a result of FCR provision. As shown, the PEM dynamics are considerably fast, and it can track the reference signal in less than five seconds. Therefore, the PEM electrolysis can be run at different power levels with a high degree of reactivity and is able to provide FCR adequately.

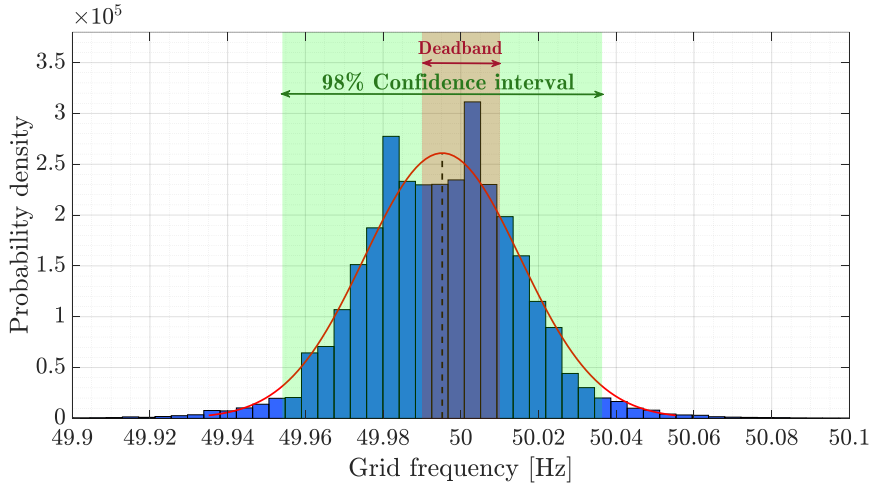

Figure 3.11: Grid frequency distribution in one year.

Fig. 3.13 illustrates the first compressor performance in the H_2 feed stream. As a result of primary level control, the hydrogen production fluctuates based on the grid frequency variation. Therefore, the first compressor in the compression stage is controlled to deliver a constant discharge pressure at different H_2 flow rates. As shown, the cascaded controller tracks the hydrogen variation by regulating the compressor speed. The variable compressor speed is obtained by regulating the motor torque. As shown, the discharge pressure and temperature are adequately regulated around their desired levels with minimal deviations.

The following four compressors in the compression stage are controlled to adjust their rotational speed based on the first compressor discharge flow rate. Fig. 3.14 illustrates the fifth compressor performance representing the last four compressors in the compression stage with the pressure and temperature of H_2 at the reactor inlet. The control diagram of the compressors is shown in Fig. 3.8. The reference speed signal is generated based on the H_2 flow rate using a lookup table obtained from the compressor performance map. As illustrated in Fig. 3.14, the motor speed, and consequently the power, are regulated to

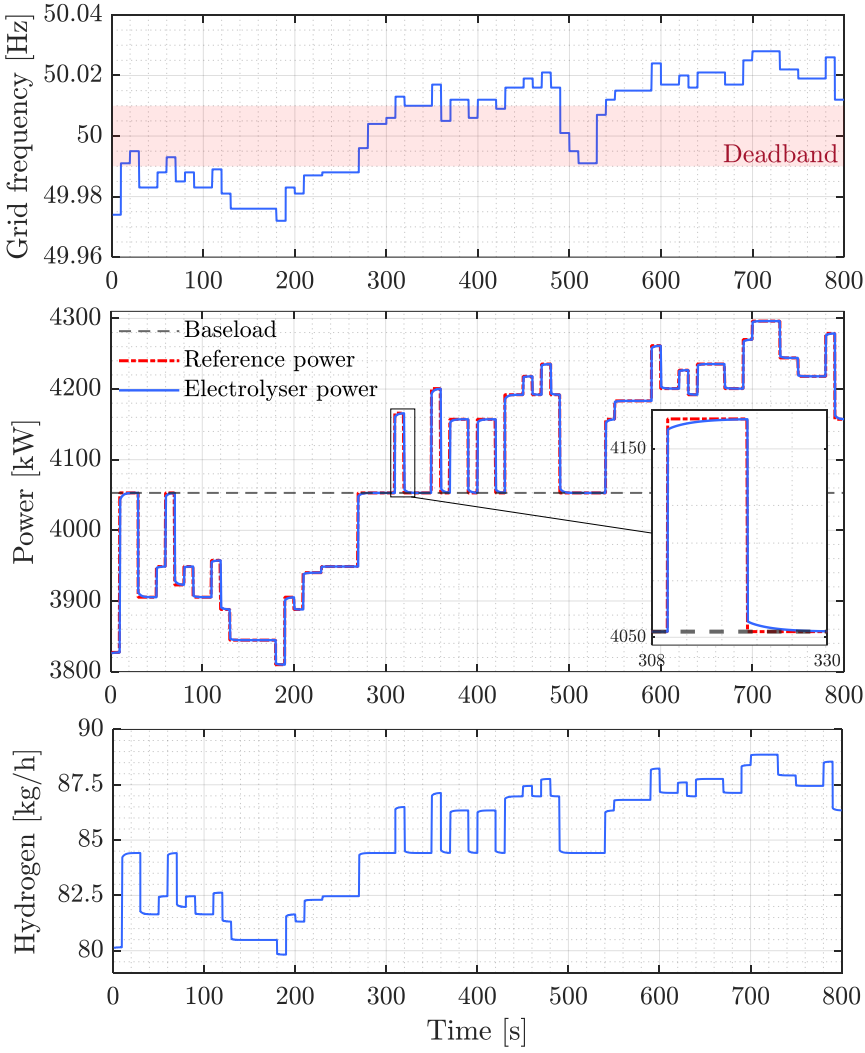

Figure 3.12: The dynamic performance of the PEM electrolyser under FCR provision strategy.

produce the desired pressure. As can be seen, the proposed control strategy can maintain the pressure and the temperature of H_2 at the optimal values.

Fig. 3.15 shows the dynamic performance of the first compressor in the CO_2 compression stage. The first compressor in the CO_2 stream is responsible for modifying the CO_2 flow rate such that the required $^{CO_2}/_{H_2}$ ratio is maintained at the reactor while supplying the desired discharge pressure. The compressor speed is regulated to adjust the CO_2 flow rate based on flow rate variation in the H_2 stream. As illustrated, the CO_2 and H_2 flow rate ratio is maintained at the

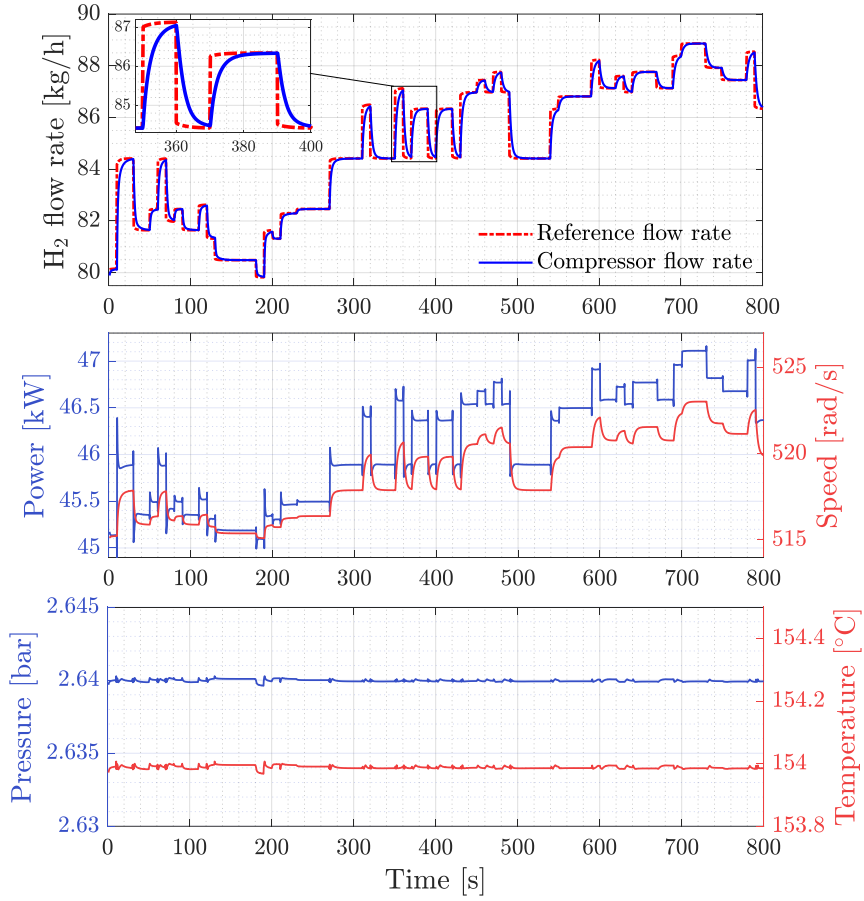

Figure 3.13: The dynamic performance of the first compressor in the H_2 compression stage.

desired level despite the variation in hydrogen production while the discharge pressure is maintained at a nearly constant level. In Fig. 3.16, the corresponding compressor performance for the 800 s simulation is illustrated on the efficiency map. As shown, for around 10% flow rate variation, the compressor operates at its maximum efficiency while the pressure ratio is maintained at the desired value.

Similar to the H_2 compression stage, the next four compressor speeds are regulated based on the first compressor discharge flow rate to keep the output pressures at the desired level. Fig. 3.17 illustrates the fifth compressor performance representing the last four compressors in the CO_2 compression stage. As the result of variable speed operation, the pressure and temperature of the CO_2 are maintained at the reactor's optimal operating condition.

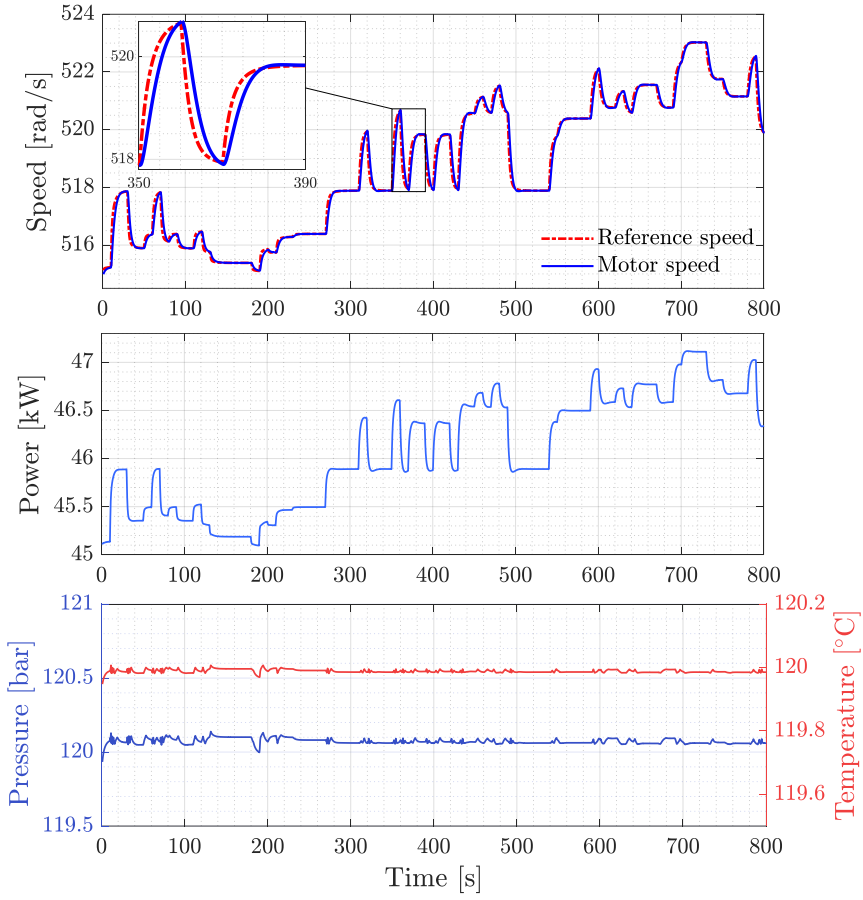

Figure 3.14: The dynamic performance of the fifth compressor in the H_2 compression stage and reactor inlet pressure and temperature.

The simulations have been carried out for different frequency profiles to evaluate the control performance. The Root Mean Square (RMS), mean and Standard Deviation (SD) of the error are calculated for the controlled variables and the reactor operating parameters. As given in Table 3.2, the control system has a robust performance with limited errors in different operating conditions.

Since the pressure and temperature are optimally controlled, the reactor product can only be influenced by the variations in the hydrogen flow rate. Fig. 3.18 illustrates the reactor performance under FCR provision. The AAR, productivity, and CO_2 conversion behave as a function of hydrogen flow rate. As the grid frequency rises, the hydrogen flow rate and productivity increases as well. Consequently, the AAR and CO_2 conversion rate decrease. This is

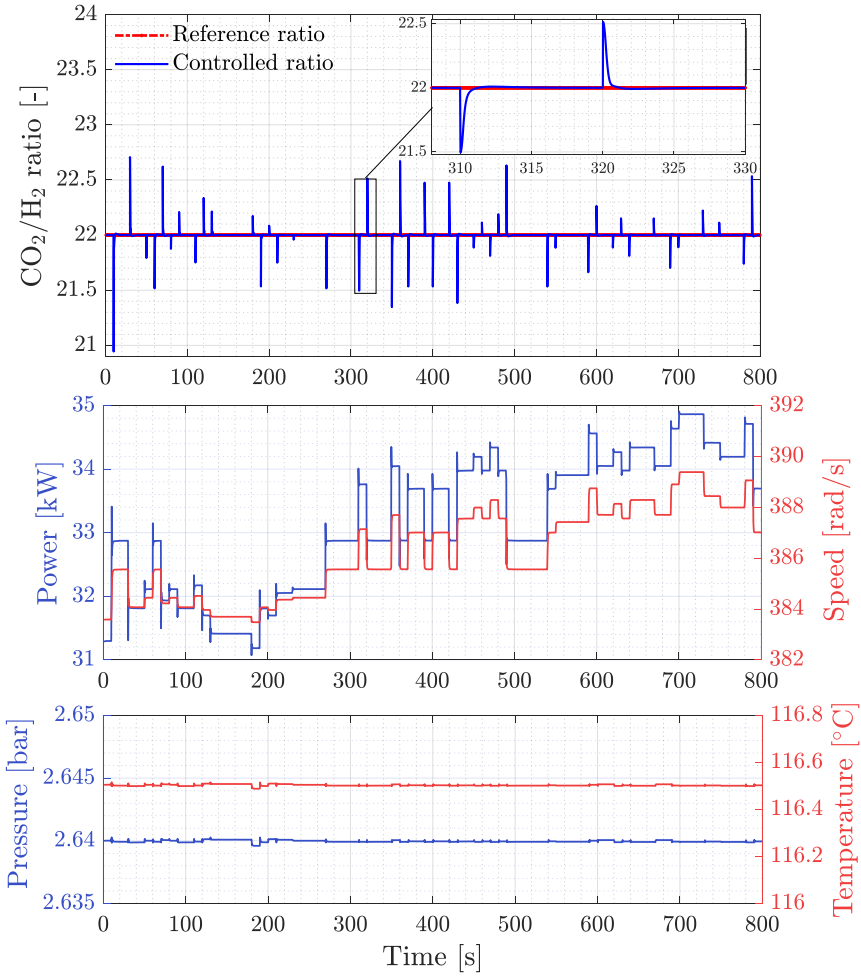

Figure 3.15: The dynamic performance of the first compressor in the CO_2 compression stage.

to be expected since the flow rate increases reducing the residence time. As observed, for the system studied [32], 10% changes in the H_2 flow have a small effect in the CO_2 conversion rate (< 1%), and even smaller changes in the AAR (< 0.02%). Such variations must be considered by the separation process and are expected to have no effect in the overall efficiency of the separation [49,50]. However, they need to be accounted for in the equipment sizing.

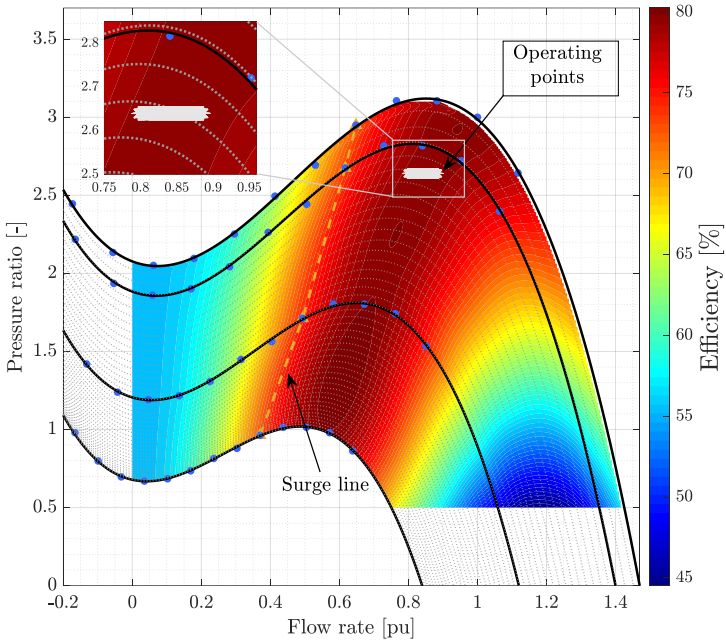

Figure 3.16: The performance of the first compressor in the CO_2 compression stage on the efficiency map.

3.6 Discussion and Conclusions

Chemical plants with intensive electricity consumption can be engaged in grid balancing programs by providing a megawatt-scale power reserve. However, providing grid requirements is challenging due to the chemical process constraints. The chemical processes should operate flexibly to allow active participation of the chemical plant in the ancillary market. The flexible operating strategy must satisfy the grid requirements while respecting the process efficiency and constraints. Therefore, dynamic plant models and control algorithms are needed to achieve the optimal flexible operation of a chemical process. In this article, a flexible operating strategy is proposed to facilitate the integration of an energy-intensive CCU based process into the power grid. The flexible operation is realised through a cooperative operation of the PEM electrolyser and the multi-stage compression systems in the process. The chemical process uses CO_2 and H_2 as raw materials to produce formic acid, which is a valuable multi-purpose chemical compound. The process is based on the continuous hydrogenation of CO_2 over heterogenised ruthenium catalysis. Dynamic models representing the flexible and energy-intensive process stages have been employed to investigate the FCR provision by an industrial-scale plant. The dynamic model of the process consists of a PEM electrolyser, compression

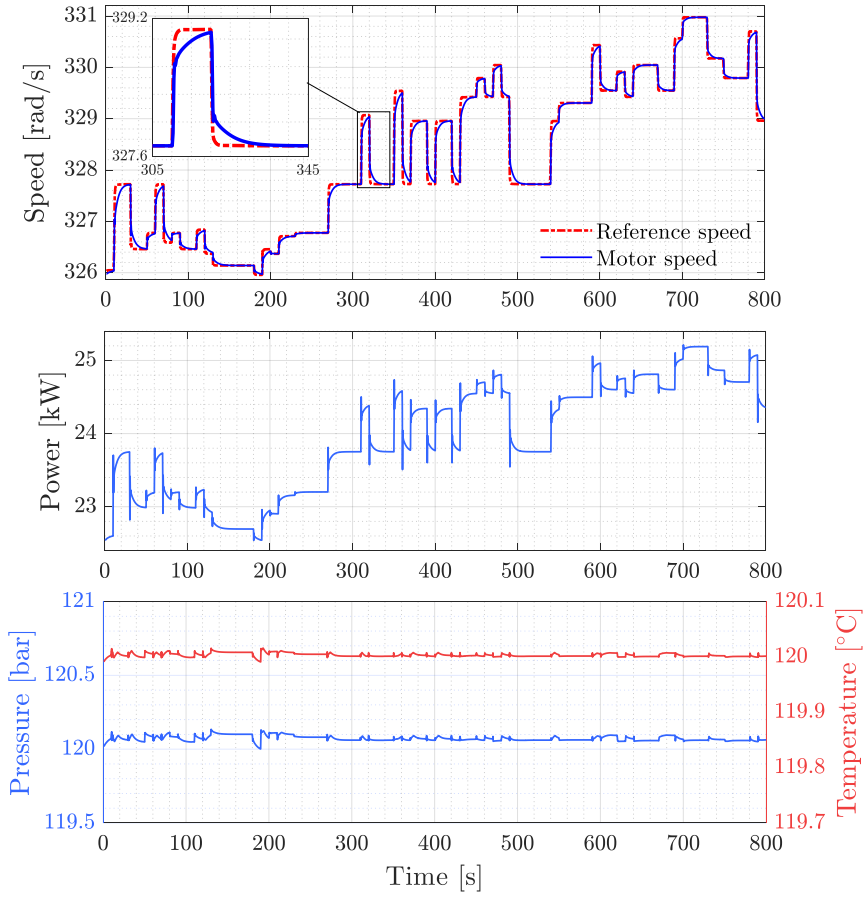

Figure 3.17: The dynamic performance of the fifth compressor in the CO_2 compression stage and reactor inlet pressure and temperature.

stages and a reactor developed for formic acid synthesis. A control algorithm has been designed to enhance the flexibility of the process for FCR provision. The implemented control system regulates the dynamics of the process components, i.e., electrolyser and compressors, to provide ancillary services concerning process efficiency and constraints. The control system reacts to the grid frequency variations by regulating the electrolyser's power input at the primary control level. At the same time, the compressors' capacity is controlled to maintain the optimal operating condition, i.e., CO_2 and H_2 ratio, pressure and temperature. The techno-economic performance of a flexible operating strategy is assessed, and the optimal operating baseload is determined. As a result, the following conclusions can be drawn:

Table 3.2: Error statistics for controlled variables.

	Control system	RMS	Mean	SD
H_2 stream	Electrolyser Power (kW)	1.4572	-0.0114	1.4571
	Compressor 1 Flow rate (kg/h)	0.3532	-0.0027	0.3532
	Compressor 5 Rotational speed (rad/s)	0.2031	-0.0015	0.2031
	Reactor Inlet pressure (bar)	0.1178	0.1171	0.0127
	Reactor Inlet temperature (°C)	0.0871	0.0870	0.0034
CO_2 stream	Compressor 1 Flow rate ratio (CO_2/H_2)	0.0351	0.0001	0.0351
	Compressor 5 Rotational speed (rad/s)	0.0931	-0.0011	0.0931
	Reactor Inlet pressure (bar)	0.1180	0.1173	0.0128
	Reactor Inlet temperature (°C)	0.0033	0.0024	0.0023

- Offering FCR is a valid option to create additional revenue from ancillary services.
- The optimal economic strategy is to run the electrolyser at a baseload of 73% while providing the remaining capacity as a power reserve.
- Although the formic acid production is decreased by 13%, the overall economic performance is increased by 10% by operating the process at the optimal baseload.
- Optimal operating parameters, i.e., ratio, pressure and temperature, are maintained at the reaction stage.
- FCR can be provided with a limited impact on the reaction efficiency (<1%).
- The control algorithm is robust for different operational conditions and grid frequency variations.
- The offered control strategy does not violate the reactor pressure limits.

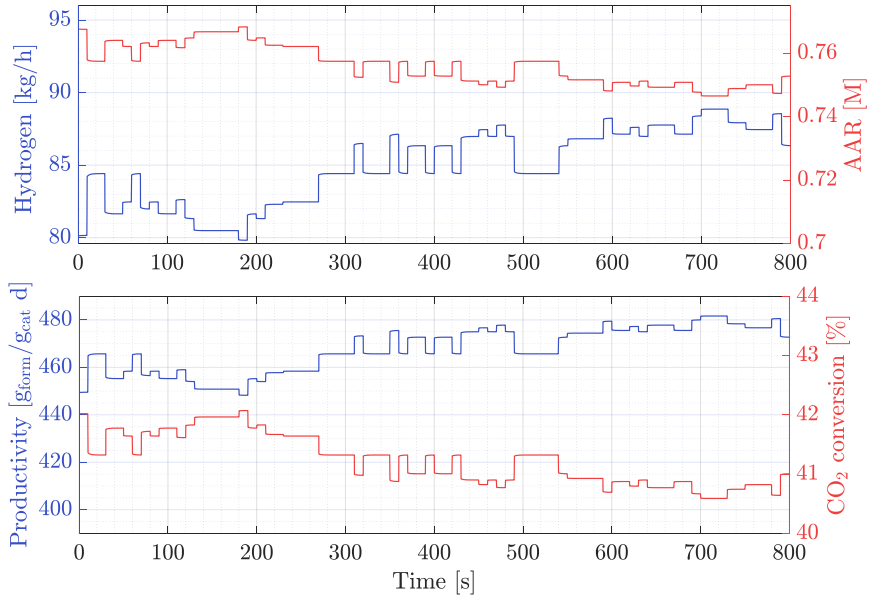

Figure 3.18: Reactor performance under FCR provision.

This paper provides incentive information that can encourage more chemical plants to actively participate in the ancillary market and support the grid. Note that the proposed strategy in this paper is applicable to a variety of chemical processes in which electrolysis and compression are present, e.g., processes for direct conversion of CO_2 and hydrogen to value-added chemicals such as formic acid, methane and methanol. Moreover, since the proposed strategy enables the chemical process to provide FCR as the most time-critical frequency regulation product, the strategy can be efficiently applied to provide ancillary services that require a longer response time, e.g., aFRR and mFRR.

Although the proposed operating strategy enables the FCR provision and improves the process's financial revenue, a number of economic and technical considerations should be taken into account for implementation and future research and development. According to the current TSO regulations, the minimum power reserve of 1 MW is required for FCR provision, which sets a lower boundary on the process size. Therefore, smaller chemical processes with FCR reserves less than 1 MW are not allowed to participate in the ancillary market. In this work, the compressors' capacity and operating points are determined for the proposed flexible operation, while existing compression stages in chemical processes are already designed based on the process requirement without considering the FCR provision. Therefore, the available power reserve might be limited by the capacity of the compressors, and an upgrade might be

required for the optimal operation, e.g., adding compression stages or adapting the compressors. Thus, the most effective approach for optimal contribution in the ancillary market is to consider the proposed demand response operation during the planning phase rather than later in the upgrading phase, which guarantees technical and economic feasibility. Moreover, the optimal baseload and power reserve might be influenced by the uncertain behaviour of the energy and reserve markets. Therefore, applying stochastic optimisation and prediction techniques in future work can improve the bidding strategy to deal with the uncertainties in the market price and support optimal operating decisions. Furthermore, the operational flexibility offered by the proposed strategy facilitates the cooperative operation of the chemical plant with renewable energy sources, where the chemical process can operate as a buffer, utilising the excess generated power for upward and downward regulation services.

Bibliography

[1] A. E. Samani, J. D. M. De Kooning, C. A. Urbina Blanco, and L. Vandevelde, "Flexible operation strategy for formic acid synthesis providing frequency containment reserve in smart grids," *International Journal of Electrical Power & Energy Systems*, vol. 139, p. 107969, 2022. DOI: 10.1016/j.ijepes.2022.107969.

[2] "Communication from the Commission to the European Parliament, the Council, the European Economic and Social Committee and the Committee of the Regions. A policy framework for climate and energy in the period from 2020 up to 2030 (2014)." URL: https://eur-lex.europa.eu/legal-content/EN/ALL/?uri=celex%3A52014DC0015.

[3] S. D. Ahmed, F. S. Al-Ismail, M. Shafiullah, F. A. Al-Sulaiman, and I. M. El-Amin, "Grid integration challenges of wind energy: A review," *IEEE Access*, vol. 8, pp. 10857–10878, 2020. DOI: 10.1109/ACCESS.2020.2964896.

[4] N. Mansouri, A. Lashab, J. M. Guerrero, and A. Cherif, "Photovoltaic power plants in electrical distribution networks: a review on their impact and solutions," *IET Renewable Power Generation*, vol. 14, no. 12, pp. 2114–2125, 2020. DOI: 10.1049/iet-rpg.2019.1172.

[5] M. Musau, "Security and stability aspects of multi objective dynamic economic dispatch with renewable energy and HVDC transmission lines," *Journal of Power and Energy Engineering*, vol. 6, no. 09, p. 165, 2018. DOI: 10.4236/jpee.2018.69013.

[6] M. Paulus and F. Borggrefe, "The potential of demand-side management in energy-intensive industries for electricity markets in germany," *Applied Energy*, vol. 88, no. 2, pp. 432–441, 2011. DOI: 10.1016/j.apenergy.2010.03.017.

[7] M. Manana, A. Zobaa, A. Vaccaro, A. Arroyo, R. Martinez, P. Castro, A. Laso, and S. Bustamante, "Increase of capacity in electric arc-furnace steel mill factories by means of a demand-side management strategy and ampacity techniques," *International Journal of Electrical Power & Energy Systems*, vol. 124, p. 106337, 2021. DOI: 10.1016/j.ijepes.2020.106337.

[8] L. C. Brée, K. Perrey, A. Bulan, and A. Mitsos, "Demand side management and operational mode switching in chlorine production," *AIChE Journal*, vol. 65, no. 7, p. e16352, 2019. DOI: 10.1002/aic.16352.

[9] B. Bruns, A. Di Pretoro, M. Grünewald, and J. Riese, "Flexibility analysis for demand-side management in large-scale chemical processes: An ethylene oxide production case study," *Chemical Engineering Science*, vol. 243, p. 116779, 2021. DOI: 10.1016/j.ces.2021.116779.

[10] C. Tsay, A. Kumar, J. Flores-Cerrillo, and M. Baldea, "Optimal demand response scheduling of an industrial air separation unit using data-driven dynamic models," *Computers & Chemical Engineering*, vol. 126, pp. 22–34, 2019. DOI: 10.1016/j.compchemeng.2019.03.022.

[11] A. Caspari, C. Tsay, A. Mhamdi, M. Baldea, and A. Mitsos, "The integration of scheduling and control: Top-down vs. bottom-up," *Journal of Process Control*, vol. 91, pp. 50–62, 2020. DOI: 10.1016/j.jprocont.2020.05.008.

[12] D. L. Summerbell, D. Khripko, C. Barlow, and J. Hesselbach, "Cost and carbon reductions from industrial demand-side management: Study of potential savings at a cement plant," *Applied energy*, vol. 197, pp. 100–113, 2017. DOI: 10.1016/j.apenergy.2017.03.083.

[13] X. Xu, M. Abeysekera, C. Gutschi, M. Qadrdan, K. Rittmannsberger, W. Markus, J. Wu, and N. Jenkins, "Quantifying flexibility of industrial steam systems for ancillary services: a case study of an integrated pulp and paper mill," *IET Energy Systems Integration*, vol. 2, no. 2, pp. 124–132, 2020. DOI: 10.1049/iet-esi.2019.0082.

[14] K. Seo, T. F. Edgar, and M. Baldea, "Optimal demand response operation of electric boosting glass furnaces," *Applied Energy*, vol. 269, p. 115077, 2020. DOI: 10.1016/j.apenergy.2020.115077.

[15] D. Fabozzi, N. F. Thornhill, and B. C. Pal, "Frequency restoration reserve control scheme with participation of industrial loads," in *2013 IEEE Conference*, (Grenoble, France), 2013. DOI: 10.1109/PTC.2013.6652104.

[16] K. Arnold and T. Janßen, "Demand side management in industry : necessary for a sustainable energy system or a backward step in terms of improving efficiency?," in *Going beyond energy efficiency to deliver savings, competitiveness and a circular economy : ECEEE Industrial Summer Study proceedings ; 12-14 September 2016, Die Kalkscheune, Berlin, Germany*, (Stockholm), pp. 339 – 350, Europ. Council for an Energy Efficient Economy, 2018. URL: https://nbn-resolving.org/urn:nbn:de:bsz:wup4-opus-69405.

[17] M. Cheng, J. Wu, S. J. Galsworthy, C. E. Ugalde-Loo, N. Gargov, W. W. Hung, and N. Jenkins, "Power system frequency response from the control of bitumen tanks," *IEEE Transactions on Power Systems*, vol. 31, no. 3, pp. 1769–1778, 2015. DOI: 10.1109/TPWRS.2015.2440336.

[18] X. Zhang, G. Hug, J. Z. Kolter, and I. Harjunkoski, "Demand response of ancillary service from industrial loads coordinated with energy storage," *IEEE Transactions on Power Systems*, vol. 33, no. 1, pp. 951–961, 2017. DOI: 10.1109/TPWRS.2017.2704524.

[19] J. I. Otashu and M. Baldea, "Scheduling chemical processes for frequency regulation," *Applied Energy*, vol. 260, p. 114125, 2020. DOI: 10.1016/j.apenergy.2019.114125.

[20] F. Klaucke, C. Hoffmann, M. Hofmann, and G. Tsatsaronis, "Impact of the chlorine value chain on the demand response potential of the chloralkali process," *Applied Energy*, vol. 276, p. 115366, 2020. DOI: 10.1016/j.apenergy.2020.115366.

[21] D. Todd, M. Caufield, B. Helms, A. P. Generating, I. M. Starke, B. Kirby, and J. Kueck, "Providing reliability services through demand response: A preliminary evaluation of the demand response capabilities of alcoa inc," *ORNL/TM*, vol. 233, 2008. DOI: 10.2172/948544.

[22] A. E. Samani, A. D'Amicis, J. D. M. De Kooning, D. Bozalakov, P. Silva, and L. Vandevelde, "Grid balancing with a large-scale electrolyser providing primary reserve," *IET Renewable Power Generation*, vol. 14, no. 16, pp. 3070–3078, 2020. DOI: 10.1049/iet-rpg.2020.0453.

[23] A. Dadkhah, D. Bozalakov, J. D. M. De Kooning, and L. Vandevelde, "On the optimal planning of a hydrogen refuelling station participating in the electricity and balancing markets," *International*

Journal of Hydrogen Energy, vol. 46, no. 2, pp. 1488–1500, 2021. DOI: 10.1016/j.ijhydene.2020.10.130.

[24] L. Allidières, A. Brisse, P. Millet, S. Valentin, and M. Zeller, "On the ability of PEM water electrolysers to provide power grid services," *International Journal of Hydrogen Energy*, vol. 44, no. 20, pp. 9690–9700, 2019. DOI: 10.1016/j.ijhydene.2018.11.186.

[25] M. Pérez-Fortes, E. Tzimas, *et al.*, "Techno-economic and environmental evaluation of CO_2 utilisation for fuel production," *Synthesis of methanol and formic acid, 2016*. , DOI: 10.2790/89238.

[26] A. Álvarez, A. Bansode, A. Urakawa, A. V. Bavykina, T. A. Wezendonk, M. Makkee, J. Gascon, and F. Kapteijn, "Challenges in the greener production of formates/formic acid, methanol, and DME by heterogeneously catalyzed CO_2hydrogenation processes," *Chemical reviews*, vol. 117, no. 14, pp. 9804–9838, 2017. DOI: 10.1021/acs.chemrev.6b00816.

[27] D. Mellmann, P. Sponholz, H. Junge, and M. Beller, "Formic acid as a hydrogen storage material–development of homogeneous catalysts for selective hydrogen release," *Chemical Society Reviews*, vol. 45, no. 14, pp. 3954–3988, 2016. DOI: 10.1039/C5CS00618J.

[28] J. Artz, T. E. Müller, K. Thenert, J. Kleinekorte, R. Meys, A. Sternberg, A. Bardow, and W. Leitner, "Sustainable conversion of carbon dioxide: an integrated review of catalysis and life cycle assessment," *Chemical reviews*, vol. 118, no. 2, pp. 434–504, 2018. DOI: 10.1021/acs.chemrev.7b00435.

[29] "Marketsandmarkets. formic acid market by types, application & geography," , 2019, URL: https://www.marketsandmarkets.com/Market-Reports/formic-acid-Market-69868960.html.

[30] "Oec. formic acid product trade, exporters and importers, the observatory of economic complexity," , URL: https://oec.world/en/profile/hs92/formic-acid?redirect=true.

[31] Z. Ma, U. Legrand, E. Pahija, J. R. Tavares, and D. C. Boffito, "From co_2 to formic acid fuel cells," *Industrial & Engineering Chemistry Research*, vol. 60, no. 2, pp. 803–815, 2020. DOI: 10.1021/acs.iecr.0c04711.

[32] K. Park, G. H. Gunasekar, S.-H. Kim, H. Park, S. Kim, K. Park, K.-D. Jung, and S. Yoon, "CO_2 hydrogenation to formic acid over heterogenized ruthenium catalysts using a fixed bed reactor with separation units," *Green Chemistry*, vol. 22, no. 5, pp. 1639–1649, 2020. DOI: 10.1039/C9GC03685G.

[33] Q. Wang, S. Santos, C. A. Urbina-Blanco, W. Y. Hernández, M. Impéror-Clerc, E. I. Vovk, M. Marinova, O. Ersen, W. Baaziz, O. V. Safonova, *et al.*, "Solid micellar Ru single-atom catalysts for the water-free hydrogenation of CO_2 to formic acid," *Applied Catalysis B: Environmental*, vol. 290, p. 120036, 2021. DOI: 10.1016/j.apcatb.2021.120036.

[34] Y. Matsubara, D. C. Grills, and Y. Koide, "Thermodynamic cycles relevant to hydrogenation of CO_2 to formic acid in water and acetonitrile," *Chemistry Letters*, vol. 48, no. 7, pp. 627–629, 2019. DOI: 10.1246/cl.190180.

[35] J. J. Anderson, D. J. Drury, J. E. Hamlin, and A. G. Kent, "Process for the preparation of formic acid," no. WO1986002066A1. 2019, URL: https://patentscope.wipo.int/search/en/detail.jsf?docId=WO1986002066.

[36] M. Mohanpurkar, Y. Luo, D. Terlip, F. Dias, K. Harrison, J. Eichman, R. Hovsapian, and J. Kurtz, "Electrolyzers enhancing flexibility in electric grids," *Energies*, vol. 10, no. 11, p. 1836, 2017. DOI: 10.3390/en10111836.

[37] B. W. Tuinema, E. Adabi, P. K. Ayivor, V. G. Suárez, L. Liu, A. Perilla, Z. Ahmad, J. L. R. Torres, M. A. van der Meijden, and P. Palensky, "Modelling of large-sized electrolysers for real-time simulation and study of the possibility of frequency support by electrolysers," *IET Generation, Transmission & Distribution*, vol. 14, no. 10, pp. 1985–1992, 2020. DOI: 10.1049/iet-gtd.2019.1364.

[38] R. F. Mann, J. C. Amphlett, M. A. Hooper, H. M. Jensen, B. A. Peppley, and P. R. Roberge, "Development and application of a generalised steady-state electrochemical model for a PEM fuel cell," *Journal of power sources*, vol. 86, no. 1-2, pp. 173–180, 2000. DOI: 10.1016/S0378-7753(99)00484-X.

[39] M. Rubio, A. Urquia, and S. Dormido, "Diagnosis of PEM fuel cells through current interruption," *Journal of Power Sources*, vol. 171, no. 2, pp. 670–677, 2007. DOI: 10.1016/j.jpowsour.2007.06.072.

[40] C. Martinson, G. Van Schoor, K. Uren, and D. Bessarabov, "Equivalent electrical circuit modelling of a proton exchange membrane electrolyser based on current interruption," in *2013 IEEE International Conference on Industrial Technology (ICIT)*, pp. 716–721, IEEE, 2013. DOI: 10.1109/ICIT.2013.6505760.

[41] K. Darowicki and L. Gawel, "Impedance measurement and selection of electrochemical equivalent circuit of a working PEM fuel cell cathode," *Electrocatalysis*, vol. 8, no. 3, pp. 235–244, 2017. DOI: 10.1007/s12678-017-0363-0.

[42] C. A. Martinson, G. Van Schoor, K. Uren, and D. Bessarabov, "Characterisation of a PEM electrolyser using the current interrupt method," *International journal of hydrogen energy*, vol. 39, no. 36, pp. 20865–20878, 2014. DOI: 10.1016/j.ijhydene.2014.09.153.

[43] J. D. De Kooning, J. Van de Vyver, B. Meersman, and L. Vandevelde, "Maximum efficiency current waveforms for a PMSM including iron losses and armature reaction," *IEEE Transactions on Industry Applications*, vol. 53, no. 4, pp. 3336–3344, 2017. DOI: 10.1109/TIA.2017.2681619.

[44] B.-H. Bae, S.-K. Sul, J.-H. Kwon, and J.-S. Byeon, "Implementation of sensorless vector control for super-high-speed PMSM of turbocompressor," *IEEE Transactions on Industry Applications*, vol. 39, no. 3, pp. 811–818, 2003. DOI: 10.1109/TIA.2003.810658.

[45] "FCR service design note," , April 2019, URL: https://www.elia.be/-/media/project/elia/elia-site/electricity-market-and-system—document-library/balancing—balancing-services-and-bsp/2019/2019-design-note-fcr-for-2020.pdf.

[46] "Establishing a guideline on electricity transmission system operation," *Official Journal of the European Union*, 2017. URL: https://eur-lex.europa.eu/.

[47] M. Pérez-Fortes, J. C. Schöneberger, A. Boulamanti, G. Harrison, and E. Tzimas, "Formic acid synthesis using CO_2 as raw material: Techno-economic and environmental evaluation and market potential," *International Journal of Hydrogen Energy, volume=41, number=37, pages=16444–16462, year=2016, publisher=Elsevier, note=DOI: 10.1016/j.ijhydene.2016.05.199*.

[48] "Frequency and fcr demand per 10 seconds," URL: https://opendata.elia.be/explore/dataset/ods057/information/.

[49] K. Narita and M. Sekiya, "Vapor-liquid equilibrium for formic acid-triethylamine system examined by the use of a modified still. formic acid-trialkylamine azeotropes," *Chemical and Pharmaceutical Bulletin*, vol. 25, no. 1, pp. 135–140, 1977. DOI: 10.1248/cpb.25.135.

[50] J. Hietala, A. Vuori, P. Johnsson, I. Pollari, W. Reutemann, and H. Kieczka, "Formic acid," *Ullmann's encyclopedia of industrial chemistry*, vol. 1, pp. 1–22, 2016. DOI: 10.1002/14356007.a12_013.pub3.

Chapter 4

Flexible operation of wind turbines to provide ancillary services

As the share of renewable energy increases in the world's energy supply, an effective integration of wind power into the grid becomes increasingly important. Classically, wind turbines were designed and controlled to maximise energy yield in low wind regimes and generate nominal power at high wind speeds while limiting the structural loads. With a higher integration of wind power into the grid, there is an increasing interest in providing ancillary services through a flexible operation of wind turbines or wind farms. The output power is regulated based on the grid frequency and the flexible operating strategy. The effective contribution of wind power in the ancillary market can be beneficial for both grid operators and wind plant owners/operators. The flexible operation capability can support the grid stability and reliability while reducing the cost of energy, leading to a higher level of renewable integration. In this context, a novel control design is required to enable the flexible operation of wind turbines while minimising the load on wind turbine components.

Different control designs have been investigated for the flexible operation of wind turbines in frequency regulation schemes. However, there are a number of challenges that need to be addressed to enable the FCR provision and to respond to the frequency variations to a full extent. One of the challenges is the ramp rate, i.e., the rate of change in output power concerning the fast frequency variation of the grid, which is limited by the rotor inertia and the delay of the pitch actuator. Moreover, the flexible operation creates a higher load on the pitch mechanism and the structure of wind turbines. In particular, floating wind turbines experience even higher structural loads and more elevated tower and platform oscillations, leading to a significant reduction in the expected life of a

wind turbine. Therefore, the need arises for an advanced control to enhance the flexibility of the wind turbines while mitigating the loads on the wind turbine components.

This chapter introduces Horizontal Axis Wind Turbine (HAWT) drivetrain models, including a pitch and torque control system design. Two control strategies, i.e., the pitch-to-stall and pitch-to-feather control concepts, are compared in terms of power regulation, the impact on structural loads and the pitch mechanism in the whole operating region. The performance of the control strategies is investigated to realise the potential advantages that each strategy can offer for flexible operation of HAWTs to provide ancillary services, i.e., ramp rate in power reference tracking and structural loads. The control performance and its impact on the pitch mechanism and structural loads are validated in uniform and turbulent winds.

The contents of this chapter are published in [1, 2].

The Impact of Pitch-to-Stall and Pitch-to-Feather Control on the Structural Loads and the Pitch Mechanism of a Wind Turbine

Arash E. Samani, Jeroen D. M. De Kooning, Nezmin Kayedpour, Dimitar Bozalakov, Narender Singh, Lieven Vandevelde

Published in in "Energies", 2020

Abstract *This article investigates the impact of the pitch-to-stall and pitch-to-feather control concepts on horizontal axis wind turbines (HAWTs) with different blade designs. Pitch-to-feather control is widely used to limit the power output of wind turbines in high wind speed conditions. However, stall control has not been taken forward in the industry because of the low predictability of stalled rotor aerodynamics. Despite this drawback, this article investigates the possible advantages of this control concept compared to pitch-to-feather control with an emphasis on the control performance and its impact on the pitch mechanism and structural loads. In this study, three HAWTs with different blade designs, i.e., untwisted, stall-regulated, and pitch-regulated blades, are investigated. The control system is validated both in uniform and turbulent wind speed. The results show that pitch-to-stall control enhances the constant power control for wind turbines with untwisted and stall-regulated blade designs. Stall control alleviates the fore-aft tower loading and the blades flapwise moment of the wind turbine with stall-regulated blades in uniform winds. However, in turbulent winds, the flapwise moment increases to a certain extent compared to pitch-to-feather control. Moreover, pitch-to-stall control considerably reduces the summed blade pitch movement, despite that it increases the risk of surface damage in the rolling bearings due to oscillating movements with a small amplitude.*

4.1 Introduction

The worldwide installed wind power capacity reached over 651 GW by the end of 2019, growing with 60.4 GW in the last year alone [3]. The exponential growth of the wind turbine market challenges manufacturers to reduce the wind turbines' capital costs, which leads to a reduction of the Cost of Energy (CoE). To further reduce manufacturing costs, more attention is required for the material use in current wind turbine designs, i.e., use of steel, concrete, and composite materials. Therefore, to design future wind turbines with lower material costs, the knowledge and reduction of mechanical loads on the structure of wind turbines are crucial. The fatigue loads are strongly determined by the

actions of the control system, e.g., pitch control, variable speed control and yaw control. A proper control system design requires a compromise between several conflicting objectives, i.e., power output regulation versus limiting the mechanical loads. In this regard, different control concepts have been developed to improve performance and reduce structural loads and fatigue. Individual pitch systems have been implemented to mitigate the load without modifying the blade [4, 5]. However, these systems have a higher energy consumption and have a limited impact on load reduction [6]. The research on active flow control, e.g., trailing edge flaps, microtabs and synthetic jet actuators, had much progress in the last decade. Although these systems reduce the structural loads, they significantly add more complexity to the blade design and blade manufacturing [7, 8].

The Operations and Maintenance (O&M) costs are estimated to amount up to 30% of the Total Cost of Ownership (TCO) [9]. Therefore, enhancing the reliability of wind turbines is one of the important determinants in reducing the Cost of Energy (CoE). A well-designed control system can ensure the wind turbines reliability by reducing failure rates and downtime. The pitch system accounts for one of the critical sub-assemblies with high failure rates, especially for offshore wind turbines [10]. For blade bearings, four-point contact rolling bearings are usually used to minimise the bearings' friction moment, and to avoid undesired large pitching. The separating lubrication film is formed if the rolling bearings rotate continually under nearly constant load and speed [11]. One of the concerns in the pitch system is the risk of surface wear in the blade bearings, i.e., adhesive and abrasive wear caused by oscillating pitch movements with a small amplitude. The bearings movement pattern is dictated by the pitch control strategy, i.e., Collective Pitch Control (CPC), Individual Pitch Control (IPC), pitch-to-stall, and pitch-to-feather. In [12], Stammler et al. compared the IPC and CPC effect on the loads and blade bearing movements of wind turbines. The results show that despite the expected negative impact of IPC on the blade bearings' lifetime, the risk of wear decreases because of the reduction in small pitch movements. Therefore, besides the impact of the blade pitching strategy on the structural loads, its impact on the pitch mechanism needs to be analysed as well.

In high wind speeds, the rotor speed can be limited by a blade pitching system either by pitching the blades to feather or to stall. The pitch-to-stall control concept has not been widely used in wind industry because of the uncertainty of the rotor aerodynamics in the stall condition. Larsen and Hansen monitored the pitch-to-stall impact on the performance of an offshore HAWT with a pitch-regulated blade design. The simulation results showed that the stall control improved the constant power generation and tower stability compared to pitch control [13]. Also, Jonkman tested pitch-to-stall control on the NREL 5 MW offshore wind turbine with a pitch-regulated blade design. The results

verified that active stall control again improved the rotor speed and power control, though it does not dampen the barge-pitch motions [14]. Macquart and Maheri redesigned the original pitch regulated blade of the NREL 5 MW wind turbine to reach a better performance in stall-regulated operation. It was shown that the amplitude of the cyclic loads was reduced in pitch-to-stall control [15]. In [16], it is shown that back-twisted blades together with pitch-to-stall control improve the tower axial fatigue life and power output generation of a semi-submersible floating offshore wind turbine. In [17], Loza et al. performed a comparative fatigue life assessment for a small wind turbine operating as a stall-regulated and pitch-regulated turbine. The stall control is implemented by regulating the generator torque at high wind speeds while the pitch angle is kept at a fixed value, i.e., speed stall control. The results show that stall regulation leads to higher fatigue loads on the blades. However, the impact is smaller than thought before, and stall regulation may be a valid option for a cost-effective design for small wind turbines.

This article provides a thorough investigation of the potential benefits of the pitch-to-stall versus the pitch-to-feather control strategies. The dynamic performance under uniform and turbulent winds, the structural loading of the blades and tower, and the blade bearing movements in the pitch system will be investigated. This will be done for three wind turbines with fundamentally different blade designs, i.e., untwisted, pitch-regulated, and stall-regulated blades to represent the aerodynamic behaviour of a wide range of wind turbines in the market, i.e., from small, medium up to large scale wind turbines. The open-source FAST software, which models the wind turbine, is coupled with a Matlab/Simulink model containing the generator and control systems.

This article is organised as follows: § 4.2.1 describes the wind turbine model and generator system. § 4.2.2 explains the pitch-to-feather and pitch-to-control control systems. Their performance is validated in § 4.3.1. The wind field simulation is explained in § 4.3.2. The dynamic performance of the wind turbine in turbulent wind flow is assessed in § 4.3.3. The impact of the control on the pitch mechanism and structural loads is assessed in § 4.3.4 and § 4.3.5, respectively.

4.2 Methodology

4.2.1 Wind turbine generation system

Figure 4.1 shows the structure of a modern wind turbine system based on a Permanent Magnet Synchronous Generator (PMSG). The turbine rotor (a) harvests the kinetic energy in the wind and drives the PMSG (b). Due to the high pole pair number of the generator, a gearbox is not used in this topology, i.e., it is a direct-drive system. The output voltage of the PMSG has a variable

amplitude and frequency and is converted to a dc voltage by the rectifier (c), which also regulates the generator torque, e.g., for Maximum Power Point Tracking (MPPT). The inverter (d) injects the electrical power into the grid (e).

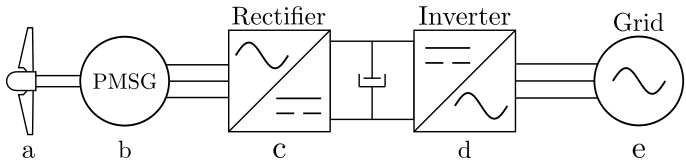

Figure 4.1: Overview of the considered wind turbine system

Three wind turbines with a different power rating and blade design are simulated in this article, i.e., the SWRT 10 kW turbine with untwisted blades, the UAE 20 kW turbine with stall-regulated blades and the WP 1.5 MW turbine with pitch-regulated blades. The specifications of these turbines are given in Table 4.1. Table 4.3 in appendix gives more details on the blade design, i.e., the aerofoil distribution and twist angles of respectively the untwisted, stall-regulated and pitch-regulated blades. Figure 4.2 shows the power coefficient C_P of the wind turbines as a function of the pitch angle θ and the tip speed ratio λ. The FAST turbine models are coupled to a generator and converter model implemented in Matlab/Simulink. The PMSG is modelled by an equivalent scheme in the rotating reference frame, including its dynamics, copper losses and iron losses [18]. A field oriented vector control is used to regulate the generator torque.

Table 4.1: Wind turbines model specification

Turbine Name	**No. Blades**	**Rotor diameter** (m)	**Rated power** (kW)	$\mathbf{C_P^{max}}$ (-)	$\boldsymbol{\lambda_{opt}}$ (-)	$\boldsymbol{\theta_{opt}}$ (°)	**Rated wind speed** (m/s)	**Rated RPM**
SWRT	3	5.8	10	0.42	5.5	7	11.5	210
UAE	2	10	20	0.42	6.4	1	10	122
WP	3	70	1500	0.50	7.3	2.5	11	22

4.2.2 Control system

As illustrated in Figure 4.3, the operating area of a wind turbine can be subdivided into four regions. In region I, below the cut-in wind speed v_{cut-in}, the turbine does not generate power. In region II, above the cut-in speed v_{cut-in}, Maximum Power Point Tracking (MPPT) is used to maximise power. Region III is a transition region between regions II and IV, and the wind turbine operates around nominal rotational speed, but below the rated power. In region IV, above the rated wind speed v_r, both power and rotor speed are limited to avoid

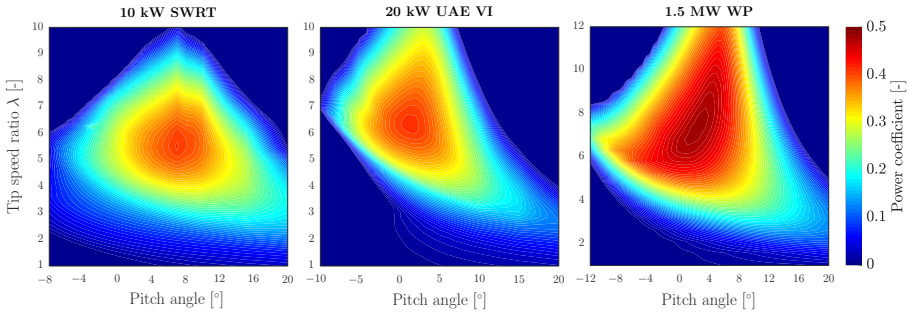

Figure 4.2: Power coefficient C_P of the wind turbines as a function of pitch angle θ and tip speed ratio λ.

exceeding their rated values. If the wind speed rises above the cut-out speed $v_{cut-out}$, the braking system brings the rotor to a standstill for safety reasons.

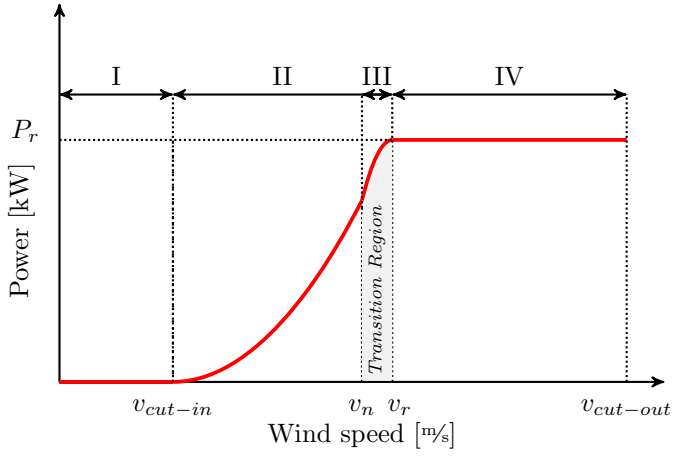

Figure 4.3: Wind turbine power curve and operational regions.

In region II, the control objective is to maximise power for any given wind speed, by maximising the power coefficient. This is achieved by regulating the generator speed and torque in a cascaded control system. The MPPT algorithm is of the Power-Signal Feedback (PSF) type, which uses a pre-defined look-up table to determine the reference power in terms of the measured rotor speed. The advantage of the PSF algorithm over the TSR method is that it does not require wind measurements. Also, the PSF method is more efficient than slow control techniques such as Hill Climb Search (HCS), which searches for the optimum in a step-by-step manner. The look-up table data are generated by

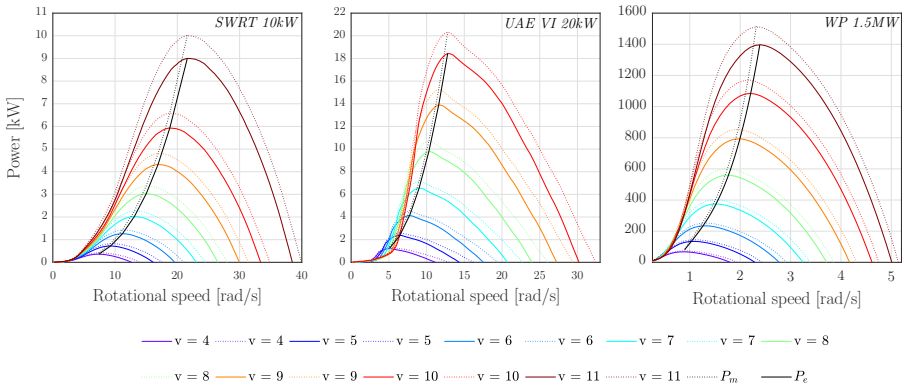

Figure 4.4: Electrical MPPT versus mechanical MPPT for SWRT, UAE and WP wind turbines.

simulating power-speed characteristic curves for different wind speeds. Figure 4.4 shows the power-speed curves of the SWRT, UAE, and WP turbines over the wind speeds in region II. In the simulations, both the mechanical power P_m of the turbine and the electrical power P_e injected into the grid are simulated. The mechanical and electrical power differ due to the losses in the system [19–21]. To reach maximum efficiency, these losses must be taken into account by the MPPT. Therefore, the look-up table data are extracted from the electrical power, not the mechanical power.

At wind speeds higher than the nominal value, the aerodynamic power is limited by reducing the lift forces on the wind turbine blades, which is obtained by regulating the angle of attack through pitching the blades. The lift coefficient C_l increases linearly when increasing the angle of attack up to a certain value, i.e., the critical or stalling angle of attack, at which the lift coefficient reaches its maximum value C_l^{max}. A further increase of the blades' angle of attack leads to a drastic reduction in lift, which is known as stall. Therefore, in the high wind region, the aerodynamic power can be limited by using two different control strategies, as described below:

- Pitch-to-feather (pitch control): The rotational speed is limited to the rated value by pitching the blades to feather. By pitching the blades' leading edge into the wind, the aerodynamic process of blade feathering occurs, which causes a reduction of the aerodynamic forces. Therefore, the speed controller increases the pitch angle, thus reducing the angle of attack, to limit the lift forces and the driving torque. The pitching rate should be high enough to keep the generator speed at its nominal value and deal with the fluctuating nature of wind.

- Pitch-to-stall (stall control): The controller turns the blades in the oppo-

site direction to the direction of pitch-to-feather, i.e., turning the blades' leading edge out of the wind, thus increasing the blades' angle of attack beyond the critical or stalling angle of attack. Therefore, the lift forces on the blades are reduced as the lift coefficient exceeds its maximum C_l^{max}.

Pitch control is typically nonlinear because the sensitivity of the system varies under different operating conditions. The pitch sensitivity, denoted by the partial derivative of aerodynamic power with respect to the pitch angle $\frac{\partial P}{\partial \theta}$, is an aerodynamic property of the rotor that depends on the wind speed, rotor speed, and pitch angle. Therefore, the blade has different responses to the pitch angle variations in region IV, which is important for determining the gains of the blade pitch speed controller. Figure 4.5 compares the pitch sensitivity of the wind turbines in the stall and pitch mode from nominal to cut-out wind speed. The blade-pitch sensitivity is calculated for the SWRT, UAE and WP turbines by performing a linearisation analysis in FAST. In each linearisation step, the pitch angle is altered at rated power, and the aerodynamic power sensitivity is calculated. As shown in Figure 4.5, the pitch sensitivity changes with pitch angle for wind speeds in region IV. The negative values of the pitch sensitivity in pitch-to-feather mode are due to the negative variation of aerodynamic power to the positive variation pitch angle, i.e., increasing the pitch angle to reduce the angle of attack. Likewise, the positive value of the pitch sensitivity in pitch-to-stall is due to a negative variation of aerodynamic power to a negative variation in pitch angle, i.e., pitching the blades to the negative direction to increase the angle of attack towards stall. As illustrated in this figure, the aerodynamic sensitivity is lower for the pitch-to-stall mode than pitch-to-feather, which means the aerodynamic power varies more slowly for the negative pitch angles. Also, much smaller pitch actions are needed to control the aerodynamic power. The lower aerodynamic sensitivity may be an advantage to reduce fatigue loads and improve the pitch mechanisms performance, i.e., the blade's pitch bearing movements. In pitch-to-feather, the blades are held in attached flow conditions giving rise to high aerodynamic sensitivity while in the pitch-to-stall process, the boundary layer separates from the upper side of the blade resulting in the low aerodynamic sensitivity. The difference in behaviour of the different wind turbines in stall mode originates from their different blade geometry. The SWRT and UAE wind turbines have thin aerofoils and a high curvature around the leading edge, which tend to stall more abruptly than the WP turbine with a thick aerofoil.

In the pitch-to-feather control mode, the pitch sensitivity varies considerably over the region IV, which requires to schedule the controller gain as a function of the pitch angle. However, the variation of the pitch sensitivity with pitch angle is nearly linear, and it follows the same trend for all three wind turbines, thus:

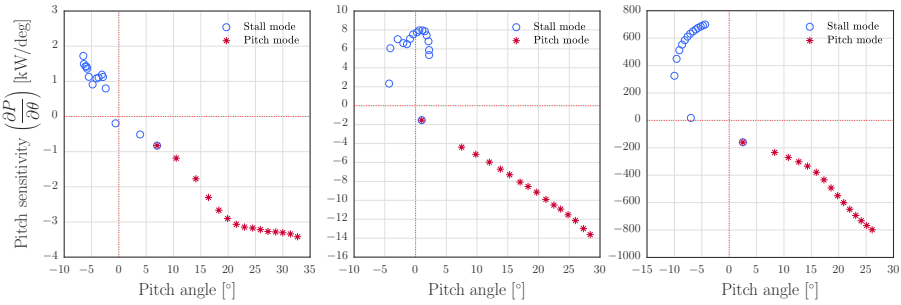

Figure 4.5: Pitch sensitivity $\frac{\partial P}{\partial \theta}$ of the SWRT (left), UAE (center), and WP wind turbines (right) at wind speeds in region IV.

$$\frac{\partial P}{\partial \theta} = \left(\frac{\frac{\partial P}{\partial \theta}(\theta = \theta_r)}{\theta_k} \right) \theta + \left(\frac{\partial P}{\partial \theta}(\theta = \theta_r) \right) \tag{4.1}$$

where $\frac{\partial P}{\partial \theta}(\theta = \theta_r)$ is the sensitivity of aerodynamic power to the pitch angle variation at the rated operating point. The pitch angle θ_k is defined as the angle at which the blade sensitivity has increased by a factor of 2, compared to its value at the rated operating point [22], i.e.:

$$\frac{\partial P}{\partial \theta}(\theta = \theta_k) = 2 \frac{\partial P}{\partial \theta}(\theta = \theta_r) \tag{4.2}$$

Based on the linear relation between the pitch sensitivity $\frac{\partial P}{\partial \theta}$ and the pitch angle θ, the gain scheduling can be implemented by defining a dimensionless gain-correction factor G_k as a function of pitch angle [22, 23]:

$$G_k = \frac{1}{1 + \frac{\theta}{\theta_k}} \tag{4.3}$$

which can be written in a more general form for wind turbines with a non-zero optimal pitch angle as:

$$G_k = \frac{1}{1 + \frac{\theta - \theta_r}{\theta_k}} \tag{4.4}$$

According to (4.4), the controller gains are varied to cope with the variation of the pitch sensitivity in region IV. A higher gain is applied where the sensitivity is low, i.e., where θ is near θ_r, and vice versa.

In the pitch-to-stall mode, the pitch sensitivity varies nonlinearly with pitch angle, and its relation depends on the blade design as well. The aerodynamic sensitivity of the SWRT turbine first decreases with the pitch angle before increasing again by pitching the blades more into the stall condition. A linear gain correction factor for pitch control is not able to deal with this variation of pitch sensitivity. Therefore, a gain correction function is proposed here for the stall control based on its nonlinear behaviour in the stall condition:

$$G_s = \frac{2}{1 + \left(\frac{\theta}{\theta_k}\right)^2} \tag{4.5}$$

The aerodynamic sensitivity of the UAE and WP wind turbines has two values at the same pitch angle, and thus the gain schedule of the stall controller is double-valued. Therefore, the pitch angle signal is not enough to identify the exact operating point. One solution is to measure the wind speed and use the signal as an additional input to determine the operating point. Also, it is possible to only use the pitch signal and detune the controller to ensure that the controller works properly at different wind speeds in region IV [24].

Figure 4.6 shows the pitch system diagram. The controller gains are tuned based on the blade pitch sensitivity in the pitch-to-stall and pitch-to-feather mode. The PI speed controller generates the reference pitch signal θ_{ref}. This signal is sent to the pitch actuator model, which is represented by a first-order transfer function with a time constant T_a. A position and rate limiter are applied to ensure that the actuator limits are not exceeded. The time constant T_a is equal to 0.1 s, and the rate limit is set at 10 °/s for all turbine models [23, 25].

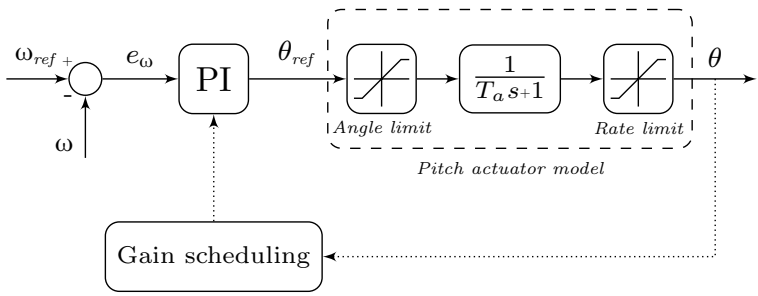

Figure 4.6: Pitch control diagram.

4.3 Verifications and results

4.3.1 Validation of control performance

The performance of both the pitch-to-stall and pitch-to-feather control systems (with gain scheduling) is first verified by simulating the wind turbines in uniform winds. The following objectives are addressed to validate the control performance:

- To maximise the energy capture in the low-speed region by maximising the aerodynamic efficiency of the wind turbine.
- To obtain an identical response for all wind turbines in the whole wind speed range of region IV, i.e., coping with the different sensitivity of the aerodynamic power to the blade pitch angle for each wind speed.

For the uniform wind simulation, the 'Inflowwind' module processes wind-inflow coupled with FAST. This module computes wind velocity components as a function of the input coordinate positions received from FAST glue code and internal time-varying parameters. The horizontal and vertical wind speeds are calculated as follows [26]:

$$\begin{aligned} V_h(x,y,z) =& V_{h_{ref}}\left(\frac{z}{\text{RefHt}}\right)^{\text{VShr}} \\ &+V_{h_{ref}}\left(\frac{\text{HLinShr}}{\text{RefLength}}\right)(x\sin(\text{Delta})+\text{y}\cos(\text{Delta})) \\ &+V_{h_{ref}}\left(\frac{\text{VLinShr}}{\text{RefLength}}\right)(z-\text{RefHt})+V_{Gust} \\ V_z(x,y,z) =& \text{VZ} \end{aligned}$$

where $V_{h_{ref}}$ is horizontal wind speed (vectorial u+v) at reference height, Delta is the wind direction, and VZ is the vertical wind speed (w component). VLinShr and HLinShr are vertical and horizontal linear wind-shear parameters, respectively. V_{Gust} is horizontal gust speed, and VShr is the vertical power-law wind-shear exponent. The Reference height (RefHt) and Reference length for linear horizontal and vertical shear (RefLength) values are set in the module's input file. The power-law wind profile is used to define the wind profile by using the following equation, where PLexp is the Power law exponent.

$$u(z) = \text{URef}\left(\frac{\text{z}}{\text{RefHt}}\right)^{\text{PLexp}} \tag{4.6}$$

For wind speeds below the nominal value, the MPPT controller regulates the generator torque by tracking the reference electrical power. Thus, the optimum

tip speed ratio is obtained by controlling the rotational speed. At the same time, the pitch control system keeps the pitch angle at its optimal value to maximise the aerodynamic efficiency. The step response of the wind turbines operating in low wind speeds is shown in Figure 4.7. As can be observed, when the wind speed increases stepwise from 4 to 7 m/s, the generator speed is regulated so that the optimum tip speed ratio is reached. Therefore, the power coefficient is maximised for all 3 turbines models, showing proper MPPT control.

In the transition zone, when the wind speed reaches the nominal value, the rotor speed is kept constant until the rated electrical power is generated. At wind speeds above the nominal, the speed controller keeps the generator speed at its rated value by pitching the blades based on two different control concepts, i.e., pitch-to-feather and pitch-to-stall. With pitch-to-feather, the pitch angle is increased to positive values, while pitch-to-stall decreases it to negative angles. Figure 4.8 compares the step response of the wind turbines to the wind variation at high wind speeds. As shown, when the wind speed increases stepwise from 14 to 17 m/s, the pitch angle is regulated to keep the rotational speed and thus the power output at the rated value. Also, an identical response of the generator speed and electrical power is obtained in all wind speeds in region IV through proper gain scheduling of the PI controllers in both operating modes, i.e., pitch-to-feather and pitch-to-stall.

As expected from the aerodynamic sensitivity analysis presented in section 4.2.2, when the wind turbine operates with the pitch-to-stall concept, smaller blade pithing is required to maintain the power at the rated value compared to pitch-to-feather. Therefore, the summed pitch manoeuvre, i.e., blade bearing movements, is reduced, and consequently, higher lifetimes of the pitch mechanism can be obtained by limiting the pitch activity. Moreover, in the stall mode, the aerodynamic power is less sensitive to the pitch angle, which increases the controllability in the high wind zone. The more stable aerodynamic response in the pitch-to-stall mode is an advantage for the control system, especially when the trade-off between the rapid changes in pitch angle on the one hand and the abrupt power increase on the other hand is needed, i.e., the power transient caused by a sudden increase of wind speed. The most significant factor in the power limiting strategy of the pitch control system is its fast response to sudden variations in the aerodynamic torque generated by the wind. The rotational speed of a wind turbine can be regulated very quickly by pitching the blades to feather with a fast pitch rate [27]. However, this requires a pitch actuator with a high pitch rate capacity. Also, the fatigue damage rate of the pitch bearings increases when increasing the pitch rate [28].

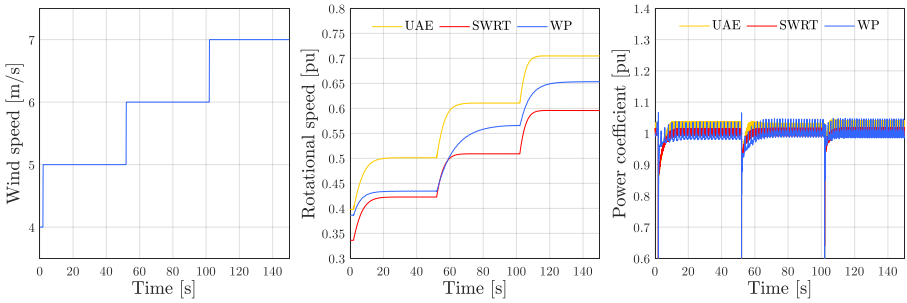

Figure 4.7: Dynamic performance of the SWRT, UAE, and WP wind turbines in the low wind region.

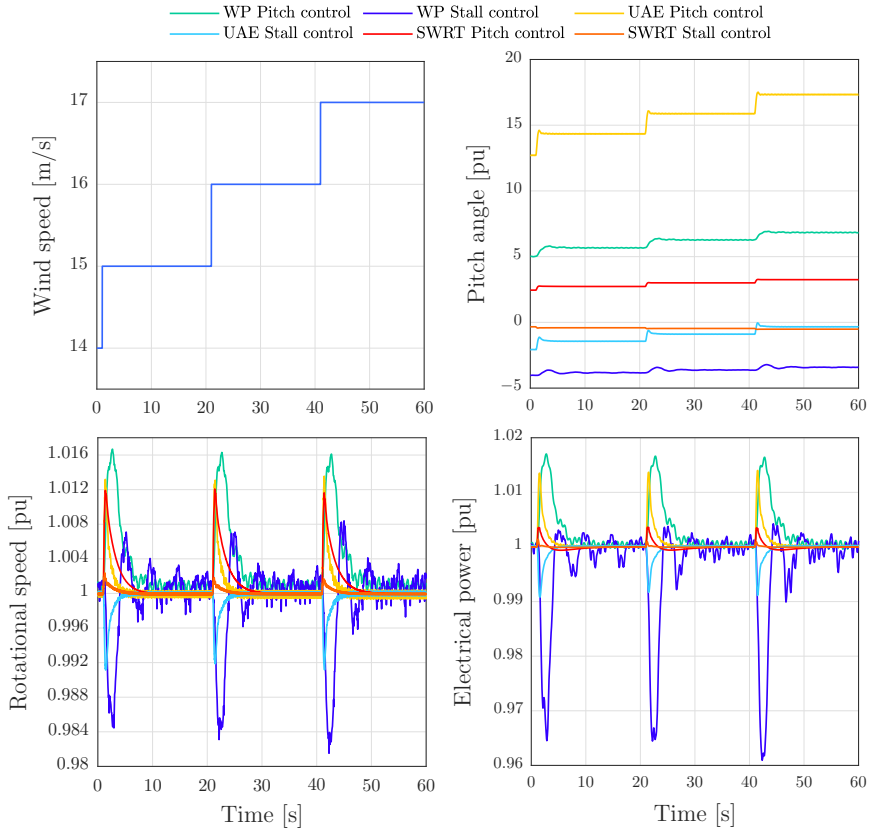

Figure 4.8: Dynamic performance of the SWRT, UAE, and WP wind turbines in the high wind region.

4.3.2 Turbulent wind field simulation

The numerical simulation of the wind field is an essential part of the horizontal axis wind turbine structural analysis, due to the nonlinearity of atmospheric turbulence and its impact on the aerodynamic loads of wind turbines. The structure of the wind turbine experiences higher loads caused by the atmospheric turbulence encountered by the rotor blades. Therefore, for the dynamic aeroelastic simulation of a wind turbine, the inflow wind should be simulated such that it includes the specific characteristics of the inflow wind which have a significant impact on the dynamic response of wind turbine. For the numerical simulation of a full-field flow, the TurbSim inflow stochastic turbulence code is used [29]. TurbSim includes many of the important fluid dynamic features that have an impact on the aeroelastic response of wind turbines. The Turbsim simulator uses a modified version of the Sandia method, which is a method for numerically simulating a three-dimensional field of turbulent wind speed, specifically for the structural analysis of horizontal axis wind turbines [30].

In TurbSim, the rotor hub is assumed to be centred on a grid of points that each represents the three-dimensional wind speed. For each wind turbine, the grid size is considered large enough to cover the whole rotor such that no part of the rotor blade lies outside the grid, even during the wind turbine displacement. The NWTCUP spectral model is used to simulate the turbulent wind, which generates a turbulent inflow that characterises the highly turbulent conditions. This model generates default spatial coherence parameters based on experimental data performed at the National Renewable Energy Laboratory's National Wind Technology Center (NWTC) [31]. The NWTCUP spectrum for stable flows are defined as [29]

$$S_K(f) = \sum_{i=1}^{\mathrm{NumPeaks_K}} p_{i,K} S_{\mathrm{K,SMOOTH}}\left(F_{i,K} f\right) \tag{4.7}$$

where $NumPeaks_K$ is equal to 2 for all wind components. $p_{i,K}$ and $F_{i,K}$ are scaling factors, and they are functions of the gradient Richardson number. The spectrum is characterised by adding scaled versions of the RisÃ¸ smooth-terrain spectral model (SMOOTH), which is defined by the following equations:

$$S_K(f) = UStar^2 \frac{s_{1,K}\left(\frac{z}{\bar{u}\phi_M}\right)\left(\frac{\phi_E}{\phi_M}\right)^{2/3}}{1 + s_{2,K}\left(\frac{fz}{\bar{u}\phi_M}\right)^{5/3}} \tag{4.8}$$

where f is the cyclic frequency, $UStar$ is the friction velocity input parameter, $\bar{u}$ is the mean wind speed at height z, and ϕ_E and ϕ_M are functions of the

stability parameter, i.e., the gradient Richardson number. s_1 and s_2 are defined as

$$\left\langle s_{1,K}, s_{2,K} \right\rangle = \begin{cases} \langle 79.0, 263.0 \rangle & K = u \\ \langle 13.0, 32.0 \rangle & K = v \\ \langle 3.5, 8.6 \rangle & K = w \end{cases} \tag{4.9}$$

For unstable flows, the NWTCUP model modifies the SMOOTH-model as:

$$S_K(f) = p_{1,K} S_{\mathrm{K,low,SMOOTH}}(F_{1,K} f) + p_{2,K} S_{\mathrm{K,high,SMOOTH}}(F_{2,K} f) \tag{4.10}$$

where $P_{1,K}$, $P_{2,K}$, $F_{1,K}$, and $F_{2,K}$ are the scaling factors that are derived from spectra calculated using velocity measurements.

The turbulent wind fields are generated with a high turbulence intensity, a vertical mean flow (uptilt) angle of 8° and a horizontal mean flow (skew) angle of 15°. The mean wind speeds are selected so that the wind profiles cover both region II, where torque control is used for MPPT and pitch control is inactive, and IV, where both torque and pitch control are active to limit the power and rotor speed. Figure 4.9 illustrates the spatial wind field components in streamwise, crosswise, and vertical direction in different time slots for a simulation of 300 seconds with an average speed of 14 m/s. The wind field simulation parameters are given in table 4.2.

Table 4.2: Wind field simulation parameters

Time step	0.050 [s]
Mean wind speed at hub height	14 [m/s]
Turbulent Intensity(TI)	13 [%]
Vertical grid-point matrix dimension	40
Horizontal grid-point matrix dimension	40
Surface roughness length	0.021 [m]
Hub height	34.6 [m]
Assumed rotor diameter	10 [m]

4.3.3 Performance in turbulent wind

To test the control system in more realistic operating conditions, the dynamic performance of the wind turbines is now analysed for a three-dimensional turbulent wind field. Figure 4.10 compares the performance of the turbines operating with the pitch-to-feather and pitch-to-stall strategies in turbulent winds. The simulation results show that the electrical power and rotor speed are regulated at their rated values with a limited error. The control transitions between

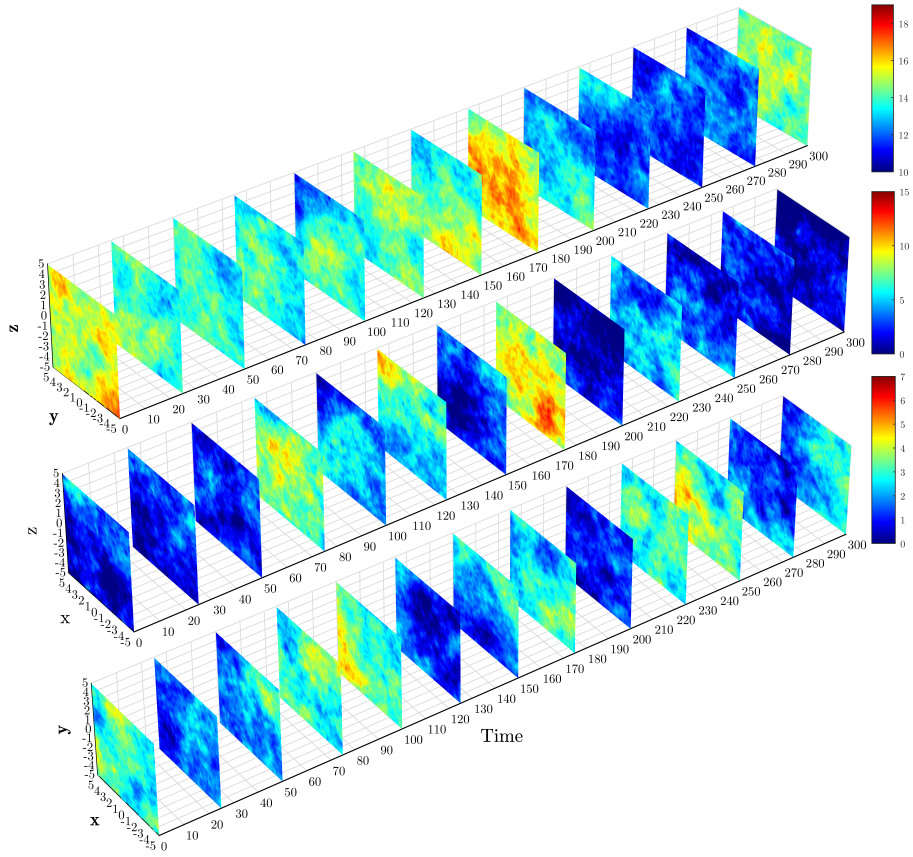

Figure 4.9: Turbulent wind field simulation in streamwise (top), crosswise (middle), and vertical direction (bottom).

region II and IV are smooth without transients. Despite the satisfactory performance of the control system in the whole operating region, wind turbines have different dynamic responses under pitch-to-stall and pitch-to-feather control. The first column shows the SWRT turbine operating as a pitch regulated turbine compared with the same turbine operating as a stall controlled turbine in turbulent wind. As can be observed, the power is well-maintained within 3% of its rated value with pitch-to-feather. However, the fluctuations in the rotor speed and electrical power are considerably smaller when using pitch-to-stall control. As expected from the aerodynamic sensitivity analysis, the aerodynamic power is less sensitive to wind speed variations in region IV. Therefore, the fluctuations in generator speed and the power transients are reduced when using pitch-to-stall control. To illustrate, when the wind turbine operates at wind speeds fluctuating between 12 to 19 m/s (Figure (4.10, time $\approx$ 10-40s) the power generator is well-preserved within 1% of its rated value. More-

over, due to the lower aerodynamic sensitivity, and thus smaller pitch action in pitch-to-stall mode, smoother control with much more moderate pitch movement is obtained. The second column of Figure 4.10 illustrates the dynamic performance of the two-bladed UAE turbine with stall-regulated blade design. Also, here, the rotor speed and power output are regulated well around the nominal value with a limited error. However, pitch-to-stall control presents smaller fluctuations in turbulent wind conditions. As can be observed, when the wind turbine operates around the transition region between II and IV, with a sudden change in wind speed (time ≈ 40-60s), a smaller peak power is obtained above the rated for pitch-to-stall control due to the lower sensitivity and smaller pitch actions in the stall mode. The third column of Figure 4.10 illustrates the performance of the WP turbine under turbulent wind conditions. As shown, pitch-to-stall control does not have the reduction effect on the fluctuations of rotational speed and power output. This behaviour of the WP turbine is due to its pitch-regulated blade design that tends to stall more slowly compare to the SWRT and UAE wind turbines with untwisted and stall-regulated blade designs. The corresponding time histories of tower and blade moments in turbulent wind are represented in Figure 4.11.

4.3.4 Control impact on the pitch mechanism

According to [10], the pitch system accounts for one of the most critical subassemblies in terms of failure rates and downtime. Pitch oscillations with an amplitude of a few degrees increase the risk of surface damage in the rolling contacts of the blade bearings [12]. In a rolling bearing, the rolling elements are separated from the raceway by a thin film of lubricant formed by the nearly constant rotation of bearing under constant or almost constant loads and speeds [11]. In the blade bearings, the blade pitch manoeuvres with relatively small amplitudes often do not build up the lubricant film, which gives rise to an unlubricated contact between the rolling elements and the bearing raceway [32]. Therefore, to increase the reliability of the pitch mechanism, small oscillating movements of blade bearings must be minimised. Cycle analysis is performed to compare the pitch movements of the wind turbines operating with the two investigated control strategies, i.e., pitch-to-stall and pitch-to-feather.

The wind turbines are operated in the full operating region, i.e., from rated wind speed v_r to cut-out wind speed $v_{cut-out}$. The wind fields are generated so that the wind speed sweeps all wind speeds in region IV with a turbulence intensity of 20%. The simulations have been run during 660 seconds, and the corresponding blade pitch movements are monitored. The rainflow method, as implemented in MATLAB, is used to count the cycles for the pitch time history according to the ASTM E 1049 standard. Figure 4.12 illustrates the results of the cycle counting of small blade pitch oscillations. For the SWRT wind

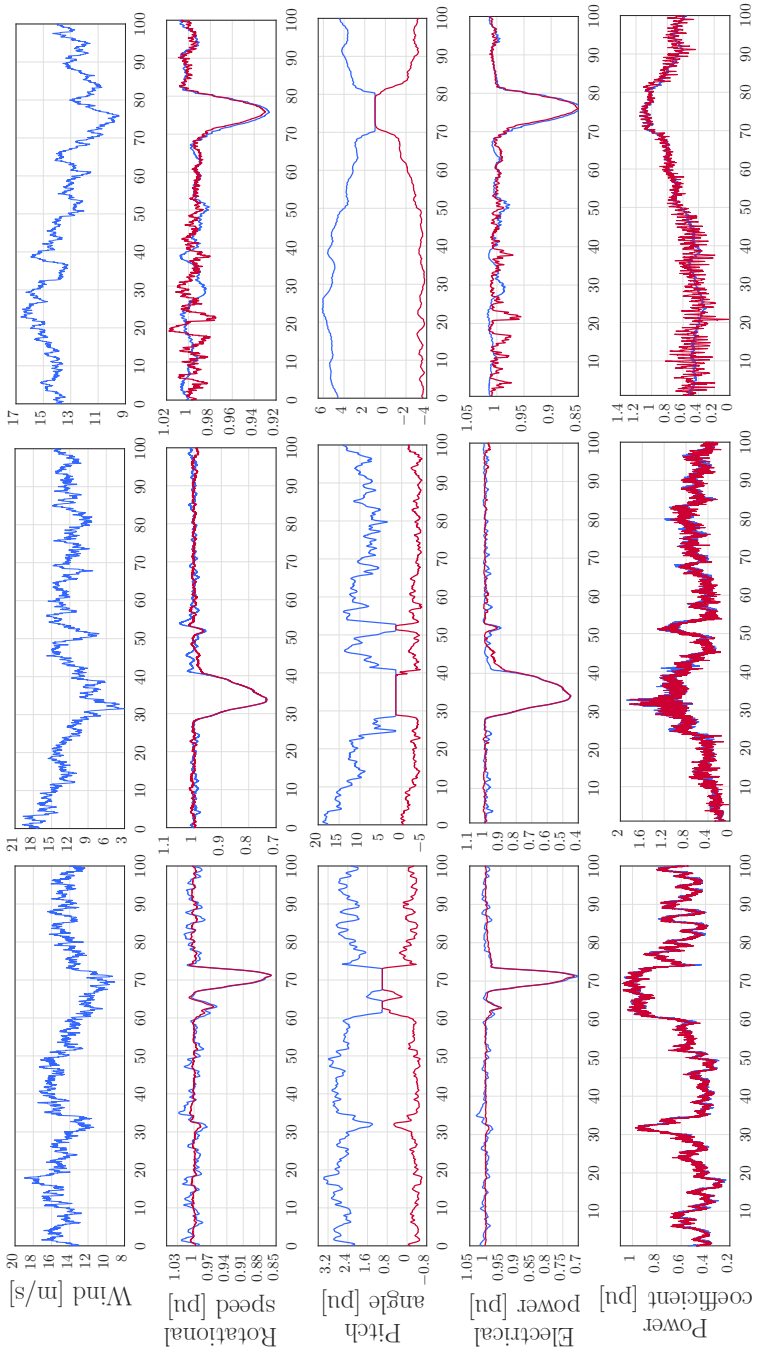

Figure 4.10: Dynamic performance of the SWRT, UAE, and WP wind turbines in turbulent wind.

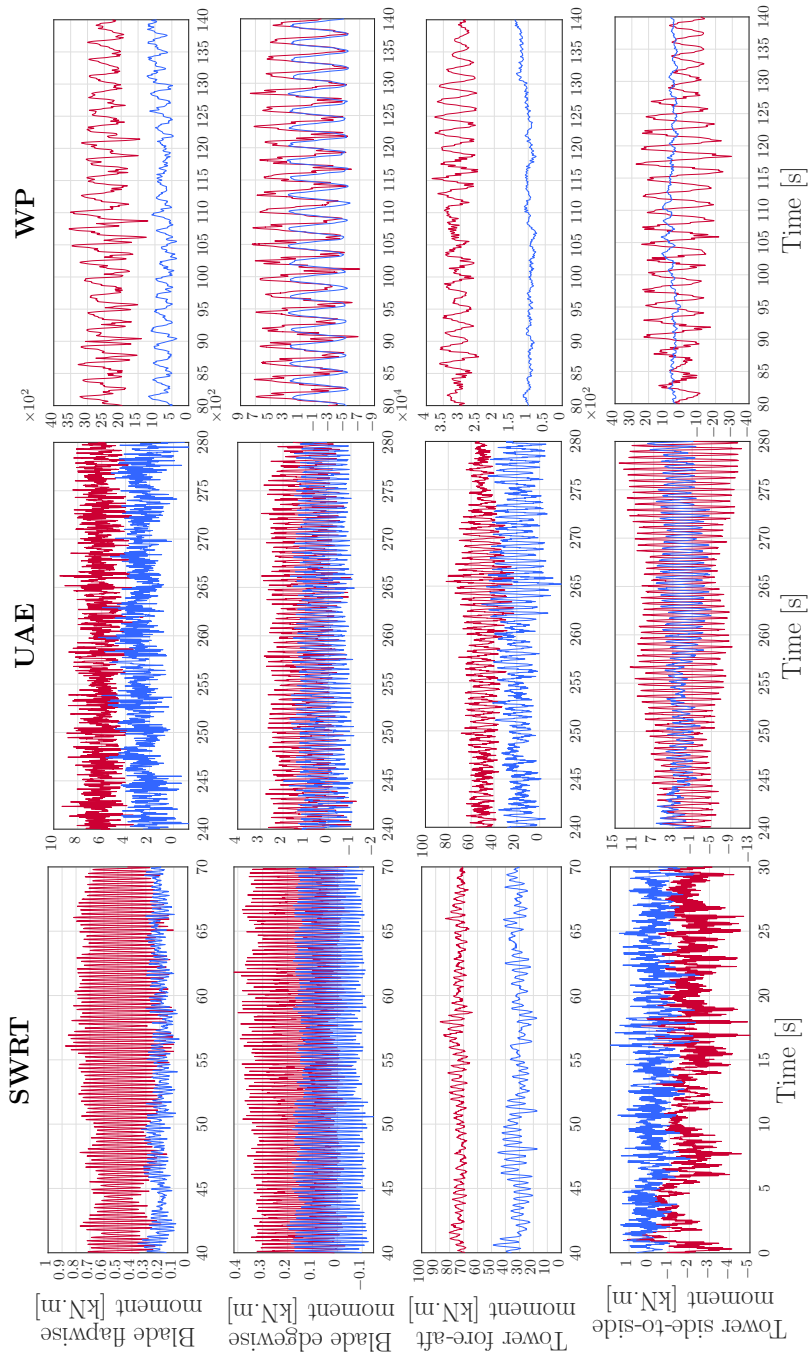

Figure 4.11: Comparison of the structural bending moments of the SWRT, UAE, and WP wind turbines in turbulent wind.

turbine with untwisted blades, the summed pitch movement is reduced from 1607° in pitch-to-feather control to 746° in pitch-to-stall control. However, a higher number of pitch movements with small oscillations are observed in pitch-to-stall control, especially in the range below 0.3°. This behaviour can be explained by the fact that in the stall condition and for wind speeds between 15 and 25 m/s, less pitch variation (≈ 4° [-7 -3]) is required to keep the power at the rated value (Figure 4.5). Therefore, the frequent small pitch variations are expected to limit the rotational speed. Also, pitch-to-stall control increases the cycles with an amplitude smaller than 1.5° for the UAE wind turbine, though a higher number of pitch movements are observed in the range between 1.5 and 5°. Also here, the pitch-to-stall control reduces the summed pitch movement to 15096°, compared to 1655° in pitch-to-feather control. The explanation lies in the way the boundary layer separates from the surface of the blades. SWRT and UAE wind turbines tend to stall more abruptly because of their geometry, where the separation starts around the leading edge of the aerofoil. Therefore, the entire boundary layer may detach almost simultaneously with a drastic decrease in the lift coefficient. The pitch system behaviour in the WP turbine is in contrast with previous models. Due to the pitch-regulated design of the blades, i.e., the airfoils' geometry with a more rounded leading edge, the lift coefficient reduced with a gentle slope, which also can be observed in . Therefore, the blades remain in soft stall conditions, where fine adjustment of the blades is less required.

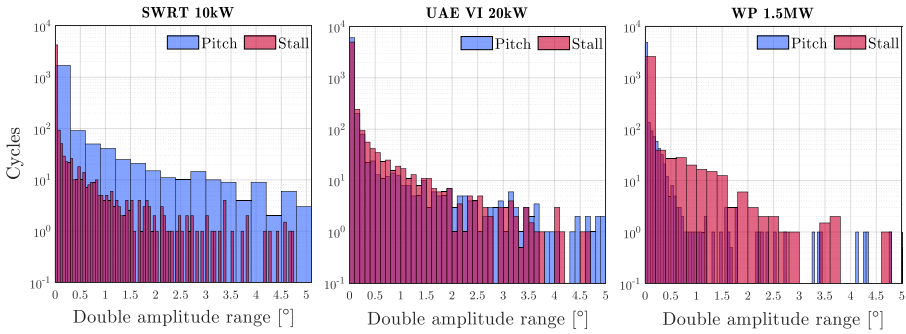

Figure 4.12: Number of cycles pitch-to-feather and pitch-to-stall in comparison for small oscillation amplitude ranges.

4.3.5 Control impact on structural loads

Having discussed the performance of the wind turbines with two different control concepts, i.e., pitch-to-stall and pitch-to-feather, this section investigates

the impact of these control systems on the structural loads. A profound understanding of the structural loads is needed to optimise the design to reduce the capital cost of wind turbines, and to guarantee a safe operation at high wind speeds. The increasing size of wind turbines over the past decade has made fatigue loads a critical issue in the construction of wind turbines. Higher system reliability and considerable cost reduction, i.e., material and maintenance costs, can be achieved by reducing the fatigue loads. According to [33], a load mitigation of 10% - 20% may bring considerable savings for the main components, such as the blade, tower and drivetrain. Additionally, the loads on the structure of the wind turbine must be estimated to ensure a safe operation throughout its lifespan, especially in strong and gusty winds. The extreme wind conditions can lead to an accumulated fatigue damage of the blades.

The impact of the control system on the structural loads of the blades and tower is calculated by using FAST in uniform and realistic winds, including turbulence. The blade root bending moments, i.e., flapwise and edgewise moments, and tower base bending moments, i.e., fore-aft and side-to-side moments, are monitored. The blade flapwise moments and the tower fore-aft moments are caused by the thrust forces, which tend to deflect the blades and tower in the downwind direction. The blades edgewise moments and tower side-to-side moments stem from the tangential forces which tend to bend the blades and tower in the rotor plane.

Figure 4.13 and 4.14 compare the mean load and amplitude of the cyclic component of the blade root and tower base bending moment of the SWRT turbine in uniform and turbulent winds, respectively. In high wind speeds, the mean load on the blades of the pitch regulated wind turbine is reduced compared to the stall controlled wind turbine, in which the mean load rises when increasing the wind speed. The mean load difference is considerably larger at cut-out wind speed, which is an advantage to mitigate the loads when the turbine brakes bring the rotor to a standstill. As it can be observed in these figures, the blades edgewise and flapwise moments amplitude increases when the wind turbine operates as a stall regulated wind turbine. Therefore, the blades experience higher fatigue loads compared to the pitch regulated turbine. However, the stall control has a reduction effect on the tower fatigue loads in a downwind direction. As shown, the tower base fore-aft bending moment reduces in the pitch-to-stall concept, while the side-to-side moment increases. The explanation of load reduction on the tower is because of increasing the drag loading, and hence the thrust loading, on the turbine in stall mode. Though the thrust loads are higher in pitch-to-stall, they become more stable and are less sensitive to pitch angle changes.

Figure 4.15 compares the mean load and amplitude of the blade root and tower base bending moment of the UAE turbine in uniform wind. The wind speed is increased stepwise with the time interval of 30 seconds, and the ampli-

tude of the fatigue load is calculated after the initial transition phase, i.e., when the load is stabilised at the corresponding wind speed. As illustrated in this figure, the pitch-to-stall control lightens the fore-aft bending loads on the blade compared to the pitch-to-feather control, which extends the fatigue loads on the blades in higher wind speeds. However, the tower base of the stall regulated wind turbine experiences a higher fatigue load in the downwind direction. The control systems have an opposite impact on in-plane loads compared to the out-plane loads. The blade edgewise moment of a stall regulated wind turbine is higher than the pitch regulated wind turbine. However, the towers side-to-side moment of the stall regulated wind turbine is reduced compared to the same wind turbine operating as a pitch regulated wind turbine. Comparing the pitch and stall control, it is observed that, in the stall control, the structural loads initial transition occurs in a longer time. Figure 4.16 reflects alternating components of moments on the structure of the UAE turbine operating in turbulent wind. Despite the mitigation effect of stall control on the blades root flapwise moment in uniform wind, the alternating component of the blade root loads increases in turbulent wind, i.e., flapwise and side-to-side fatigue loads. However, the tower experiences lower fore-aft fatigue loads in the turbulent wind, while the amplitude of side-to-side moment increases. One can notice that the difference in blade loading between pitch-to-stall and pitch-to-feather is much smaller for the SWRT wind turbine. This load reduction on the structure stems from a more stable thrust loading in the stall mode, where the tower fore-aft and blade flapwise moments are less sensitive to pitch variation.

Figure 4.17 compares the amplitude of the cyclic components the blade root and tower base bending moments of the WP turbine in uniform wind. As shown in this figure, the pitch-to-stall control has an inconsistent effect on the blade fatigue loads, and the amplitude of the flapwise moment significantly increases at a certain range of wind speeds, i.e., the range of 18-25 m/s. Also, the blades of the stall regulated wind turbine experience higher side-to-side fatigue loads at high wind speeds compared to the pitch regulated wind turbine. Comparing the tower moments of the WP turbine operating with pitch and stall control, it is observed that pitch-to-stall control magnifies the tower base fore-aft and side-to-side fatigue loads. The tower base and the blade rood moment of the WP turbine are also monitored in turbulent wind. Figure 4.18 compares the magnitudes of the alternating components of the blade root and tower base bending moments of the WP turbine in turbulent wind. A significant increase in the tower fore-aft fatigue load of the stall regulated turbine tower can be observed, caused by resonances due to negative damping which is known to occur in stall operation [34]. Moreover, pitch-to-stall control magnifies the side-to-side fatigue loads of the tower base.

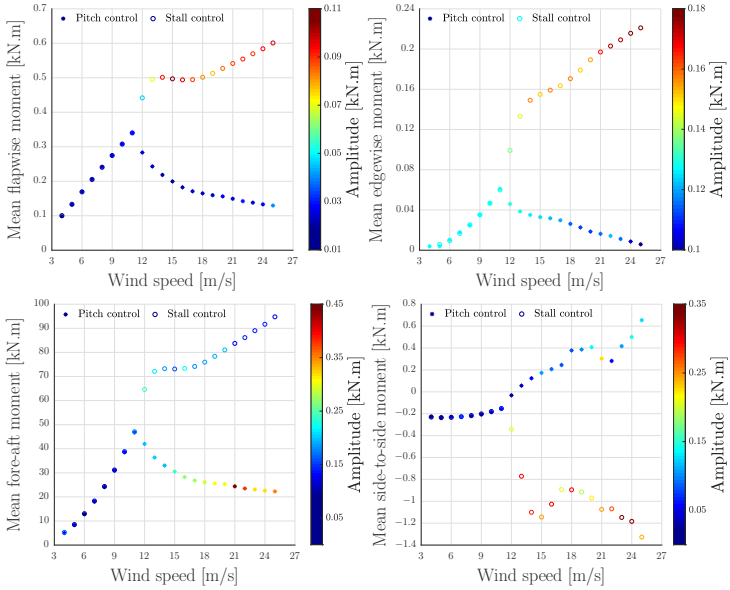

Figure 4.13: Comparison of the fatigue loads on the structure of the SWRT wind turbine operating with pitch-to-stall and pitch-to-feather control in the whole wind speed range.

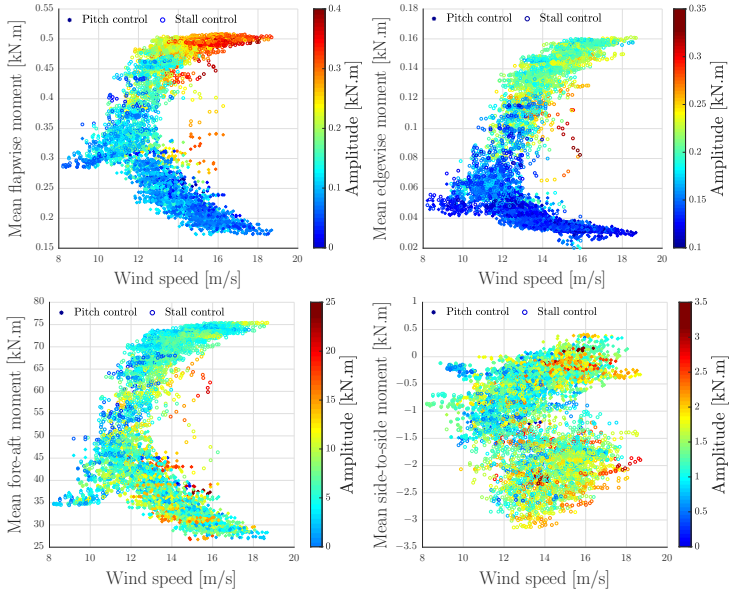

Figure 4.14: Comparison of the fatigue loads on the structure of the SWRT wind turbine operating with pitch-to-stall and pitch-to-feather control in the turbulent wind.

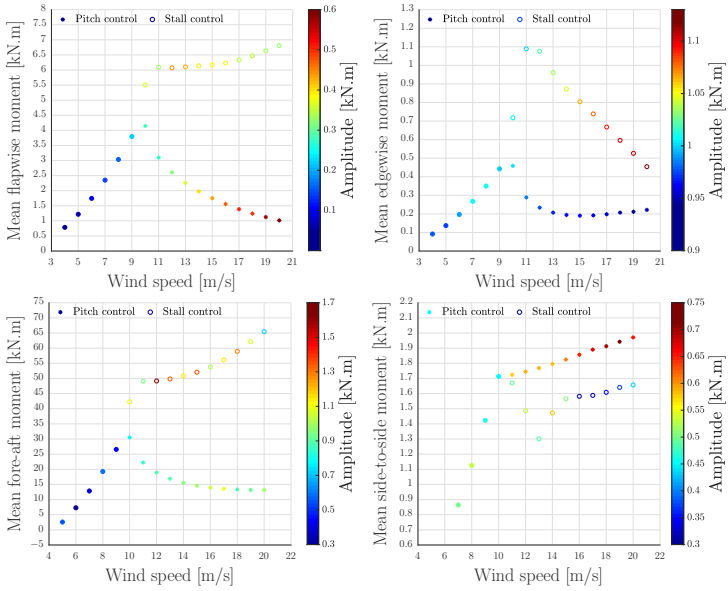

Figure 4.15: Comparison of the fatigue loads on the structure of the UAE wind turbine operating with pitch-to-stall and pitch-to-feather control in the whole wind speed range.

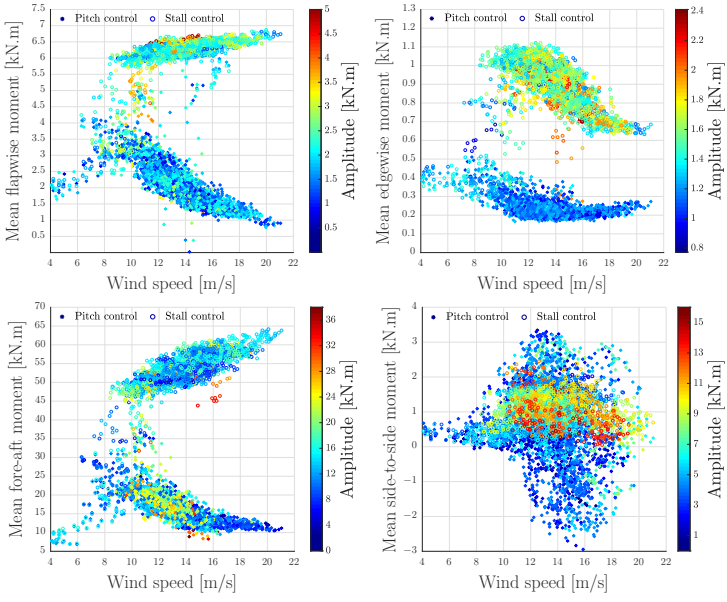

Figure 4.16: Comparison of the fatigue loads on the structure of the UAE wind turbine operating with pitch-to-stall and pitch-to-feather control in the turbulent wind.

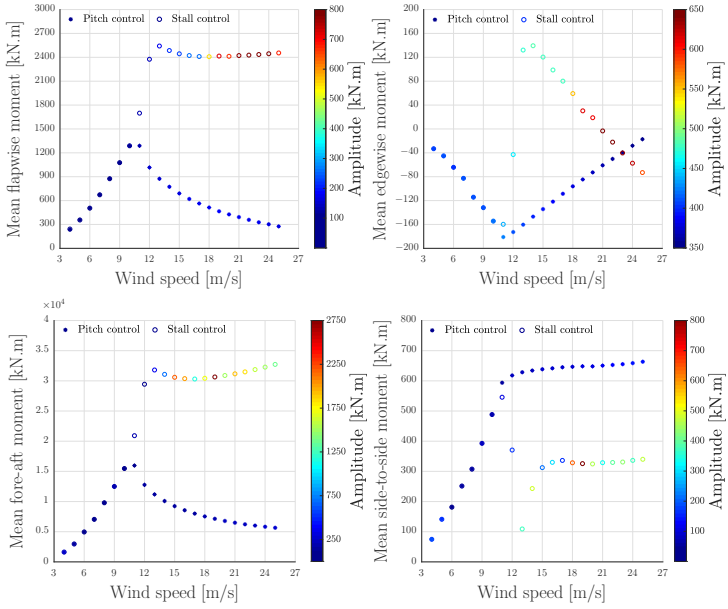

Figure 4.17: Comparison of the fatigue loads on the structure of the WP wind turbine operating with pitch-to-stall and pitch-to-feather control in the whole wind speed range.

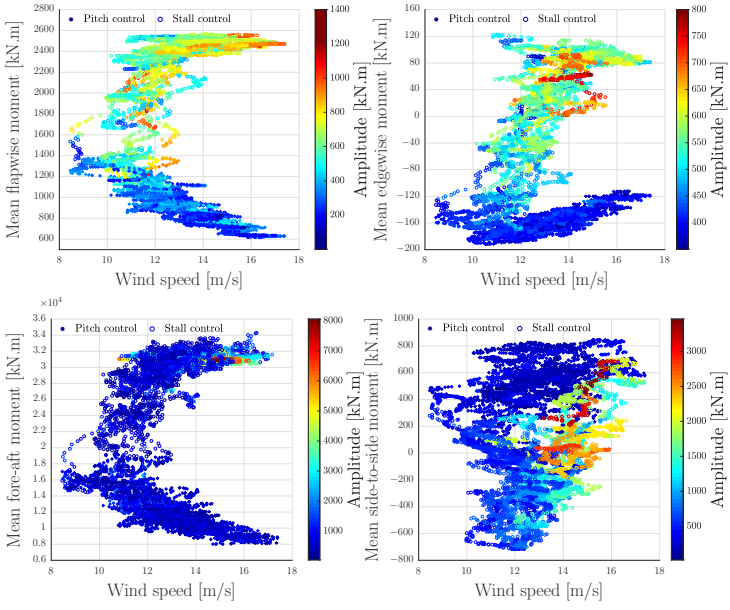

Figure 4.18: Comparison of the fatigue loads on the structure of the WP wind turbine operating with pitch-to-stall and pitch-to-feather control in the turbulent wind.

4.4 Conclusion and discussion

In this article, a comparative analysis was carried out between pitch-to-feather and pitch-to-stall control, in order to investigate the potential benefits of stall control for HAWTs. The impact of these different control schemes was investigated in terms of dynamic performance under turbulent flows, structural loading, and pitch system behaviour for three HAWTs with different blade designs, i.e., untwisted, stall-regulated, and pitch-regulated blades. A control system was designed to control the wind turbine in the whole operating region (II,III, and IV). An MPPT algorithm was applied to maximise the power coefficient in the low wind region. To validate the control systems performance with gain scheduling based on aerodynamic sensitivity, the dynamic response of the wind turbines was monitored in the whole wind speed range. The dynamic performance of the wind turbines was tested in a realistic operating condition in the presence of three-dimensional turbulent wind fields. Moreover, the oscillating movements of the blade pitch system were compared by performing cycle analysis. Considering the results, the following conclusions can be drawn:

- Pitch-to-stall control reduces the rotor speed oscillations and power transients, as compared to pitch-to-feather, for the SWRT and UAE wind turbines with untwisted and stall-regulated blade designs, respectively.
- Pitch-to-stall control reduces the fore-aft fatigue load on the tower, as compared to pitch-to-feather, of the wind turbines with untwisted and stall-regulated blade designs.
- For SWRT and UAE wind turbines, pitch-to-stall control decreases the flapwise moment on the blades in uniform wind, and stabilises it in turbulent wind. However, the amplitude of the cycling component increases in turbulent wind.
- Pitch-to-stall control magnifies the side-to-side tower fatigue loading and the blades flapwise and edgewise fatigue loads in turbulent winds. However, the difference with pith-to-feather control is minimised for the UAE wind turbines due to its stall-regulated blade design.
- Although the pitch-to-stall control reduces the summed blade pitch movements of SWRT and UAE wind turbines, the pitch movements with small amplitude oscillation increases, which increases the risk of wear in the rolling contacts of the blade bearings.
- Pitch-to-stall control has a negative impact on the WP wind turbine (with pitch-regulated blade design) in terms of dynamic performance and structural loading.

To conclude, pitch-to-stall control has the most positive impact on HAWTs with a stall-regulated blade design in terms of dynamic performance and fore-aft tower loading in turbulent wind, with a minimum increase of the blades flapwise moment. However, it should be considered that although pitch-to-stall control reduces the summed blade pitch movements, it increases the risk of surface damage in the blades bearing due to the oscillating movements with a small amplitude.

4.5 Appendix: Blade characteristic of wind turbine models

Table 4.3: Aerofoil distribution and twist angle of untwisted, stall-regulated, pitch-regulated blades

SWRT 10 kW			**UAE 20 kW**			**WP 1.5 MW**		
Blade radius (m)	Twist angle (°)	Aerofoils	Blade radius (m)	Twist angle (°)	Aerofoils	Blade radius (m)	Twist angle (°)	Aerofoils
0	2	SH3052	0	0	cylinder	0	11.1	cylinder
0.0865	0	SH3052	0.136	0	cylinder	1.108	11.1	cylinder
0.432	0	SH3052	0.448	-0.098	cylinder	3.325	11.1	S818
0.605	0	SH3052	0.8	19.423	S809	5.541	11.1	S818
0.779	0	SH3052	1.076	14.318	S809	7.758	11.1	S818
0.952	0	SH3052	1.277	10.971	S809	9.975	8.38	S818
1.125	0	SH3052	1.495	8.244	S809	12.191	6.35	S818
1.298	0	SH3052	1.713	6.164	S809	14.408	4.33	S818
1.471	0	SH3052	1.914	4.689	S809	16.625	2.85	S825
1.644	0	SH3052	2.116	3.499	S809	18.841	2.22	S825
1.817	0	SH3052	2.334	2.478	S809	21.058	1.58	S825
1.990	0	SH3052	2.552	1.686	S809	23.275	0.95	S825
2.164	0	SH3052	2.753	1.115	S809	25.491	0.53	S825
2.337	1.6	SH3052	2.954	0.666	S809	27.708	0.38	S825
2.510	3.2	SH3052	3.172	0.267	S809	29.925	0.23	S826
2.596	3.2	SH3052	3.390	-0.079	S809	32.141	0.08	S826
			3.591	-0.381	S809	33.25	0.08	S826
			3.792	-0.679	S809			
			3.968	-0.933	S809			
			4.144	-1.184	S809			
			4.345	-1.466	S809			
			4.521	-1.711	S809			
			4.597	-1.815	S809			

Bibliography

[1] A. E. Samani, J. D. De Kooning, N. Kayedpour, N. Singh, and L. Vandevelde, "The impact of pitch-to-stall and pitch-to-feather control on the structural loads and the pitch mechanism of a wind turbine," *Energies*, vol. 13, no. 17, p. 4503, 2020. DOI: 10.3390/en13174503.

[2] N. Kayedpour, A. E. Samani, L. De Kooning, Jeroen D. M.and Vandevelde, and G. Crevecoeur, "Model predictive control with a cascaded hammerstein neural network of a wind turbine providing frequency

containment reserve," *IEEE Transactions on Energy Conversion*, 2021. DOI: 10.1109/TEC.2021.3093010.

[3] G. W. E. Council, "Global wind report 2019," 2020. URL: https://gwec.net/global-wind-report-2019/.

[4] E. A. Bossanyi, "Individual blade pitch control for load reduction," *Wind Energy: An International Journal for Progress and Applications in Wind Power Conversion Technology*, vol. 6, no. 2, pp. 119–128, 2003. DOI: 10.1002/we.76.

[5] S. Park and Y. Nam, "Two lqri based blade pitch controls for wind turbines," *Energies*, vol. 5, no. 6, pp. 1998–2016, 2012. DOI: 10.3390/en5061998.

[6] T. Macquart, A. Maheri, and K. Busawon, "Microtab dynamic modelling for wind turbine blade load rejection," *Renewable energy*, vol. 64, pp. 144–152, 2014. DOI: 10.1016/j.renene.2013.11.011.

[7] K. He, L. Qi, L. Zheng, and Y. Chen, "Combined pitch and trailing edge flap control for load mitigation of wind turbines," *Energies*, vol. 11, no. 10, p. 2519, 2018. DOI: 10.3390/en11102519.

[8] V. Maldonado, "Active flow control of wind turbine blades," *Wind Turbines-Design, Control and Applications, In-Tech, Rijeka*, pp. 303–324, 2016. DOI: 10.8772/63480.

[9] I. Dinwoodie, D. McMillan, M. Revie, I. Lazakis, and Y. Dalgic, "Development of a combined operational and strategic decision support model for offshore wind," *Energy Procedia*, vol. 35, pp. 157–166, 2013. DOI: 10.1016/j.egypro.2013.07.169.

[10] C. Dao, B. Kazemtabrizi, and C. Crabtree, "Wind turbine reliability data review and impacts on levelised cost of energy," *Wind Energy*, vol. 22, no. 12, pp. 1848–1871, 2019. DOI: 10.1002/we.2404.

[11] T. A. Harris and M. N. Kotzalas, *Advanced concepts of bearing technology: rolling bearing analysis*. CRC press, 2006. DOI: 10.1201/9781420006582.

[12] M. Stammler, P. Thomas, A. Reuter, F. Schwack, and G. Poll, "Effect of load reduction mechanisms on loads and blade bearing movements of wind turbines," *Wind Energy*, 2019. DOI: 10.1002/we.2428.

[13] T. J. Larsen and T. D. Hanson, "A method to avoid negative damped low frequent tower vibrations for a floating, pitch controlled wind turbine," in *Journal of Physics: Conference Series*, vol. 75, p. 012073, IOP Publishing, 2007. DOI: 10.1088/1742-6596/75/1/012073.

[14] J. M. Jonkman, "Dynamics modeling and loads analysis of an offshore floating wind turbine," tech. rep., National Renewable Energy Lab.(NREL), Golden, CO (United States), 2007. DOI: 10.2172/921803.

[15] T. Macquart and A. Maheri, "A stall-regulated wind turbine design to reduce fatigue," *Renewable energy*, vol. 133, pp. 964–970, 2019. DOI: 10.1016/j.renene.2018.10.089.

[16] D. Ward, M. Collu, and J. Sumner, "Reducing tower fatigue through blade back twist and active pitch-to-stall control strategy for a semi-submersible floating offshore wind turbine," *Energies*, vol. 12, no. 10, p. 1897, 2019. DOI: 10.3390/en12101897.

[17] B. Loza, J. Pacheco-Chérrez, D. Cárdenas, L. I. Minchala, and O. Probst, "Comparative fatigue life assessment of wind turbine blades operating with different regulation schemes," *Applied Sciences*, vol. 9, no. 21, p. 4632, 2019. DOI: 10.3390/app9214632.

[18] J. D. M. De Kooning, J. Van de Vyver, B. Meersman, and L. Vandevelde, "Maximum efficiency current waveforms for a pmsm including iron losses and armature reaction," *IEEE Transactions on Industry Applications*, vol. 53, no. 4, pp. 3336–3344, 2017. DOI: 10.1109/TIA.2017.2681619.

[19] J. D. M. De Kooning, T. L. Vandoorn, J. Van de Vyver, B. Meersman, and L. Vandevelde, "Displacement of the maximum power point caused by losses in wind turbine systems," *Renewable energy*, vol. 85, pp. 273–280, 2016. DOI: 10.1016/j.renene.2015.06.052.

[20] Z. Cui and L. Song, "Improvement of maximum power point tracking for a new wind power system," in *2018 13th IEEE Conference on Industrial Electronics and Applications (ICIEA)*, pp. 1665–1670, IEEE, 2018. DOI: 10.1109/ICIEA.2018.8397977.

[21] S. M. R. Kazmi, H. Goto, H.-J. Guo, and O. Ichinokura, "A novel algorithm for fast and efficient speed-sensorless maximum power point tracking in wind energy conversion systems," *IEEE Transactions on Industrial Electronics*, vol. 58, no. 1, pp. 29–36, 2010. DOI: 10.1109/TIE.2010.2044732.

[22] J. Jonkman, S. Butterfield, W. Musial, and G. Scott, "Definition of a 5-mw reference wind turbine for offshore system development," tech. rep., National Renewable Energy Lab.(NREL), Golden, CO (United States), 2009. DOI: 10.2172/947422.

[23] M. H. Hansen, A. D. Hansen, T. J. Larsen, S. Øye, P. Sørensen, and P. Fuglsang, "Control design for a pitch-regulated, variable speed wind turbine," 2005. URL: https://www.osti.gov/etdeweb/biblio/20567534.

[24] E. A. Bossanyi, "The design of closed loop controllers for wind turbines," *Wind energy: An International Journal for Progress and Applications in Wind Power Conversion Technology*, vol. 3, no. 3, pp. 149–163, 2000. DOI: 10.1002/we.34.

[25] M. Singh, E. Muljadi, J. Jonkman, V. Gevorgian, I. Girsang, and J. Dhupia, "Simulation for wind turbine generators–with fast and matlab-simulink modules," tech. rep., National Renewable Energy Lab.(NREL), Golden, CO (United States), 2014. DOI: 10.2172/1130628.

[26] A. Platt, B. Jonkman, and J. Jonkman, "Inflowwind users guide," *Technical Report*, 2016. DOI: https://openfast.readthedocs.io/en/dev/source/user/inflowwind.

[27] E. Muljadi and C. P. Butterfield, "Pitch-controlled variable-speed wind turbine generation," *IEEE transactions on Industry Applications*, vol. 37, no. 1, pp. 240–246, 2001. DOI: 10.1109/28.903156.

[28] K. Hammerum, P. Brath, and N. K. Poulsen, "A fatigue approach to wind turbine control," in *Journal of Physics: Conference Series*, vol. 75, p. 012081, 2007. DOI: 10.1088/1742-6596/75/1/012081.

[29] B. Jonkman, "Turbsim user's guide v2. 00.00," *Natl. Renew. Energy Lab*, 2016. DOI: 10.2172/891594.

[30] P. S. Veers, "Three-dimensional wind simulation," tech. rep., Sandia National Labs., Albuquerque, NM (USA), 1988. URL: https://www.osti.gov/biblio/6633902.

[31] N. Kelley, M. Hand, S. Larwood, and E. McKenna, "The nrel large-scale turbine inflow and response experiment: preliminary results," in *Wind Energy Symposium*, vol. 7476, pp. 412–426, 2002. DOI: 10.1115/WIND2002-64.

[32] M. Stammler, G. Poll, and A. Reuter, "The influence of oscillation sequences on rolling bearing wear," vol. 4, pp. 19–25, 2019. URL: https://d-nb.info/1235076768/34#page=19.

[33] P. S. Veers, T. D. Ashwill, H. J. Sutherland, D. L. Laird, D. W. Lobitz, D. A. Griffin, J. F. Mandell, W. D. Musial, K. Jackson, M. Zuteck, *et al.*, "Trends in the design, manufacture and evaluation of wind turbine blades," *Wind Energy: An International Journal for Progress and Applications in Wind Power Conversion Technology*, vol. 6, no. 3, pp. 245–259, 2003. DOI: 10.1002/we.90.

[34] V. Riziotis and H. A. Madsen, "Aeroelasticity and structural dynamics of wind turbines," in *Wind Energy Systems*, pp. 46–111, Elsevier, 2011. DOI: 10.1533/9780857090638.1.46.

Chapter 5

Demand response operation of hybrid systems

Carbon dioxide emission reduction and increasing integration of renewables into the power system are the challenging solutions to combat global warming and climate change. On the one hand, the power systems' flexibility needs to be extended with the increasing penetration of renewables into the grid due to its variability and inertia-less characteristics. In a system with a high penetration of renewables and inadequate flexibility, renewable power generation is curtailed to maintain grid stability and reliability. On the other hand, the emerging technologies for direct conversion of CO_2 to value-added chemicals are energy-intensive processes and represent low economic viability. Therefore, renewables, CCU based processes and power systems form an interconnected system in which the elements have a considerable impact on each other. In this complex techno-economic system, the sustainable solution would be the optimal collaborative operation of the elements. The cooperative operation of renewables and CCU based processes based on the grid condition can tackle three challenges at the same time:

1. Carbon dioxide emissions are reduced by utilising a CCU based process.
2. The chemical plant is operated by renewable power, reducing the energy costs of the chemical plant.
3. The cooperative approach can support the power grid by using the chemical process as a buffer, allowing the integration of more renewable energy sources into the power system.

Given these advantages, the chemical industry can play a key role in accelerating the transition towards a low carbon future. However, the uncertain behaviour of renewable resources and the energy market has a considerable impact on system

reliability. Therefore, stochastic optimisation techniques are required to deal with these uncertainties and support optimal operating/investment decisions.

This chapter proposes a cooperative control strategy for the flexible operation of the chemical process coupled with renewable energy sources. CO_2-based chemical processes can offer a vast potential of new forms of flexible operation using storage capabilities and adaptive control design. Based on the proposed control scheme, wind turbines in all operating regions provide the power input of a CCU based chemical plant. An optimal cooperative two-stage stochastic programming model is formulated for a novel flexible operation strategy of the chemical process coupled with wind turbines. The collaborative decision model is developed to ensure optimal energy sharing among the chemical plant, wind energy, and the grid requirements under variabilities and uncertainties. Wind turbines are connected to the grid and actively participate in the day-ahead energy and reserve markets, considering the chemical plant as a buffer. Therefore, a day ahead pricing system is considered for scheduling the power consumption and reserve capacity by optimal FCR contribution to shift demand from peak to non-peak intervals. The designed architecture allows the coupling of detailed dynamic models to assess the proposed optimisation framework and the operational restrictions. Furthermore, an equivalent scenario-based model of the proposed optimisation problem is suggested using the Group Method of Data Handling (GMDH) for a data-driven prediction of stochastic variables.

The contents of this chapter have been submitted to IEEE Transactions on Sustainable Energy where it is currently under review.

An Optimal Cooperative Strategy for Flexible Operation of a CCU Process with Wind Energy

Arash E. Samani, Nezmin Kayedpour, Farjam Kayedpour, Jeroen D. M. De Kooning, Guillaume Crevecoeur and Lieven Vandevelde

Submitted to "IEEE Transactions on Sustainable Energy"

Abstract *Improving power system flexibility by responsive demand is essential for integrating wind energy with a high level of variability in power systems. Carbon dioxide-based chemical processes as energy-intensive industrial loads may offer a vast potential of new forms of flexible operation due to their existing control infrastructure and storage capabilities. However, a collaborative decision model is needed for optimal energy sharing among the chemical plant and the grid under the variations and uncertainties of wind power. This study develops an optimal cooperative two-stage stochastic programming model for a novel flexible operation strategy of the chemical process coupled with wind turbines. Based on the proposed control scheme, the wind turbines' available power in partial and full load regions provides the power input of a carbon dioxide-based chemical plant. Wind turbines are connected to the grid and actively participate in the day-ahead energy and reserve markets, considering the chemical plant as a source of flexibility. The designed architecture allows the coupling of detailed dynamic models to assess the proposed optimization framework and the operational restrictions. An equivalent scenario-based model of the proposed optimization problem is suggested using the Group Method of Data Handling (GMDH) for a data-driven prediction of stochastic variables. Simulation results demonstrate the effectiveness and significance of the proposed approach for an optimal and cooperative contribution in the ancillary market of a carbon dioxide-based chemical plant supplied by wind energy.*

5.1 Introduction

the global energy consumption has dramatically increased since the industrial revolution. During the nineteenth century, the excessive use of fossil fuels such as coal, natural gas, and oil has significantly added an extreme amount of carbon dioxide and other greenhouse gases to the atmosphere. The excessive emission of carbon dioxide subsequently results in global warming and other severe environmental problems. The Paris Agreement global framework for avoiding climate change has set out targets to minimize carbon dioxide emission [1]. The European Union (EU) has also conducted a schedule for Europe's

neutral climate till 2050 by supporting the sustainable expansion of renewable energy and Carbon Capture and Utilization (CCU) technologies. This policy makes Europe a global leader in tracking the record of decarbonizing power systems [2]. Currently, wind energy has the most extensive contribution to the EU's renewable energy production and is responsible for providing up to 759 TWh by 2030, which will be 23% of the total electricity request [3]. The EU has decided to reduce its net greenhouse gas emissions by at least 55% by the end of this decade before eventually attaining net-zero by 2050 [4]. The EU's regulations ensure the development of technologies that make it possible to integrate the energy produced from renewable sources into CCU based processes.

CCU processes require access to H_2 as a raw material to synthesize added value chemicals such as polyols, polyurethane, formic acid, methane, and methanol [5,6]. H_2 can be obtained from water electrolysis or biomass gasification using electricity sources. However, electrolysis has a significant electricity consumption rate in these processes, known as an indication of high operating costs. Thus, it is highly recommended for CCU processes to have access to low-cost renewable energy to significantly decrease their costs and increase market competitiveness, considering both environmental and economic points of view [7, 8]. Many studies have considered opportunities for integrating CCU processes with renewable energy sources [7, 9–11]. [12] used methanol production via carbon dioxide hydrogenation as a case study to conceptually analyze the flexibility of chemical processes that can operate with a varying load, while meeting a reliable production target. This study reveals evident potential advantages of process flexibility under a high penetration level of renewable energy. Although chemical processes conventionally prefer to operate at a steady-state with a constant load, combining variable renewable energy can be addressed by optimal coordination between flexible energy generation and flexible chemical production [13, 14].

Coupling CCU processes with variable renewable sources is an efficient path to decrease greenhouse gas emission rates. However, few studies look into the potential role of these sources in power system flexibility and demand response. Nevertheless, integrating CCU processes with renewables can be complementary with energy storage devices for surplus electricity generation and even an adequate resolution to provide grid balancing services. In [15], a case study for the UK and Spain is presented to use methanol and hydrogen as chemical storage compounds for wind and solar energy. The study used nonlinear programming to solve a trade-off between investment and production capacity. In [16], an optimal integration of renewable-based processes for several products is studied. However, no proposal with a relevant business model and actual power market operation is reported in this study. In [17], a flexible operation strategy is proposed for formic acid synthesis providing

frequency containment reserve in smart grids. In [18], the requirements needed for an environmentally and economically viable methanol producing carbon dioxide utilization process explored for participating in the energy system with consideration of the day-ahead or intraday bidding system, including the seasonality of wind.

The flexibility of the power system has become essential with an evolving electricity market landscape to cancel the effects of uncertainties and variabilities that are evident due to the increased penetration of renewable energy in the energy mix [19, 20]. Therefore, a collaborative energy-sharing strategy is required for CCU processes coupled with renewables to actively participate in the ancillary services such that the power system can accommodate even the most extensive deviation range of uncertainties. This solution can significantly accelerate the integration of intermittent electricity sources, assist demand flexibility, and decrease the dependence on renewables support schemes [21].

Although little attention is shown to the capacity of CCU processes coupled with renewables in demand response and grid balancing services, several studies suggest a collaborative energy-sharing optimization model among other responsive demands with flexible operation, the power grid and renewable energy. [22] proposed a controlled electric vehicle charging strategy to optimize the peak-valley difference of the grid, considering the regional wind and photovoltaic (PV) power outputs using probabilistic models. In [23], a stochastic model based on chance constraints is suggested for network congestion management in the day-ahead power market with consideration of the uncertainty of wind power and demand-side response in order to determine the optimal daily dispatch of generators and loads, and to minimize the risk of transmission congestion. In [24], a two-stage energy sharing framework is proposed for a new prosumer microgrid with renewable energy generation, multiple storage units, and load shifting. The proposed robust energy sharing schedule reveals the potential to overcome the uncertainties of market prices and renewable energy.

The main contribution of this study is an optimal cooperative strategy for the flexible operation of a carbon dioxide-based chemical process synthesizing formic acid connected to a wind energy source that actively participates in the day-ahead energy and reserve markets. The significance of the energy sharing concept in the proposed arrangement is explored in which wind turbines can support the power grid while delivering the energy consumption of the process based on economic viability and the plant owners' willingness under different scenarios and system actions. The total profit is maximized by an optimal contribution of the wind power in the electricity/reserve market and/or by producing formic acid. Maximization of profit as the optimization criterion resolves the bidding strategy that should be set before the day-ahead market's closure. Therefore, a two-stage stochastic optimization framework

is suggested, considering the likelihood of different scenarios of wind power and grid demand for the day ahead. Thus, the chemical plant baseload can be decided while (1) maximizing the share of electricity/reserve offering to the market, considering stochastic behavior of wind and grid frequency in a day ahead, and (2) maximizing the formic acid production and CO_2 capture, guaranteeing the profitability of the process and the decarbonization policy.

The article is structured as follows: Section II introduces the wind turbine and chemical plant models. Section III formulates the methodology and optimization problem based on wind and grid frequency prediction. Section IV provides an overview of the outcomes and results, while Section V presents a discussion and conclusions.

5.2 System description

This section describes and illustrates the wind turbine model and the design of the flexible CCU based chemical process. Fig. 5.1 gives a general overview of the system under study. Wind power is allocated close to the chemical process, which captures carbon dioxide and produces formic acid. The system is also connected to the power grid and can deliver ancillary services for grid balancing. The chemical plant's baseload and the share of Frequency Containment Reserve (FCR) [25] should be determined based on the available wind power, electricity/reserve prices and the marginal profit of formic acid production, taking into account the variability of wind energy and grid frequency within a scenario-based stochastic framework. In what follows, the system component models will be described in more details. These models will be used to validate

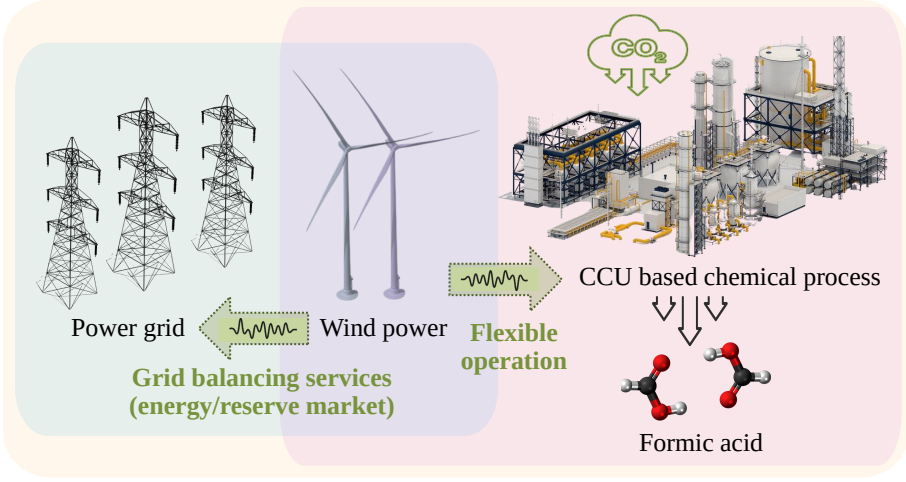

Figure 5.1: Overview of the hybrid system.

the proposed optimization strategy under different operational conditions.

5.2.1 Wind turbine model

The wind energy source in this article consists of two NREL 5MW wind turbines [26]. The NREL 5MW baseline wind turbine model is implemented and coupled to a generator and converter model. The generator is a direct-drive PMSG, which is modeled with an equivalent scheme in the rotating reference frame, as presented in [27]. The efficiency curve is included in the model as a function of different operating points [28]. As shown in Fig. 5.2, the wind turbine operating mode depends on the wind speed. Three operating regions can be defined. In the partial load region, where the wind speed is below the rated value, the pitch angle is kept in an optimal position, and the generator-torque controller aims to maximize power capture by means of Maximum Power Point Tracking (MPPT). The transition zone can be considered as an extension of the first zone. In this region, the primary objective is to regulate generator speed at rated power by using pitch control. The blade-pitch controller aims to regulate the generator speed at its rated value in the full load region, where the wind speed is above the rated value. Proportional integral (PI) controllers are used for the pitch and torque control systems. The used control system is discussed in more detail in [29, 30]. The total electrical power obtained from each wind turbine can be expressed as:

$$P_{\mathrm{wt}} = \begin{cases} 0 & , v_{\mathrm{w}} < v_{\mathrm{w}}^{ci} \\ \frac{1}{2}\rho\pi R^2 v_{\mathrm{w}}^3 \eta_{\mathrm{g}}\eta_{\mathrm{c}} C_P^{\max}(\lambda_{\mathrm{opt}}, \theta_{\mathrm{opt}}) & , v_{\mathrm{w}}^{ci} \leqslant v_{\mathrm{w}} \leqslant v_{\mathrm{w}}^{n} \\ \frac{1}{2}\rho\pi R^2 v_{\mathrm{w}}^3 \eta_{\mathrm{g}}\eta_{\mathrm{c}} C_P(\lambda, \theta) & , v_{\mathrm{w}}^{n} \leqslant v_{\mathrm{w}} \leqslant v_{\mathrm{w}}^{cu} \end{cases} \tag{5.1}$$

where the air density is represented by ρ, the blade length is indicated by R and the wind speed is denoted by v_{w}. C_P represents the power coefficient as a function of the tip speed ratio λ and the blade pitch angle θ. The generator and converter efficiency are characterized by η_{g} and η_{c}, respectively, which vary depending on the operating point.

In order to obtain the realistic power curve of the wind turbine, the turbine is operated under different wind conditions, i.e., mean wind speed and turbulent intensity, and the power out pout of the wind turbine is measured. The data points are obtained from 20 simulations over 200 minutes for mean wind speeds of 5 to 20 m/s and turbulence intensity of 10 to 20%. After data preprocessing and eliminating the outliers that exist due to turbulence, a cubic polynomial curve fitting is used to fit the wind turbine power curve, which can be defined as:

$$P_{\text{wt}} = \begin{cases} 0 & , \quad 0 < v_{\text{w}} < v_{\text{w}}^{ci} \\ a\, v_{\text{w}}^3 + b\, v_{\text{w}}^2 + c\, v_{\text{w}} + d & , \quad v_{\text{w}}^{ci} \leqslant v_{\text{w}} \leqslant v_{\text{w}}^{n} \\ 5 & , \quad v_{\text{w}}^{n} \leqslant v_{\text{w}} \leqslant v_{\text{w}}^{cu} \end{cases} \tag{5.2}$$

where v_{w}^{ci}, v_{w}^{cu} and v_{w}^{n} are respectively the cut-in, cut-out and rated wind speeds in m/s. P_{wt} is a wind turbine electrical power in MW. a, b, c and d are the parameters of a cubic polynomial fitted to the data. The parameter values are:

$$\begin{aligned} &v_{\text{w}}^{\text{ci}} = 3, \quad v_{\text{w}}^{\text{n}} = 11.9, \quad v_{\text{w}}^{\text{cu}} = 25 \\ &a = 0.0019, \quad b = 0.0227, \quad c = -0.1140, \quad d = 0.1359 \end{aligned} \tag{5.3}$$

A piecewise linearization is employed to divide the nonlinear function of two wind turbines into several linear sections as follows:

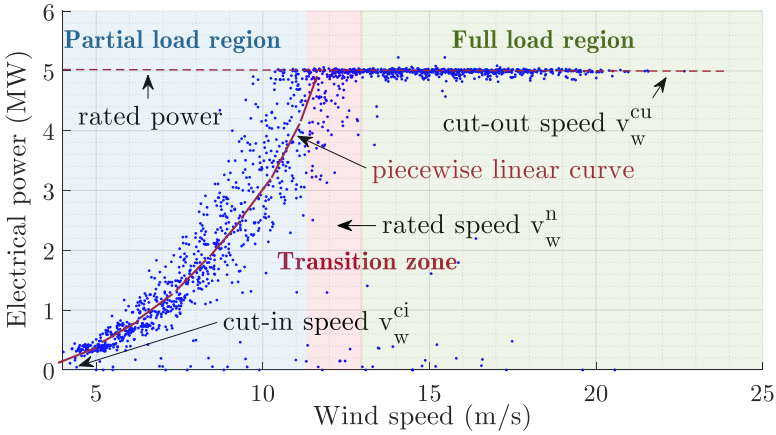

Figure 5.2: 5MW wind turbine power curve.

$$P_{\mathrm{wt}} = \begin{cases} 0 & \text{if} \quad v_{\mathrm{w}} < v_{\mathrm{w}}^{\mathrm{ci}} \\ 0.1152 \cdot v_{\mathrm{w}} - 0.2961 & \text{if} \quad v_{\mathrm{w}}^{\mathrm{ci}} \leq v_{\mathrm{w}} < 4 \\ 0.2062 \cdot v_{\mathrm{w}} - 0.6601 & \text{if} \quad 4 \leq v_{\mathrm{w}} < 5 \\ 0.3086 \cdot v_{\mathrm{w}} - 1.1721 & \text{if} \quad 5 \leq v_{\mathrm{w}} < 6 \\ 0.4224 \cdot v_{\mathrm{w}} - 1.8549 & \text{if} \quad 6 \leq v_{\mathrm{w}} < 7 \\ 0.5476 \cdot v_{\mathrm{w}} - 2.7313 & \text{if} \quad 7 \leq v_{\mathrm{w}} < 8 \\ 0.6842 \cdot v_{\mathrm{w}} - 3.8241 & \text{if} \quad 8 \leq v_{\mathrm{w}} < 9 \\ 0.8322 \cdot v_{\mathrm{w}} - 5.1561 & \text{if} \quad 9 \leq v_{\mathrm{w}} < 10 \\ 0.9916 \cdot v_{\mathrm{w}} - 6.7500 & \text{if} \quad 10 \leq v_{\mathrm{w}} < 11 \\ 0.8425 \cdot v_{\mathrm{w}} - 5.1100 & \text{if} \quad 11 \leq v_{\mathrm{w}} < v_{\mathrm{w}}^{\mathrm{n}} \\ 5 & \text{if} \quad v_{\mathrm{w}}^{\mathrm{n}} \leq v_{\mathrm{w}} \leq v_{\mathrm{w}}^{\mathrm{cu}} \end{cases} \tag{5.4}$$

5.2.2 Chemical plant model

The chemical process under study produces formic acid by thermo-catalysis through hydrogenation of CO_2 over heterogenised ruthenium catalysts. Formic acid is a basic chemical that finds use in a variety of applications such as leather and rubber production, textiles, pharmaceuticals, preservatives and antibacterial agents in livestock feed. Fig. 5.3 shows the process flow diagram for conversion of CO_2 and H_2 to formic acid based on the process developed in [31]. The synthesis process comprises five sections: (I) the compression stage of H_2 and CO_2, (II) the reaction stage, (III) the formic acid enrichment stage to concentrate the reactor product, (IV) the amine exchange stage and (V) the distillation stage for formic acid formation and purification. The process uses 2464 kg/h of CO_2 and 112 kg/h of H_2 to produce 10 kt/yr of formic acid. In this model, it is assumed that the captured CO_2 is available at atmospheric pressure. Therefore, a compression stage is required to increase the pressure up to the optimal operating pressure of the reactor. The required H_2 is supplied by a 5.79 MW Polymer Electrolyte Membrane (PEM) electrolyser. The CO_2 and H_2 are pressurized before feeding into the reactor. In the reaction stage, CO_2 is hydrogenated in the presence of theritelamin (Et_3N) to drive the thermodynamically limited equilibrium of the hydrogenation via the formation of a stable adduct, Et_3NH^+:$HCOO^-$ [32]:

$$CO_2(g) + H_2(g) \rightarrow HCOOH(aq) \tag{5.5}$$

$$CO_2(g) + H_2(g) + Et_3N(aq) \rightleftharpoons Et_3NH^+{:}HCOO^-(aq) \tag{5.6}$$

The liquid stream from the catalytic reactor is fed into the evaporator to concentrate the Et_3NH^+:$HCOO^-$ adduct at an Acid to Amine Ratio (AAR)

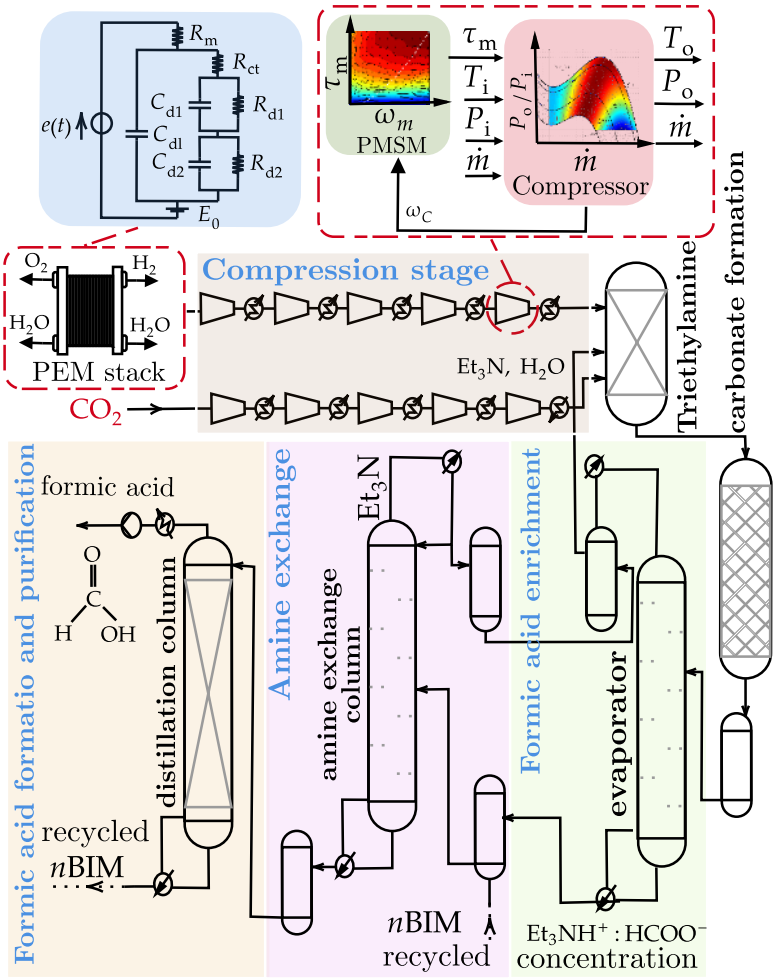

Figure 5.3: Process flow diagram.

of 2.3 by removing water and excess triethylamine, which allows the amine exchange in the next stage. Since the Et_3NH^+:$HCOO^-$ adduct can not be directly separated into formic acid and triethylamine, the concentrated Et_3NH^+:$HCOO^-$ is combined with n-butyl imidazole (*n*BIM) to form *n*BIMH^+ : $HCOO^-$ [33]. Then, the product is introduced into a separation column to produce pure formic acid according to reactions (3.3) and (3.4):

$$Et_3NH^+{:}HCOO^-(l) + n\text{BIM}(l) \rightleftharpoons n\text{BIMH}^+{:}HCOO^-(l) + Et_3N(l) \tag{5.7}$$

$$n\text{BIMH}^+{:}HCOO^-(l) \rightarrow HCOOH(l) + n\text{BIM}(l) \tag{5.8}$$

A dynamic model of the chemical process is developed to represent the process dynamics under flexible operation. In this process, the PEM electrol-

yser and compression stages are selected as the main electrical components to provide flexibility due to their fast dynamic response and significant power consumption. Therefore, the dynamic model is developed based on the fast dynamic response of the PEM electrolyser and the compressors, while monitoring the impact on the subsequent stages. The process elements are individually modelled in Matlab/Simulink. Then they are integrated to build a complete model of the synthesis process. A Randles-Warburg (RW) impedance equivalent is used to model the electrochemical dynamics of the PEM electrolyser.

Hydrogen and carbon dioxide input streams are pressurized in two separate compression stages to reach the reactor pressure of 120 bar. The compression stages are first modelled in Aspen HYSYS to determine the required specifications to reach the desired pressure level at the reactor, i.e., the number of stages and the size of the compressors. Then, the compressors are modelled based on the acquired data, and they are coupled with models of Permanent Magnet Synchronous Motors (PMSM) with a variable speed drive to enable the compressors to operate at variable speeds. The dynamic model of the PMSMs is developed in the rotating $d-q$ synchronous reference frame, including copper losses, iron losses and armature reaction effects [27]. The compressors are modelled based on the compressor's mechanical dynamics using the first-order equation of motion, including rotational inertia and the compressor and motor torques. The variable-speed operation is performed by regulating the motor torque by using field-oriented control, and the corresponding output pressure and temperature at each rotational speed is obtained by using an approximation of the compressor performance map. The reactor model is developed based on the data available in [31], assuming a constant ratio of CO_2 and H_2 at the reactor. Based on the developed model, the formic acid production is obtained as a function of the power consumption of the process $g(P_{\text{fa}}(\omega))$:

$$g(P_{\text{Fa}}(\omega)) = -31.79 \cdot P_{\text{Fa}}(\omega)^2 + 433.16 \cdot P_{\text{Fa}}(\omega) - 61.97 \tag{5.9}$$

where g is the numerical value of the formic acid production expressed in kg/h. This function is piecewise linearized, resulting in:

$$g(P_{\text{Fa}}(\omega)) = \begin{cases} 368.65 \cdot P_{\text{Fa}}(\omega) - 35.28, & \text{if } 0.57 \leqslant P_{Fa}(\omega) < 1.44 \\ 313.50 \cdot P_{\text{Fa}}(\omega) + 44.54, & \text{if } 1.44 \leqslant P_{\text{Fa}}(\omega) < 2.31 \\ 258.35 \cdot P_{\text{Fa}}(\omega) + 172.27, & \text{if } 2.31 \leqslant P_{\text{Fa}}(\omega) < 3.18 \\ 203.01 \cdot P_{\text{Fa}}(\omega) + 348.50, & \text{if } 3.18 \leqslant P_{\text{Fa}}(\omega) < 4.05 \\ 147.82 \cdot P_{\text{Fa}}(\omega) + 527.18, & \text{if } 4.05 \leqslant P_{\text{Fa}}(\omega) < 4.92 \\ 92.75 \cdot P_{\text{Fa}}(\omega) + 843.21, & \text{if } 4.92 \leqslant P_{\text{Fa}}(\omega) < 5.79 \end{cases} \tag{5.10}$$

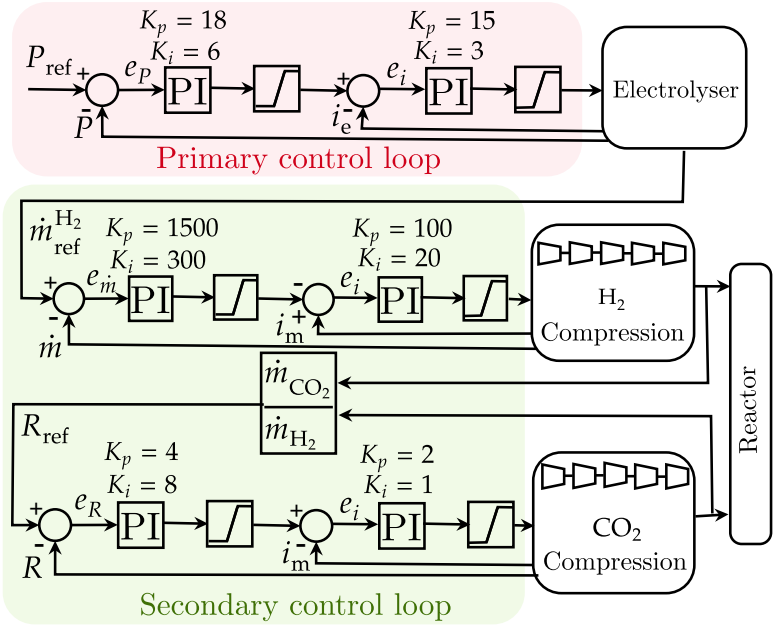

Figure 5.4: Control system for flexible operation of the PEM electrolyser and the CO_2 and H_2 compression stages.

In order to facilitate the cooperative operation of the CCU based process with wind energy, a control design is needed to enhance the process flexibly at the operational level. The control system must be able to track the reference power while maintaining the process efficiency at the desired level. Fig. 5.4 illustrates the proposed control scheme for flexible operation of the process. The primary control loop tracks the power signal by regulating the power consumption of the PEM electrolyser. The secondary control loop follows the primary controller and regulates the compressors' speed to maintain the correct hydrogen and carbon dioxide ratio, and the optimal pressure and temperature at the reactor. The simulation results show the propose control system enables the dynamic operation of the process while maintain the optimal operating condition for the CO_2 conversation reaction [17].

5.3 Optimization problem formulation

The decision-making of the proposed stochastic optimization framework consists of two objectives. The first objective is to determine the strategic bidding for the scheduled electricity and reserve quantity in the day-ahead market. The second objective is to optimize the formic acid production the next day, satisfying the scheduled bidding quantities as much as is feasible. Once the

participant decides the bidding quantity, it will not be allowed to change its decision on the next day against the signed corresponding transaction agreement. Therefore, a two-stage stochastic optimization process is formulated to support decision-making during the different stages and periods. The two-stage stochastic energy sharing model allows the participant in the first stage to make an optimal decision considering the day-ahead electricity and reserve transactions while optimizing tomorrow's real-time chemical plant operations. In the second stage, the deviation from the promised reserve quantities will be compensated by upward or downward reserves provided by the chemical plant. The central assumption is that the decision-maker can estimate the expected value of possible scenarios related to wind speed and grid frequency when offering its bidding quantity in the day-ahead electricity/reserve market. On the next day, the decision-maker then optimizes the baseload of formic acid production based on available wind power and grid frequency. Fig. 5.5 shows the cooperative strategy for energy sharing among formic acid production $P_{\mathrm{Fa}}(\omega)$, and the power injected into the grid $P_g(\omega)$. This includes both electricity $P_e(\omega)$ and reserve quantities for upward $P_r^+(\omega)$ and downward $P_r^-(\omega)$ regulation. As the flexible operation region illustrates in Fig. 5.5, the available reserve margin can be allocated to both formic acid production and the electricity market based on grid frequency and the Transmission System Operator's (TSO) demand.

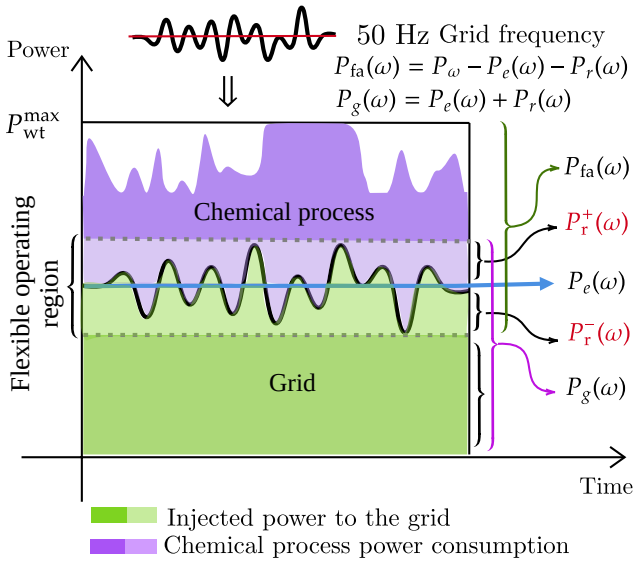

Figure 5.5: Cooperative strategy for energy sharing.

5.3.1 Scenario analysis and time-series prediction

One of the main issues in the decision-making of power systems is how to estimate the uncertainty and variability nature of wind power and how this variability can be incorporated into optimization modeling. The bidding decision variables in the day-ahead market are selected based on possible wind speed scenarios and average expected grid frequency. However, in stochastic programming, the run-time highly depends on the number of scenarios. Therefore, an efficient scenario reduction approach is required to reduce the computational time required for simulating a large number of cases over a year. In [34], the advantages of incorporating a deep learning-based time-series forecasting method into a multistage stochastic programming framework are discussed. In this study, as Fig. 5.6 shows, the Group Method of Data Handling (GMDH) is used as a deep learning method to estimate the likelihood of four wind scenarios, which their occurrence has a major impact on the bidding strategy. The GMDH employs a combination of quadratic and higher polynomial functions in a particular number of layers and maps input features to the expected output by creating a multistage nonlinear pattern [35]. In this study, the GMDH is mainly used as a prediction tool to overcome the difficulties of adequately selecting the other neural network-based structures, which usually require many try/error attempts or evolutionary algorithms to find the optimal tuning parameters. The structure of the GMDH network can be created automatically, only based on prepared training and testing data sets. Moreover, since the GMDH is a self-organizing algorithm that gradually sorts out complicated polynomial models and selects the best solution using the external criterion, it usually needs less training data to overcome the prediction problem.

As mentioned, reducing the number of scenarios representing the underlying uncertainty is often essential to finding efficient numerical solutions. Finding a smaller subset of scenarios reduces the numerical complexity while keeping the error at an acceptable level. Therefore, a computationally efficient methodology is used to tackle the scenario reduction problem. A clustering method based on the K-means algorithm is used to partition the scenario sets. Each cluster represents the scenario that best mirrors the conditional objective values for that specific operational condition. Four scenarios are foreseen based on wind speed distribution to cover all the wind turbines operating regions gradually. The wind speed is above the rated value in the fourth scenario ω_4. Therefore, the surplus power is consumed by the formic acid plant, which results in further CO_2 capture. In the first scenario ω_1, wind power is less than half of the maximum capacity of the chemical process. In the second and third scenarios ω_2 and ω_3, the wind speed is below the rated value and above the maximum capacity of the chemical process. Furthermore, the grid

frequency situation can be determined by estimating the mean frequency on a quarter-hourly basis depending on the TSO's penalty mechanism. Using K-means finding the mean value and considering the density of data points located below or above nominal frequency. Fig 5.6 shows an example of the grid frequency that seems to be occurring below the nominal value, where the average of the central clusters outside the dead-band zone is 49.985 Hz.

Fig. 5.7 reveals the results of the wind speed and grid frequency prediction using historical datasets over five years, i.e., from January 2015 till December 2019. The Mean, Root Mean Square Error (RMSE), Mean Square Error (MSE), and Standard Deviation (SD) of the absolute errors are the evaluation metrics used for assessing the results. Four scenarios are foreseen based on wind speed distribution to cover all the wind turbines operating regions gradually. The wind speed is above the rated value in the fourth scenario. Therefore, the surplus power is consumed by the formic acid plant, which results in further CO_2 capture. In the first scenario, wind power is less than half of the maximum capacity of the chemical process. In the second and third scenarios, the wind speed is below the rated value and above the maximum capacity of the chemical process.

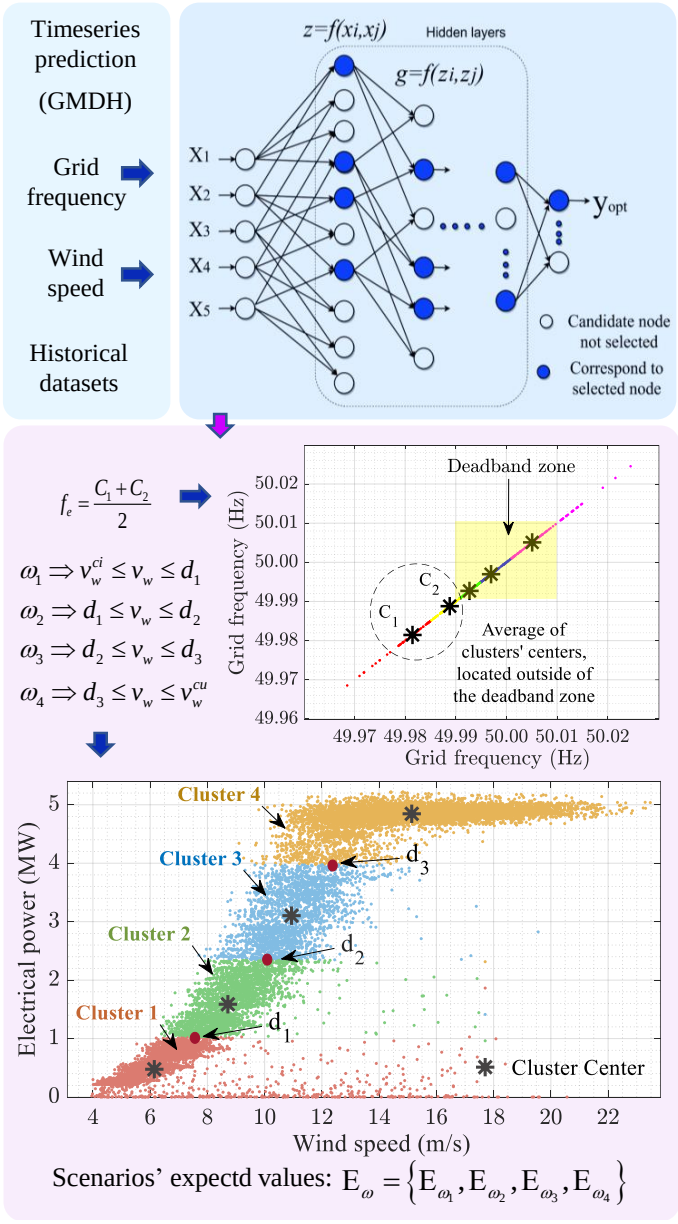

Figure 5.6: Estimating expected value of each scenario based on day-ahead predictions of wind speed and grid frequency.

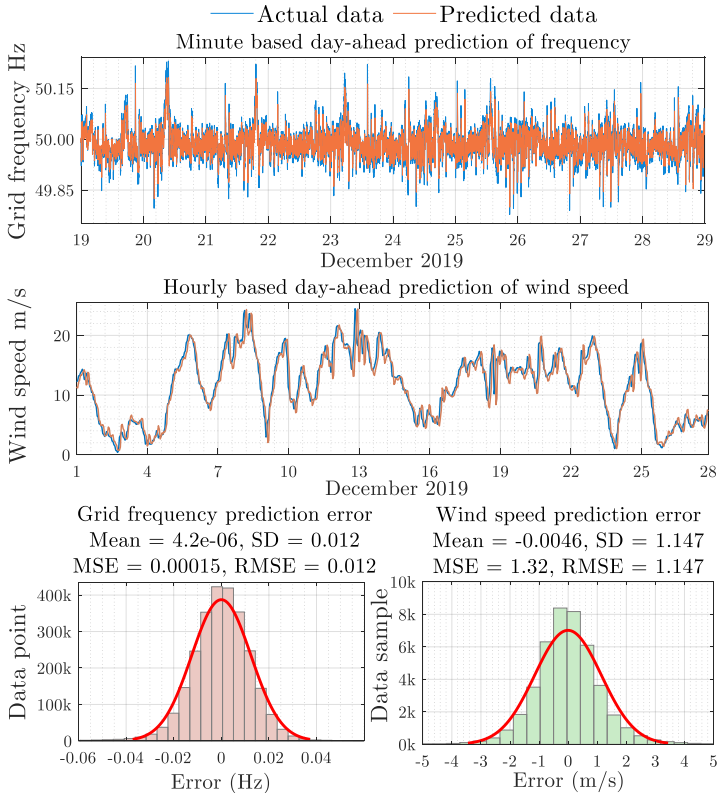

Figure 5.7: Wind speed and grid frequency day-ahead prediction.

5.3.2 Stochastic optimization

The bidding decision variables of electricity P_e^{sch} and reserve P_r^{sch} are defined as first-stage decision variables. These should be scheduled in the day-ahead market. The decision variables related to formic acid production $P_{\text{Fa}}^{\text{sch}}$, electricity and reserve commitments, $P_e(\omega)$ and $P_r(\omega)$ respectively, are defined as second-stage variables. The decision-maker does not need to select the formic acid production schedule in the day-ahead but can take advantage of the plant's flexibility to optimize the baseload of formic acid production $P_{\text{Fa}}^{b}(\omega)$ according to the different wind speed scenarios that may occur. Therefore, the two-stage stochastic optimization model and its constraints are formulated, based on the above considerations, as follows:

$$\begin{aligned}\max \quad & P_e^{\text{sch}} \cdot \lambda_e^{\text{sch}} + P_r^{\text{sch}} \cdot \lambda_r^{\text{sch}} + \\ & \mathbb{E}_\omega \left[g(P_{\text{Fa}}(\omega)) \cdot \lambda_{\text{Fa}} + \Delta P_e(\omega) \cdot \lambda_{\Delta e} + \Delta P_r(\omega) \cdot \lambda_{\Delta r} \right]\end{aligned} \tag{5.11}$$

$$\Delta P_e(\omega) \cdot \lambda_{\Delta e} = \Delta P_e^{+}(\omega) \cdot \lambda_{\Delta e}^{+} + \Delta P_e^{-}(\omega) \cdot \lambda_{\Delta e}^{-} \tag{5.12}$$

$$P_\omega = 2 \cdot P_{wt} \tag{5.13}$$

$$\Delta P_r(\omega) \cdot \lambda_{\Delta r} = \Delta P_r^{+}(\omega) \cdot \lambda_{\Delta r}^{+} + \Delta P_r^{-}(\omega) \cdot \lambda_{\Delta r}^{-} \tag{5.14}$$

$$P_r^{\text{sch}} = 200\text{mHz} \cdot K \quad (K \text{ is droop constant}) \tag{5.15}$$

$$P_r(\omega) = \Delta f \cdot K \tag{5.16}$$

$$\Delta f = f_e - f_{\text{ref}} \quad (f_{\text{ref}} \text{ is 50 Hz}) \tag{5.17}$$

where λ_e^{sch}, λ_r^{sch} and λ_{Fa} are the electricity, reserve and formic acid prices respectively. $\mathbb{E}_\omega$ is the probability of scenario ω. $\Delta P_e{}^{+}(\omega)$, $\Delta P_e{}^{-}(\omega)$, $\Delta P_r{}^{+}(\omega)$ and $\Delta P_e{}^{+}(\omega)$ are additional and deficiency of power injection to the grid and reserve provision. $\lambda_{\Delta e}^{-}$, $\lambda_{\Delta e}^{+}$, $\lambda_{\Delta r}^{-}$ and $\lambda_{\Delta r}^{+}$ are revenue and penalty for additional power and reserve injected to the grid as well. In the first and second stage of the optimization, the objective function (5.11) is subject to the following boundary conditions:

s.t.(first stage)

$$0 \leqslant P_e^{\text{sch}} \leqslant P_\omega^{\max} \tag{5.18}$$

$$0 \leqslant P_r^{\text{sch}} \leqslant \frac{P_{\text{Fa}}^{\max} - P_{\text{Fa}}^{\min}}{2} \tag{5.19}$$

The constraint 5.19 limits the symmetric upward and downward scheduled power reserve to guarantee the continuous operation of electrolyzer and avoid any start-up and shut-down time required to purge the nitrogen. s.t.(second stage)

$$P_{\text{Fa}}^{\min} \leqslant P_{\text{Fa}}(\omega) \leqslant P_\omega \tag{5.20}$$

$$P_{\mathrm{Fa}}(\omega) = P_{\omega} - P_e(\omega) - P_r(\omega) \quad \text{if} \quad 49.8 \leqslant f_e \leqslant 49.99 \tag{5.21}$$

$$P_{\mathrm{Fa}}(\omega) = P_{\omega} - P_e(\omega) + P_r(\omega) \quad \text{if} \quad 50.01 \leqslant f_e \leqslant 50.2 \tag{5.22}$$

$$0 \leqslant P_e(\omega) \leqslant P_{\omega} - P_{\mathrm{Fa}}(\omega) \tag{5.23}$$

$$0 \leqslant P_r(\omega) \leqslant \frac{P_{\mathrm{Fa}}(\omega)}{2} \tag{5.24}$$

$$\Delta P_e^{+}(\omega) = P_e(\omega) - P_e^{\mathrm{sch}} \quad \text{if} \quad P_e(\omega) > P_e^{\mathrm{sch}} \tag{5.25}$$

$$\Delta P_r^{+}(\omega) = P_r(\omega) - P_r^{\mathrm{sch}} \cdot \Delta f \quad \text{if} \quad P_r(\omega) > P_r^{\mathrm{sch}} \tag{5.26}$$

$$\Delta P_e^{-}(\omega) = P_e(\omega) - P_e^{\mathrm{sch}} \quad \text{if} \quad P_e(\omega) \leqslant P_e^{\mathrm{sch}} \tag{5.27}$$

$$\Delta P_r^{-}(\omega) = P_r(\omega) - P_r^{\mathrm{sch}} \cdot \Delta f \quad \text{if} \quad P_r(\omega) \leqslant P_r^{\mathrm{sch}} \tag{5.28}$$

The nonlinear functions P_{wt} and $P_{\mathrm{Fa}}(\omega)$ and their piece-wise linearizations are given in (5.3), (5.4), (5.9) and (5.10), which are discussed in detail in § 5.2.1 and § 5.2.2. The proposed two-stage stochastic optimization is solved with both the nonlinear function of formic acid (5.9) and the linearized form (5.10). The best results are obtained using a mixed integer nonlinear programming (MILNP), for which the nonlinear solvers guarantee the global optimum.

5.4 Results

5.4.1 The impact of variable wind power on decision making

One of the most critical issues with the bidding strategies of the flexible demand, integrated with renewable sources, is the trade-off between the power consumption and the injection of additional renewable power into the grid. If the decision-maker offers a too high bidding quantity, it will not satisfy grid requirements in low wind power scenarios. It will be subject to penalties, leading to an additional cost. However, a low bidding quantity of reserve and electricity causes extra wind power curtailment and declines revenue. Hence, the optimization criteria proposed in this study guarantee an offer which is a compromise between an aggressive decision with a high bidding quantity and a conservative decision with a low bidding quantity, considering the variability of wind and grid frequency. Table 5.1 gives the optimal allocation of available wind power to the electricity/reserve markets and the formic acid production for proposed and baseline strategies. No operational flexibility and FCR provision are considered for the baseline approach, and the available wind power is only decided to be optimally distributed between the chemical process and the electricity market. It can be understood that the purpose strategy suggests almost zero contribution to the electricity market on an almost windless day when the wind speed is too low. However, a marginal reserve contribution

Table 5.1: Optimal decision for the proposed and baseline strategies in different days, various wind and frequency conditions.

		P_e^{sch}	P_r^{sch}	f_e	$P_{\mathrm{Fa}}(\omega)$ (MW)				Z
Days of 2019	Operation mode	day a head schedule		Hz	ω_1	ω_2	ω_3	ω_4	euro
Almost windless: $v_w \leq 4\ m/s$	Proposed strategy	0	0.33	50.122	0.44	1.48	4.00	0	173.68
	Baseline approach	0	No FCR		0.44	1.47	4.00	0	138.94
Windless: $3\ m/s \leq v_w \leq 6\ m/s$	Proposed strategy	0.86	0	49.948	0	2.16	4.95	0	504.57
	Baseline approach	1.31	No FCR		0	2.15	4.53	0	408.91
Varoable wind: $4\ m/s \leq v_w \leq 12\ m/s$	Proposed strategy	4.58	0.50		0.57	0.99	4.61	4.92	730.25
	Baseline approach	5.54	No FCR	50.101	0.57	1.49	4.06	4.45	617.47
Windy: $v_w \geq 10\ m/s$	Proposed strategy	4.14	1.01		0	2.02	4.61	4.84	910.43
	Baseline approach	5.64	No FCR	49.921	0	3.03	4.06	4.35	768.22
Extremely windy: $v_w \geq 12\ m/s$	Proposed strategy	2.26	2.58		0	0	5.16	5.16	1041.70
	Baseline approach	5.62	No FCR	49.916	0	0	4.12	4.38	874.511

is decided since the maximum frequency deviation rises to 50.122 Hz, and the chemical process can play a demand response role in consuming excessive supplied power. Instead, any available wind speed will be allocated to formic acid production. Thus, there will be a minimum formic acid production even in the first scenario ω_1 when the average estimated frequency exceeds 50 Hz. This condition does not happen so often due to some degree of correlation between wind speed and grid frequency. Nevertheless, for the following case, which is an almost windless day when the wind speed is between $3to6m/s$, and the maximum frequency deviation drops to 49.948 Hz, no reserve is arranged to avoid activation penalties for the windless condition. Contrarily, a maximum contribution in electricity and reserve markets will be selected for windy and extremely windy days. According to Table 5.1, the results of the proposed optimization problem for an extremely windy day show an almost equal amount of bids for both scheduled electricity and reserve. The average wind speed is above the rated value on a windy day, but it may also drop for a meaningful period. Therefore, a higher contribution to the electricity market is suggested to avoid extra penalties of the reserve that will be asked for activation, especially when the maximum estimated grid frequency is below 50 Hz. An even more conservative policy is taken for the day, meeting variable wind conditions. The results show that the proposed strategy effectively prioritizes formic acid production based on available wind power over all the scenarios and actively participates in the reserve and electricity market to enhance the expected revenue z. At the same time, the baseline approach only guarantees the optimal baseload of formic acid production and relatively increases the electricity market share by rising wind speed up to the rated power (10 MW). Fig. 5.8 shows wind variation and grid frequency situation for the first 100 days of 2019. Fig. 5.9 also shows the performance of the two-stage stochastic programming for the same wind and frequency situation when the prices mentioned above are competitive, and the decision maker is willing to participate in all the markets. It shows that whenever the wind speed is above the rated value (11.9 m/s), the maximum reserve bidding quantity is decided, which is half of the maximum capacity of the formic acid process, around 2.60 MW, to satisfy the symmetric (upward and downward) FCR. However, the priority is to produce formic acid when wind speed is expected to drop significantly. For the expected unstable wind and variable frequency conditions, the preference is to offer a higher electricity contribution to avoid FCR penalties in low wind speed events. Also, in Fig. 5.9, the total income considering the proposed operational strategy is compared with the baseline strategy, where no flexibility and reserve contribution is supported, and the wind power is only allocated to the chemical process and the electricity market. The average revenue is increased for the proposed strategy compared to the baseline approach as a result of the offered flexibility and FCR provision, especially in above-rated wind speeds.

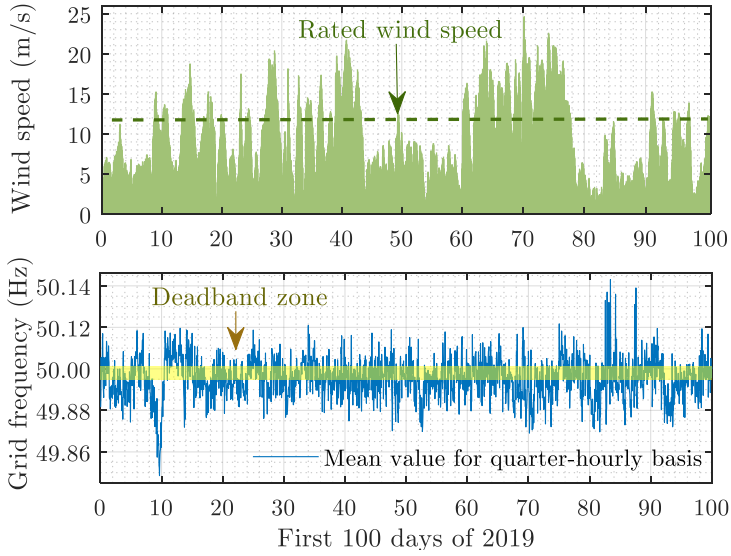

Figure 5.8: Wind and grid frequency behaviour for the first 100 days of 2019.

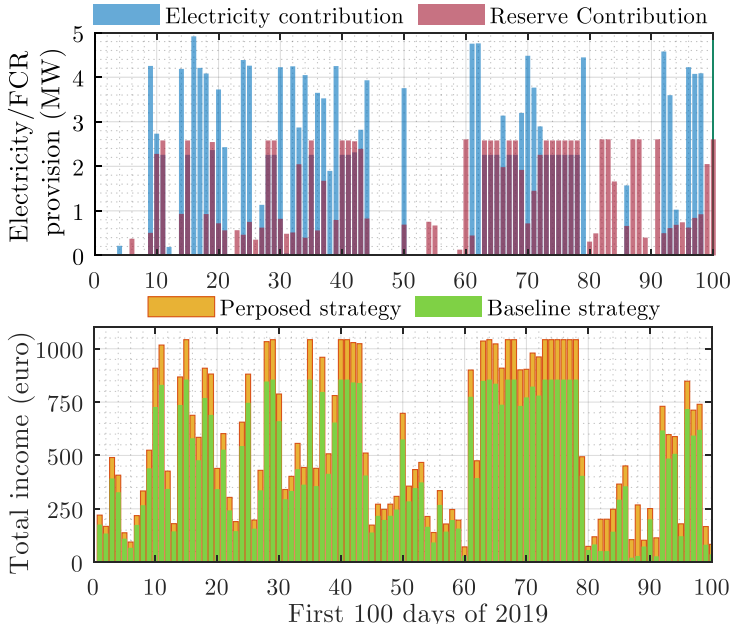

Figure 5.9: The two-stage stochastic programming performance for the first 100 days of 2019.

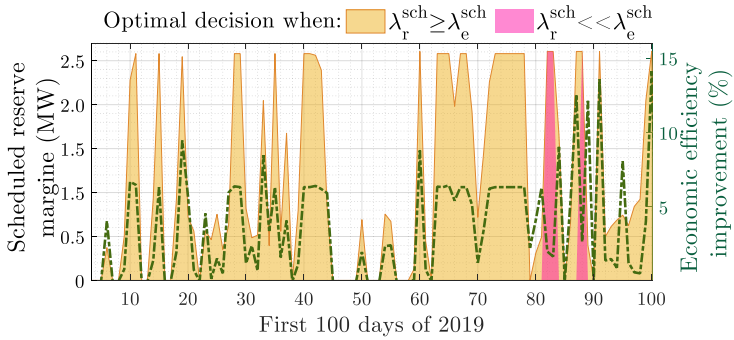

Figure 5.10: Economic efficiency considering two pricing conditions.

5.4.2 The economic efficiency

Although the primary goal of the proposed two-stage stochastic programming is to deal with wind power uncertainty, the optimization's parameters are set to obtain the maximum sensitivity to electricity, reserve and formic acid prices. Fig. 5.9 shows the performance of the two-stage stochastic programming for the first 100 days of 2019 when the prices mentioned above are competitive, and the decision maker is willing to participate in all the markets. It shows that whenever the wind speed is above the rated value, the maximum reserve bidding quantity is decided, which is half of the maximum capacity of the formic acid process, around 2.60 MW, to satisfy the symmetric (upward and downward) FCR. However, the priority is to produce formic acid when wind speed is expected to drop significantly. For the expected unstable wind and variable frequency conditions, the preference is to offer a higher electricity contribution to avoid FCR penalties in low wind speed events. Moreover, Fig. 5.10 compares the economic efficiency of the proposed model for two pricing conditions. First, when the reserve price is competitive to the electricity price ($\lambda_r^{\text{sch}} \geq \lambda_e^{\text{sch}}$) and second, when the reserve price is much lower than the electricity price ($\lambda_r^{\text{sch}} << \lambda_e^{\text{sch}}$). The first pricing condition is more likely to happen in the future of power systems without conventional plants, and the second pricing condition represents the lowest reserve price according to market prices in 2019. It can be witnessed that in the second pricing condition, lower economic efficiency is achieved because the stochastic programming does not suggest a high contribution in the reserve market, except for a couple of days, i.e. between days 80 and 90, where the grid frequency is foreseen to go above 50 Hz. The economic efficiency improvement EE is calculated as follows:

$$EE = \frac{Z(\lambda_r^{sch} >> \lambda_e^{sch}) - Z(\lambda_r^{sch} << \lambda_e^{sch})}{Z(baseline)} \times 100 \tag{5.29}$$

Estimation of EE shows the degree of freedom of the decision-maker and explains up to what level contributes to the reserve market based on reserve prices.

5.5 Conclusions

In this study, a two-stage stochastic programming model considering wind power uncertainty is employed to develop an optimal cooperative framework for the flexible operation of a CCU based chemical process as an energy-intensive industrial load in combination with wind power. Although demand and renewable sources are envisioned to play an essential role in the ancillary market, offering grid balancing services in a cooperative procedure is not yet well explored. Therefore, this paper suggests a decision-making algorithm, which guarantees an optimal bidding strategy for the hybrid system consisting of a CCU based process and two wind turbines, participating in the day-ahead electricity and reserve markets. The dynamic modeling of the subsystems and the proposed architecture of the chemical plant are presented in detail, and their piecewise linearization is used in the optimization algorithm. The proposed algorithm is not limited by period spans and can be applied to other markets as well, e.g., the intraday market. Instead of generating hundreds of scenarios that can make the optimization computationally expensive, the GMDH algorithm is used as a deep learning time-series prediction tool for forecasting wind speed and grid frequency in a day ahead. Accordingly, only four wind scenarios are considered that can particularly impact the optimal bidding strategy. The results show the significance of the proposed stochastic programming to find an optimal decision for the bidding strategy and the formic acid production. This approach ensures sufficient carbon-dioxide capture and an optimal provision of FCR as vital elements towards decarbonizing the grid.

Bibliography

[1] H. L. van Soest, M. G. den Elzen, and D. P. van Vuuren, "Net-zero emission targets for major emitting countries consistent with the Paris Agreement," *Nature Communications*, vol. 12, no. 1, pp. 1–9, 2021. DOI: 10.1038/s41467-021-22294-x.

[2] L. Haar, "An empirical analysis of the fiscal incidence of renewable energy support in the European Union," *Energy Policy*, vol. 143, p. 111483, 2020. DOI: 10.1016/j.enpol.2020.111483.

[3] I. Pineda, "Aiming high-rewarding ambition in wind energy," *A position paper by the European Wind Energy Association*, 2015. URL: https://www.ewea.org/publications/.

[4] C. Schwarte, "EU climate policy under the Paris Agreement," *Climate Law*, vol. 11, no. 2, pp. 157–175, 2021. DOI: 10.1163/18786561-11020002.

[5] M. Rosental, T. Fröhlich, and A. Liebich, "Life cycle assessment of carbon capture and utilization for the production of large volume organic chemicals," *Frontiers in Climate*, vol. 2, p. 9, 2020. DOI: 10.3389/fclim.2020.586199.

[6] Z. Sun, L. Zeng, C. K. Russell, S. Assabumrungrat, S. Chen, L. Duan, W. Xiang, and J. Gong, "Solar–wind–bio ecosystem for biomass cascade utilization with multigeneration of formic acid, hydrogen, and graphene," *ACS Sustainable Chemistry & Engineering*, vol. 7, no. 2, pp. 2558–2568, 2018. DOI: 10.1021/acssuschemeng.8b05546.

[7] D. Ravikumar, G. Keoleian, and S. Miller, "The environmental opportunity cost of using renewable energy for carbon capture and utilization for methanol production," *Applied Energy*, vol. 279, p. 115770, 2020. DOI: 10.1016/j.apenergy.2020.115770.

[8] B. Lee, H. Lee, D. Lim, B. Brigljević, W. Cho, H.-S. Cho, C.-H. Kim, and H. Lim, "Renewable methanol synthesis from renewable H_2 and captured CO_2: How can power-to-liquid technology be economically feasible?," *Applied Energy*, vol. 279, p. 115827, 2020. DOI: 10.1016/j.apenergy.2020.115827.

[9] H. Saboori and R. Hemmati, "Considering carbon capture and storage in electricity generation expansion planning," *IEEE Transactions on Sustainable Energy*, vol. 7, no. 4, pp. 1371–1378, 2016. DOI: 10.1109/TSTE.2016.2547911.

[10] A. I. Osman, M. Hefny, M. A. Maksoud, A. M. Elgarahy, and D. W. Rooney, "Recent advances in carbon capture storage and utilisation technologies: a review," *Environmental Chemistry Letters*, pp. 1–53, 2020. DOI: 10.1007/s10311-020-01133-3.

[11] M. Bos, S. Kersten, and D. Brilman, "Wind power to methanol: Renewable methanol production using electricity, electrolysis of water and CO_2 air capture," *Applied Energy*, vol. 264, p. 114672, 2020. DOI: 10.1016/j.apenergy.2020.114672.

[12] C. Chen and A. Yang, "Power-to-methanol: The role of process flexibility in the integration of variable renewable energy into chemical production," *Energy Conversion and Management*, vol. 228, p. 113673, 2021. DOI: 10.1016/j.enconman.2020.113673.

[13] C. Hank, S. Gelpke, A. Schnabl, R. J. White, J. Full, N. Wiebe, T. Smolinka, A. Schaadt, H.-M. Henning, and C. Hebling, "Economics & carbon dioxide avoidance cost of methanol production based on renewable hydrogen and recycled carbon dioxide–power-to-methanol," *Sustainable Energy & Fuels*, vol. 2, no. 6, pp. 1244–1261, 2018. DOI: 10.1039/C8SE00032H.

[14] N. Li, X. Zhao, X. Shi, Z. Pei, H. Mu, and F. Taghizadeh-Hesary, "Integrated energy systems with CCHP and hydrogen supply: A new outlet for curtailed wind power," *Applied Energy*, vol. 303, p. 117619, 2021. DOI: 10.1016/j.apenergy.2021.117619.

[15] M. Martín, "Methodology for solar and wind energy chemical storage facilities design under uncertainty: Methanol production from CO_2 and hydrogen," *Computers & Chemical Engineering*, vol. 92, pp. 43–54, 2016. DOI: 10.1016/j.compchemeng.2016.05.001.

[16] M. Martín and I. E. Grossmann, "Optimal integration of renewable based processes for fuels and power production: Spain case study," *Applied Energy*, vol. 213, pp. 595–610, 2018. DOI: 10.1016/j.apenergy.2017.10.121.

[17] A. E. Samani, J. D. M. De Kooning, C. A. Urbina Blanco, and L. Vandevelde, "Flexible operation strategy for formic acid synthesis providing frequency containment reserve in smart grids," *International Journal of Electrical Power & Energy Systems*, vol. 139, p. 107969, 2022. DOI: 10.1016/j.ijepes.2022.107969.

[18] I. González-Aparicio, Z. Kapetaki, and E. Tzimas, "Wind energy and carbon dioxide utilisation as an alternative business model for energy producers: A case study in spain," *Applied Energy*, vol. 222, pp. 216–227, 2018. DOI: 10.1016/j.apenergy.2018.03.114.

[19] O. Babatunde, J. Munda, and Y. Hamam, "Power system flexibility: A review," *Energy Reports*, vol. 6, pp. 101–106, 2020. DOI: 10.1016/j.egyr.2019.11.048.

[20] J. Zhao, T. Zheng, and E. Litvinov, "A unified framework for defining and measuring flexibility in power system," *IEEE Transactions on power systems*, vol. 31, no. 1, pp. 339–347, 2015. DOI: 10.1109/TPWRS.2015.2390038.

[21] M. Melliger and E. Chappin, "Phasing out support schemes for renewables in neighbouring countries: An agent-based model with investment preferences," *Applied Energy*, vol. 305, p. 117959, 2022. DOI: 10.1016/j.apenergy.2021.117959.

[22] H. Liu, P. Zeng, J. Guo, H. Wu, and S. Ge, "An optimization strategy of controlled electric vehicle charging considering demand side response and regional wind and photovoltaic," *Journal of Modern Power Systems and Clean Energy*, vol. 3, no. 2, pp. 232–239, 2015. DOI: 10.1007/s40565-015-0117-z.

[23] J. Wu, B. Zhang, Y. Jiang, P. Bie, and H. Li, "Chance-constrained stochastic congestion management of power systems considering uncertainty of wind power and demand side response," *International Journal of Electrical Power & Energy Systems*, vol. 107, pp. 703–714, 2019. DOI: 10.1016/j.ijepes.2018.12.026.

[24] S. Cui, Y.-W. Wang, J.-W. Xiao, and N. Liu, "A two-stage robust energy sharing management for prosumer microgrid," *IEEE Transactions on Industrial Informatics*, vol. 15, no. 5, pp. 2741–2752, 2018. DOI: 10.1109/TII.2018.2867878.

[25] "Establishing a guideline on electricity transmission system operation," *Official Journal of the European Union*, 2017. URL: https://eur-lex.europa.eu/.

[26] J. Jonkman, S. Butterfield, W. Musial, and G. Scott, "Definition of a 5-MW reference wind turbine for offshore system development," tech. rep., National Renewable Energy Lab (NREL), Golden, CO (United States), 2009. DOI: 10.2172/947422.

[27] J. D. M. De Kooning, J. Van de Vyver, B. Meersman, and L. Vandevelde, "Maximum efficiency current waveforms for a PMSM including iron losses and armature reaction," *IEEE Transactions on Industry Applications*, vol. 53, no. 4, pp. 3336–3344, 2017. DOI: 10.1109/TIA.2017.2681619.

[28] J. D. M. De Kooning, T. L. Vandoorn, J. Van de Vyver, B. Meersman, and L. Vandevelde, "Displacement of the maximum power point caused by losses in wind turbine systems," *Renewable Energy*, vol. 85, pp. 273–280, 2016. DOI: 10.1016/j.renene.2015.06.052.

[29] N. Kayedpour, A. E. Samani, J. D. M. De Kooning, L. Vandevelde, and G. Crevecoeur, "Model predictive control with a cascaded hammerstein neural network of a wind turbine providing frequency con-

tainment reserve," *IEEE Transactions on Energy Conversion*, 2021. DOI: 10.1109/TEC.2021.3093010.

[30] A. E. Samani, J. D. M. De Kooning, N. Kayedpour, N. Singh, and L. Vandevelde, "The impact of pitch-to-stall and pitch-to-feather control on the structural loads and the pitch mechanism of a wind turbine," *Energies*, vol. 13, no. 17, p. 4503, 2020. DOI: 10.3390/en13174503.

[31] K. Park, G. H. Gunasekar, S.-H. Kim, H. Park, S. Kim, K. Park, K.-D. Jung, and S. Yoon, "CO_2 hydrogenation to formic acid over heterogenized ruthenium catalysts using a fixed bed reactor with separation units," *Green Chemistry*, vol. 22, no. 5, pp. 1639–1649, 2020. DOI: 10.1039/C9GC03685G.

[32] Q. Wang, S. Santos, C. A. Urbina-Blanco, W. Y. Hernández, M. Impéror-Clerc, E. I. Vovk, M. Marinova, O. Ersen, W. Baaziz, O. V. Safonova, *et al.*, "Solid micellar Ru single-atom catalysts for the water-free hydrogenation of CO_2 to formic acid," *Applied Catalysis B: Environmental*, vol. 290, p. 120036, 2021. DOI: 10.1016/j.apcatb.2021.120036.

[33] J. J. Anderson, D. J. Drury, J. E. Hamlin, and A. G. Kent, "Process for the preparation of formic acid," no. WO1986002066A1. 2019, URL: https://patentscope.wipo.int/search/en/detail.jsf?docId=WO1986002066.

[34] J. Wang, M. Cevik, and M. Bodur, "On the impact of deep learning-based time-series forecasts on multistage stochastic programming policies," *INFOR: Information Systems and Operational Research*, pp. 1–32, 2021. DOI: 10.1080/03155986.2021.2015825.

[35] N. Kayedpour, A. E. Samani, J. D. M. De Kooning, L. Vandevelde, and G. Crevecoeur, "A data-driven approach using deep learning time series prediction for forecasting power system variables," in *2019 IEEE 2nd International Conference on Renewable Energy and Power Engineering (REPE)*, (Toronto, ON, Canada), pp. 43–47, IEEE, 2-4 Nov. 2019. DOI: 10.1109/REPE48501.2019.9025159.

Chapter 6

Conclusions and future research

6.1 Conclusions

This dissertation proposes different solutions to extend the flexibility of the grid, enabling a higher-level integration of renewables and energy-intensive CCU based processes into the power system. An optimal cooperative operation of CO_2-based processes, renewables, and the grid can provide the opportunity to accelerate the decarbonisation and realise the low-carbon paradigm. However, reaching an optimal collaborative approach requires new operating strategies to support the flexible operation of the variable renewable power generation and energy-intensive industries. The flexible operating strategies are extensively researched in this dissertation. Various flexible operating approaches are proposed in different emerging technologies, e.g., power-to-gas and CCU processes, to support the grid on electricity supply and demand. The research results are concluded as follows:

In chapter 2, the optimal demand response operation of power-to-hydrogen technology was investigated for the specific case of Belgium. The techno-economic analysis was performed for a large-scale PEM electrolyser, operating under price-based and grid-based strategies. The PEM electrolyser was operated based on a variable electricity price by regulating the power offtake first. In the second operating approach, the electrolyser was operated to participate in the ancillary market by responding to grid frequency variations. Furthermore, a dynamic model and control architecture was designed to evaluate the technical feasibility of the optimal operating strategy. The results show that the revenue driven from the price-based strategy could not effectively improve the economic performance, and this strategy would not be economically viable due to the high capital investment cost and low hydrogen selling price. The economic analysis confirmed that offering 100 mHz symmetric FCR can bring in further revenue from ancillary services and considerably improve the economic per-

formance, making the power-to-hydrogen system a profitable technology. As a result, operating the PEM electrolyser at a baseload of 55% and offering the remaining capacity as a power reserve maximises the system profit. In order to evaluate the controllability of the power input, the dynamic response of the system is tested to the maximum frequency variation. Dynamic simulations show that the PEM electrolyser has adequate flexibility to react to the grid frequency, i.e., below five seconds, providing the opportunity to participate in fast-paced demand response programs.

In chapter 3, a flexible operating strategy was proposed for demand response operation of energy-intensive chemical processes developed for direct conversion of CO_2 to value-added chemicals. The feasibility of providing grid balancing services was investigated in the form of FCR while using CO_2 in a thermo-catalytic formic acid synthesis process. In this process, the formic acid is produced through the hydrogenation of CO_2 over heterogenised ruthenium catalysis. The proposed strategy was designed based on the collaborative operation of the PEM electrolyser and multi-stage H_2 and CO_2 compression trains. A dynamic model of the process consisting of a PEM electrolyser, multi-stage compression systems and a reactor was developed to investigate the flexible operating strategy on the industrial-scale plant. A control architecture has been designed to respond to the grid frequency variations through regulating the process components, i.e., the electrolyser and compressors. A techno-economic analysis is performed to obtain the optimal operating baseload for the flexible operating strategy. The results show that the proposed control strategy and the control system enable the CCU based formic acid process to provide FCR for the grid concerning process efficiency and constraints. This is obtained by maintaining the optimal operating parameters, i.e., flow rate ratio, pressure and temperature, at the reaction stage through the collaborative operation of process components. The control system enhances the flexibility of the process for FCR provision, and it is designed robustly for different operational conditions and grid frequency variations. Moreover, the techno-economic optimisation showed that providing FCR is a valid option to create additional revenue and improve the economic performance of the process.

In chapter 4, the potential benefits of the pitch-to-feather and pitch-to-stall control strategies were investigated for the flexible operation of HAWTs to provide ancillary services for the grid. A comparative analysis was performed to investigate the control performance and the impact on the HAWTs' structure and pitch mechanism under different wind conditions. Three HAWTs with different blade designs are studied, i.e., untwisted, stall-regulated, and pitch-regulated blades. A control system consisting of pitch and torque control was designed to control the wind turbine in the whole operating region, coping with the nonlinearity of the system and the intermittent nature of wind. The dynamic response of the wind turbines was examined in the whole wind speed range

and realistic operating conditions considering the nonlinearity of atmospheric turbulence simulated by three-dimensional turbulent wind fields. The results show that the pitch-to-stall strategy represents less aerodynamic sensitivity in the full load operating region. Moreover, the pitch-to-stall strategy improves the wind turbine generator speed and power regulation with smaller pitch manoeuvres. The pitch-to-stall control considerably reduces the summed blade pitch movements compared to pitch-to-feather. This advantage is significant for active power control of the wind turbine in frequency regulation to enhance the reactivity of the wind turbine while reducing the load on the pitch mechanism. The pitch cycle analysis showed that, despite the advantages of pitch-to-stall control, it might increase the risk of surface damage in the blades bearing due to the increased oscillating movements with a small amplitude. The load analysis shows that pitch-to-stall control reduces the fore-aft fatigue load on the tower due to the augmented aerodynamic rotor thrust. This capability is significant to prevent negative damping for floating wind turbines, where pitch-to-feather control reduces the platform-pitch damping mode and contributes to large system-pitch motions. Besides the advantages of pitch-to-stall control, it magnifies the loads on the rotor blades. However, the increased loads are minimised for the wind turbine with a stall-regulated blade design.

In chapter 6, a flexible operating strategy was designed for a hybrid system comprising a CCU based process and wind turbines. The strategy was developed based on the optimal renewable energy sharing between the chemical plant and the grid. A dynamic model of a wind turbine and the chemical process including a PEM electrolyser, compression stages and a reactor is developed to realise the flexible operation of the system. In order to enhance the process flexibility, a control system is designed to regulate the process components adaptively based on the input power. Moreover, a two-stage stochastic optimisation model is developed to calculate the optimal bidding for the energy and reserve markets, taking the wind power uncertainty into account. In order to reduce the computational load of the optimisation, the GMDH algorithm is used as a deep learning time-series prediction tool for forecasting wind speed and grid frequency in a day ahead. Therefore, the number of wind scenarios are reduced to four main scenarios that influence the optimal bidding strategy. The results show that the proposed decision-making algorithm guarantees an optimal bidding strategy for the hybrid system, participating in day-ahead electricity and reserve markets. Therefore, wind energy was successfully integrated into the grid and supported the chemical process while offering grid balancing services in a cooperative procedure.

6.2 Future research

The presented research proposes techno-economic solutions to facilitate the integration of energy-intensive CO_2-based processes and wind power into the grid. Therefore, this research can make valuable contributions in extending the flexibility of the power system under a high penetration of renewable energy sources. Moreover, the developed flexible operating strategy for emerging CCU based technologies can further reduce carbon dioxide emissions in the paradigm shift toward net-zero emissions. During this work, some other interesting research paths were identified to be continued in future research. The most important topics are summarised here:

6.2.1 Wind turbine control strategies for FCR provision

Pitch-to-stall control for flexible operation of offshore floating wind turbines

In chapter 4, the potential advantage of the pitch-to-stall control versus pitch-to-feather is investigated for HAWTs. The results show that the pitch-to-stall strategy improves the control performance to regulate rotational speed and output power with considerably smaller pitch system manoeuvres. Also, despite the nonlinear variation of aerodynamic sensitivity in the stall regulation, blade-pitch sensitivity across the full load operating region is less prominent and adjusting the controller gains is less of a requirement. These characteristics can be advantageous for active power control of wind turbines for frequency regulation. Pitch-to-stall control can reduce the load on the pitch mechanism by reducing the pitch action while tracking the grid frequency with a relatively faster dynamic response. Moreover, the results confirmed that pitch-to-stall control reduces the fore-aft fatigue loads on the tower. This is due to the fact that thrust increases while power is regulated in increasing relative winds. The main drawback of the pitch-to-feather regulation is the reduction in steady-state rotor thrust with increasing wind speed in the full load operating region, which may result in negative damping. This is more of an issue for offshore floating wind turbines where the drop of rotor thrust introduces negative damping in the platform-pitch mode and leads to large system-pitch motions. Therefore, pitch-to-stall control can be used for more effective damping of the platform-pitch motions because of increased thrust induced by pitching the blades to stall. In future research, more work is needed to apply and test pitch-to-stall control on offshore floating wind turbines. In addition, future research should be devoted to redesigning the blades to optimise the aerodynamic performance in stall-regulated operation.

Analysis considering wind turbine control strategies in the techno-economic model

In chapter 5, a cooperative control strategy was proposed for the flexible operation of a chemical process supplied by wind energy. In the designed control scheme, the wind turbines operate at their maximum capacity while using the chemical plant as a buffer. Therefore, the ancillary service was provided for the grid by flexible operation of the chemical process. In the alternative scenario, the ancillary services can be provided by both wind turbines and the chemical plant. For instance, wind turbines can provide upward regulation while chemical plant offers downward regulation. Therefore, the hybrid system can take advantage of two flexible sources to support the grid, and thus, the flexible operation is distributed between wind turbines and the chemical plant. The decision-making algorithm will take into account operating conditions, e.g., wind, grid frequency, wind turbine structural loads and chemical plant constraints, to make the decision between the wind turbine and the chemical plant as sources of flexibility. In these circumstances, the impact of the control strategy on the wind turbine should be included in the techno-economic model, e.g., the impact on structural loads and maintenance costs. Therefore, the corresponding parameters in the optimisation problem are determined based on the applied control strategy for the flexible operation of wind turbines. The proposed operating strategy and the required adaptations in the optimisation model can be addressed in future studies.

6.2.2 Scenario generation strategies for stochastic optimisation

Scenario generation using unsupervised learning algorithms (K-means clustering)

The efficiency of the stochastic programming problem presented in chapter 5 can be significantly improved by increasing the number of wind scenarios. However, the runtime will also rise by expanding the number of wind scenarios. Therefore, an efficient scenario reduction approach is required to decrease the computational time required for simulating many scenarios. The K-means clustering method, an unsupervised learning algorithm, can group the unlabeled dataset into different clusters. Applying this method can be a promising approach for reducing the number of scenarios by setting day ahead predictions of wind speed into scenarios according to the centroid closeness of each cluster. The development of the K-means clustering algorithm as a scenario reduction technique can potentially result in a reduced computation time of the proposed stochastic problem while improving the accuracy in the outcomes [1, 2].

Wind speed prediction system using Monte Carlo and artificial intelligence algorithms

The accuracy and efficiency of the proposed prediction method in chapter 5 can be improved by applying promising hybrid prediction strategies. Since wind speed and grid frequency are among the most uncertain and volatile phenomena, using the Monte Carlo method can be promising to construct a Markov chain that is able to generate meaningful scenarios [3].

6.2.3 Stability and sensitivity-analysis for stochastic programming

Based on the primary results obtained in the last section of chapter 5, a sensitivity analysis discussion can be performed for the general optimization problem regarding reserve and electricity prices. A practical sensitivity analysis should investigate the sensitivity of the parameters of the stochastic optimization problem to price data variations. It should also allow modification of the optimal formulation and the point where the optimum is achieved concerning changing the first stage day-ahead and second stage real-time prices in both reserve and electricity markets [4, 5]. Identifying the main parameters that influence the output uncertainty in the optimal energy sharing decisions through a complete sensitivity analysis may also result in identifying risk sources in energy investments.

6.2.4 A robust fuzzy stochastic programming model for the cooperative energy sharing strategy

The proposed flexible operation of the chemical process with wind energy and the suggested energy sharing problem in chapter 5 can be an ideal case for investigating robust fuzzy stochastic programming due to a hybrid uncertainty of wind and grid frequency variability, considered as two sources of uncertainty for most of the parameters. Therefore, it is very engaging to take into account the requirements of robustifying the decision-making process. The proposed model is a mixed-integer nonlinear program using time-series wind speed and grid frequency prediction, which can be solved by employing an effective hybrid robust fuzzy stochastic method for handling uncertainty in parameters and risk-taking out of outbound decisions [6].

Bibliography

[1] M.-R. Yaghoubi-Nia, H. Hashemi-Dezaki, and A. H. Niasar, "Optimal stochastic scenario-based allocation of smart grids' renewable and non-renewable distributed generation units and protective devices," *Sustain-*

able Energy Technologies and Assessments, vol. 44, p. 101033, 2021. DOI: 10.1016/j.seta.2021.101033.

[2] A. Xuan, X. Shen, Q. Guo, and H. Sun, "A conditional value-at-risk based planning model for integrated energy system with energy storage and renewables," *Applied Energy*, vol. 294, p. 116971, 2021. DOI: 10.1016/j.apenergy.2021.116971.

[3] Y. Zhang, Y. Zhao, X. Shen, and J. Zhang, "A comprehensive wind speed prediction system based on monte carlo and artificial intelligence algorithms," *Applied Energy*, vol. 305, p. 117815, 2022. DOI: 10.1016/j.apenergy.2021.116971.

[4] E. M. Urbano, V. Martinez-Viol, K. Kampouropoulos, and L. Romeral, "Risk assessment of energy investment in the industrial framework–uncertainty and sensitivity analysis for energy design and operation optimisation," *Energy*, vol. 239, p. 121943, 2022. DOI: 10.1016/j.energy.2021.121943.

[5] A. Azizi, H. Karimi, and S. Jadid, "Daily operation of multi-energy systems based on stochastic optimization considering prediction of renewable energy generation," *IET Renewable Power Generation*, 2022. DOI: 10.1049/rpg2.12292.

[6] H. Gholizadeh, H. Fazlollahtabar, and M. Khalilzadeh, "A robust fuzzy stochastic programming for sustainable procurement and logistics under hybrid uncertainty using big data," *Journal of Cleaner Production*, vol. 258, p. 120640, 2020. DOI: 10.1016/j.jclepro.2020.120640.

Flexible integration of renewables into the decarbonised power systems.